Title

Assessing the Impacts of Land-Use Change and Ecological Restoration on CH4 and CO2 Fluxes in the Sacramento-San Joaquin Delta, California: Findings from a Regional Network of Eddy Covariance Towers

Author

Knox, Sara Helen

Publication Date

2016

Peer reviewed|Thesis/dissertation

Assessing the Impacts of Land-Use Change and Ecological Restoration on CH_4 and CO_2 Fluxes in the Sacramento-San Joaquin Delta, California: Findings from a Regional Network of Eddy Covariance Towers

by

Sara Helen Knox

A dissertation submitted in partial satisfaction of the

requirements for the degree of

Doctor of Philosophy

in

Environmental Science, Policy, and Management

in the

Graduate Division

of the

University of California, Berkeley

Committee in charge:

Professor Dennis D. Baldocchi, Chair
Professor Whendee L. Silver
Professor Iryna Dronova

Spring 2016

Assessing the Impacts of Land-Use Change and Ecological Restoration on CH_4 and CO_2 Fluxes in the Sacramento-San Joaquin Delta, California: Findings from a Regional Network of Eddy Covariance Towers

by

Sara Helen Knox

Abstract

Assessing the Impacts of Land-Use Change and Ecological Restoration on CH_4 and CO_2 Fluxes in the Sacramento-San Joaquin Delta, California: Findings from a Regional Network of Eddy Covariance Towers

by

Sara Helen Knox

Doctor of Philosophy in Environmental Science, Policy, and Management

University of California, Berkeley

Professor Dennis Baldocchi, Chair

The Sacramento–San Joaquin Delta in California was drained for agriculture and human settlement circa 1850, resulting in extreme rates of soil subsidence and CO_2 emissions due to peat oxidation. As a result of this prolonged ecosystem carbon imbalance where ecosystem respiration exceeded primary productivity, much of the land surface in the Delta now lies 5 to 8 m below sea level. To help reverse subsidence and convert Delta ecosystems from net carbon sources to carbon sinks, land managers have begun converting drained agricultural lands back to flooded ecosystems including wetlands and irrigated rice paddies. However, this comes at the cost of increased CH_4 emissions, a much more potent greenhouse gas than CO_2.

To evaluate the impacts of drained to flooded land-use change on the biosphere-atmosphere exchange of CO_2 and CH_4 in the Delta, I conducted a full year of simultaneous eddy covariance measurements at two conventional drained agricultural peatlands (a pasture and a corn field) and three flooded land-use types (a rice paddy and two restored wetlands). This research showed that the drained sites were large CO_2 and greenhouse gas (GHG) sources. However, this study also found that converting drained agricultural peat soils to flooded rice paddies or wetlands can help reduce or reverse soil subsidence and reduce GHG emissions, despite the potential for considerably higher CH_4 emissions. In particular, wetlands offer the greatest potential for reversing subsidence since both restored wetlands were large net carbon sinks.

Since natural and managed ecosystems can exhibit large year-to-year variation in CO_2 and CH_4 exchange, I analyzed 6.5 years of measurements from the irrigated rice

paddy to investigate the factors affecting CH_4 fluxes across diel to interannual timescales and quantify interannual variability in CO_2 and CH_4 budgets. Using wavelet analysis, I found that photosynthesis induced the diel pattern in CH_4 flux, but soil temperature influenced its amplitude. At the seasonal scale, linear and neural network models indicated that photosynthesis and water levels were the dominant factors regulating daily average CH_4 fluxes. However, across years, much of the variability in annual and growing season CH_4 sums was driven by soil temperature. Soil temperature also strongly influenced ecosystem respiration, resulting in large interannual variability in the net carbon budget at the paddy. This study emphasizes the need for long-term, continuous measurements particularly under changing climatic conditions.

With a growing interest in including wetlands in carbon markets worldwide due to their ability to accumulate large amounts of carbon, there is a need for models that can accurately and cheaply predict wetland CO_2 and CH_4 fluxes. In the final chapter of this dissertation, I combined eddy covariance CO_2 fluxes measurements, flux footprint analysis, and near-surface (i.e. digital cameras) or satellite remote sensing data to investigate the potential of using the light use efficiency approach to accurately and cost-effectively model photosynthesis in wetland systems. Through this analysis, I showed that digital camera and Landsat imagery can be used to model carbon uptake in wetlands, providing inexpensive means of monitoring carbon cycling in these environments that can be used in carbon markets.

By measuring trace gas exchange across multiple sites for multiple years, this dissertation provides new and important insights on the impacts of land use change in the Delta, improves our understanding of factors influencing CO_2 and CH_4 fluxes from agricultural and restored wetlands across diel to interannual timescales, and presents cost-effective and accurate ways of estimating photosynthesis in restored wetlands by combining flux measurements with near-surface and satellite remote sensing. This work helps bridge understanding between biometeorology, biogeochemistry and climate policy, and provides valuable information to help inform management decisions regarding carbon and water management of the Delta.

Table of Contents

List of Figures

List of Tables

Acknowledgments

I would like to express my deep gratitude and appreciation to my advisor, Professor Dennis Baldocchi, for the guidance and mentorship he provided to me these past five years. I am very fortunate to have had the opportunity to work with such a passionate, intelligent, creative, and supportive advisor. I also greatly appreciate the financial funding, which allowed me to focus on my studies and research. I am very grateful for the hard work and patience of Joe Verfaillie. Joe goes out of his way to ensure that our sensors are properly assembled and maintained, that our data is of the highest quality, and he's helped teach me the ins and outs of our instrumentation. I would also like to thank all my wonderful colleagues and friends in the Biomet lab, including Cove Sturtevant, Patty Oikawa, Jaclyn Hatala Matthes, Sebastian Wolf, Housen Chu, Ana Andreu Mendez, Elke Eichelmann, Kyle Hemes, Siyan Ma, Naama Raz Yaseef, Melanie Hahn, Laurie Koteen, and Martin Beland. I'd like to recognize my Dissertation Committee members, Professor Whendee Silver and Professor Iryna Dronova, for their help, advice and constructive feedback that improved the quality of this dissertation work.

I would like to thank my family for being there as a constant source of support and encouragement, for fostering my sense of curiosity, and for always believing in me. I would also like to acknowledge my friends who have been there for me over the years. In particular, I would like to thank Kate Wilkin, Lisa Kelley, Katy Seto, Ashton Wesner, and Kevi Mace whose support and advice deeply enriched my graduate school experience. And to my best friend and partner, Tyler Reid, for his endless encouragement, kindness, and patience.

Lastly, I greatly appreciate the support of the UC Berkeley Department of Environmental Science, Policy, and Management, and thanks to the National Sciences and Engineering Research Council of Canada, which generously supported my PhD studies and dissertation research from 2011-2014. Portions of the dissertation, with permission, have been reprinted from *Global Change Biology* and *Journal of Geophysical Research: Biogeosciences* and I thank the Wiley publishing company for that permission.

Chapter 1: Introduction

Wetlands play a key role in global carbon dynamics due to their large soil carbon pools, high methane (CH_4) emissions, and potential for carbon sequestration (Bridgham *et al.*, 2006). Although wetlands comprise only 5–8% of the earth's land surface, it is estimated that they store roughly 20 to 30% of the carbon in terrestrial soil reservoirs (Mitsch *et al.*, 2013). Most of this carbon resides in peatlands, defined as wetland environments with > 40 cm of surface organic matter (Bridgham *et al.*, 2006). The ability of these ecosystems to accumulate large amounts of carbon is largely a result of limited rates of decomposition in anaerobic soils and, in some cases, potential for high productivity. However, worldwide peatlands have been drained for agricultural or forestry purposes due to the high economic benefit of the fertile soil, which has resulted in vast soil subsidence and contributed to increased atmospheric carbon dioxide (CO_2) concentrations. This also includes many of the world's major river deltas which are sinking as a result of soil loss and compaction following drainage (Syvitski *et al.*, 2009). This type of land-use conversion has important consequences for global biogeochemical cycling and climate through changes to carbon dynamics and the energy exchange between the land and atmosphere.

The Sacramento–San Joaquin Delta (hereafter the Delta) in California is just one example of a delta peatland that has undergone rapid environmental change, with large changes to the carbon cycle, as a result of drainage and conversion to agriculture. Prior to drainage, the Delta existed a network of tidal marshes at the confluence of the Sacramento and San Joaquin Rivers, covering an area of ~1400 km^2 (Drexler *et al.*, 2009a). These extremely productive ecosystems with low rates of decomposition accumulated up to 15 m of peat as the marsh surface kept pace with gradual sea-level rise over about 7000 years. Wide-scale drainage of the Delta for agriculture near the end of the nineteenth century converted the most extensive stretch of wetlands on the Pacific coast into a network of islands with some of the most productive farmland in the state. However, agricultural cultivation since then has resulted in extreme rates of soil subsidence due to peat compaction and oxidation, and today the land surface of Delta islands now lies on average 5 to 8 m below sea level (Drexler *et al.*, 2009b). Islands in the Delta, better described as saucers or bowls, maintain an artificially low water table through an extensive and fragile levee network and continual pumping (Mount & Twiss, 2005). However, as the land continues to sink, the risk of levee failure and ensuing flooding increases. Levee failure would cause saltwater intrusion into the Delta, threatening an important supply of water for over 22 million people (Miller *et al.*, 2000).

Land managers and other Delta stakeholders recognize that the continued practice of drained agriculture in this region is unsustainable and consequently there is strong interest in converting drained lands back to flooded conditions, including restored wetlands or flooded rice paddies. The flooded nature of these environments can decrease the rate of peat oxidation by physically impeding the transport of oxygen required by most microbial metabolism into the soil. As such, this slows rates of decomposition and can help reverse net carbon loss. Although converting lands back to flooded conditions helps reduce the loss of soil carbon as CO_2, it also creates ideal conditions for the production of CH_4, a much more potent greenhouse gas (GHG) than CO_2. Therefore, even relatively low rates of CH_4 emissions can offset the benefit of CO_2 sequestration in terms of the net GHG benefit.

The second chapter of this dissertation evaluated the impact of drained to flooded land-use change on CO_2 and CH_4 fluxes in the Delta. The objective of this research was to analyze the net carbon and GHG trade-offs of land-use conversion from drained agricultural peatlands (a pasture and a corn field) to flooded land-use types (an irrigated rice paddy and two restored wetlands). To achieve this objective, I studied one year of simultaneous and direct ecosystem-scale measurements of CO_2 and CH_4 fluxes collected with eddy covariance flux towers at these five sites. Through analysis of annual CO_2 and CH_4 budgets, I determined that ecosystem respiration consistently exceeded CO_2 uptake by photosynthesis at the drained sites. This carbon imbalance made these sites large sources of CO_2 to the atmosphere. Moderate CH_4 emissions were observed at the pasture due to the presence of cattle and flooded depressions in the field, however, when factoring the carbon removed from the field through harvest, the corn site was the largest carbon and GHG source. Flooding resulted in lower rates of ecosystem respiration at the rice paddy that were roughly equal to rice photosynthesis, making the rice paddy near CO_2 neutral. When considering harvest and CH_4 emissions at this site, the paddy acted as both a carbon and GHG source, although carbon loss and GHG emissions were lower than at the drained peatland sites. The wetland sites offered the greatest potential for reversing subsidence; CO_2 uptake by the high photosynthetic capacity of the wetland plants exceeded ecosystem respiration, resulting in large carbon sequestration. However, the wetlands were also the largest sources of CH_4. Nonetheless, even when factoring the greater global warming potential of CH_4, the wetlands were still more beneficial from a GHG perspective than the drained sites. This work concluded that converting drained agricultural peat soils to flooded land-use types can help reduce or reverse soil subsidence and reduce GHG emissions.

Although the second chapter provided a baseline analysis of net CO_2 and CH_4 budgets across key ecosystems in the Delta, it represented only a single snapshot in time. However, natural and managed ecosystems can exhibit large year-to-year

variability in carbon and GHG exchange, highlighting the need to consider interannual variability in CO_2 and CH_4 fluxes. In the third chapter, I focused on temporal variability in CO_2 and CH_4 exchange and analyzed 6.5 years of flux measurements from the irrigated rice paddy, which represents the longest and most comprehensive data set of eddy covariance measurements of wetland rice GHG fluxes in the world. The goals of this work were to investigate the factors affecting CH_4 fluxes across diel to interannual timescales and quantify interannual variability in CO_2 and CH_4 budgets. I used a combination of linear regression models, neural network modeling, and wavelet analysis to investigate the biophysical controls on CH_4 fluxes from the rice paddy. Wavelet analysis suggested that photosynthesis induced the diel pattern in CH_4 flux, but soil temperature modulated its amplitude. At the seasonal scale, neural network models explained considerably more of the variance in daily average CH_4 flux than linear models due to their competence in modeling nonlinear relationships, and emphasized the importance of photosynthesis and water levels in regulating daily average CH_4 fluxes. However, at the interannual scale, much of the variability in annual and growing season CH_4 sums was driven by soil temperature. Higher soil temperatures also increased the annual and growing season ratio of CH_4 flux to ecosystem productivity, an observation that may help improve global estimates of CH_4 flux from rice agriculture. Finally, soil temperature strongly influenced ecosystem respiration, resulting in large year-to-year variability in the net carbon budget at the paddy. This study therefore stresses the need for long-term measurements particularly under changing climatic conditions.

While eddy flux measurements can provide important insights into the factors controlling CO_2 exchange within and among sites, bridging to larger spatial scales can be achieved by combining CO_2 flux and remotely sensed data. Furthermore, with a growing interest in carbon market-funded wetland conservation and restoration, this approach can also be used to develop low cost remote sensing-based models of carbon exchange in these environments suitable for carbon market and Cap-and-Trade systems. In the fourth chapter of this dissertation, I evaluated the potential of using digital cameras, a form of near-surface remote sensing, as simple and cost-effective means of estimating photosynthesis at the restored Delta wetlands, and assessed the suitability of using Landsat data to model productivity in these environments for regional upscaling. I showed the potential of using camera-based greenness indices and eddy covariance data to develop and parameterize a light use efficiency (LUE) model to predict daily photosynthesis. The LUE model combining camera and meteorological data was able to explain most of the variation in daily photosynthesis at the restored wetlands and accurately predict annual and multiyear CO_2 uptake. However, model performance decreased somewhat with increasing site complexity, highlighting the need to explicitly consider spatial heterogeneity in LUE models. I also tested a similar

model using Landsat-based indices and found that although model performance was high at the homogeneous site dominated by emergent vegetation, model data-model agreement was lower at the site comprised of a mixture of open water and vegetation, indicating limitations of Landsat data. Nonetheless, this research showed that digital camera and Landsat imagery can be used to model photosynthesis in restored wetlands, providing inexpensive means of monitoring carbon cycling in these environments that can be used in carbon markets, thereby advancing the opportunity to counteract the widespread degradation of wetlands worldwide.

Using a multi-site multi-year approach, this dissertation works toward a better understanding of the impacts of drained to flooded land-use change on CH_4 and CO_2 exchange, improving our understanding of the factors controlling these fluxes across a range of temporal scales, and developing cost-effective and accurate ways of estimating carbon cycling in restored wetlands by combining flux measurements with near-surface and satellite remote sensing. With a growing interest in wetland restoration for carbon sequestration and GHG mitigation, the results of this dissertation have important management implications for land managers and policy makers both in the California Delta and elsewhere. This work also highlights important challenges and new tools for future studies measuring CO_2 and CH_4 exchange from complex landscapes where fluxes can vary in both space and time. This dissertation provides new insights into CO_2 and CH_4 fluxes from drained and restored peatland ecosystems, bridging understanding between biometeorology, biogeochemistry and climate policy.

Chapter 2: Agricultural peatland restoration: effects of land-use change on greenhouse gas (CO_2 and CH_4) fluxes in the Sacramento-San Joaquin Delta

2.1. Abstract

Agricultural drainage of organic soils has resulted in vast soil subsidence and contributed to increased atmospheric carbon dioxide (CO_2) concentrations. The Sacramento-San Joaquin Delta in California was drained over a century ago for agriculture and human settlement and has since experienced subsidence rates that are among the highest in the world. It is recognized that drained agriculture in the Delta is unsustainable in the long-term, and to help reverse subsidence and capture carbon (C) there is an interest in restoring drained agricultural land-use types to flooded conditions. However, flooding may increase methane (CH_4) emissions. We conducted a full year of simultaneous eddy covariance measurements at two conventional drained agricultural peatlands (a pasture and a corn field) and three flooded land-use types (a rice paddy and two restored wetlands) to assess the impact of drained to flooded land-use change on CO_2 and CH_4 fluxes in the Delta.

We found that the drained sites were net C and greenhouse gas (GHG) sources, releasing up to 326 g C-CO_2 m^{-2} yr^{-1} as CO_2 and 11.4 g C-CH_4 m^{-2} yr^{-1} as CH_4. Conversely, the restored wetlands were net sinks of atmospheric CO_2, sequestering up to 506 g C-CO_2 m^{-2} yr^{-1}. However, they were large sources of CH_4, with emissions ranging from 43.8 to 65.2 g C-CH_4 m^{-2} yr^{-1}. In terms of the full GHG budget, the restored wetlands could be either GHG sources or sinks. The rice paddy was near CO_2 neutral, however, when considering harvest and CH_4 emissions, it acted as both a C and GHG source. Annual photosynthesis was similar between sites, but flooding at the restored sites inhibited ecosystem respiration, making them net CO_2 sinks. This study suggests that converting drained agricultural peat soils to flooded land-use types can help reduce or reverse soil subsidence and reduce GHG emissions.

2.2. Introduction

The worldwide drainage of peatlands for agricultural or forestry purposes has resulted in vast soil subsidence, due to changes in physical conditions and enhanced rates of microbial decomposition (Hirano et al., 2012, Rojstaczer & Deverel, 1993, Stephens et al., 1984, Syvitski et al., 2009). In addition to degrading peat soils and associated habitat, these ecosystems have become globally significant sources of carbon dioxide (CO_2) to the atmosphere, as large amounts of carbon (C) are lost to the

atmosphere through oxidation (Armentano, 1980, Couwenberg et al., 2010, Drösler et al., 2008). Nonetheless, this practice is widespread due to the high economic benefit of the fertile soil (Kramer & Shabman, 1993).

The Sacramento-San Joaquin Delta (referred to hereafter as the Delta) in California was drained over a century ago for agriculture and human settlement and has since experienced subsidence rates that are among the highest in the world (Rojstaczer & Deverel, 1995, Stephens et al., 1984). Prior to drainage, the Delta consisted of a network of tidal marshes at the confluence of the Sacramento and San Joaquin Rivers that covered an area of approximately 1,400 km^2 (Drexler *et al.*, 2009a, Shlemon & Begg, 1975). These highly productive ecosystems with low rates of decomposition accumulated up to 18 m of peat as the marsh surface kept pace with gradual sea-level rise over several thousand years (Atwater & Belknap, 1980, Shlemon & Begg, 1975). Since drainage, agricultural cultivation has caused high rates of peat soil oxidation and surface elevations have subsided to more than 8 m below sea level in some regions (Deverel & Leighton, 2010, Deverel & Rojstaczer, 1996, Drexler *et al.*, 2009b). Today the Delta exists as a network of islands that maintain an artificially low water table through an extensive levee network and continual pumping (Mount & Twiss, 2005). As the land continues to subside, the risk of levee failure and subsequent flooding also increases. This would cause saltwater intrusion into the Delta, threatening a critical supply of water for California, as the Delta is a transfer point for agricultural and municipal water for more than 22 million people (Miller et al., 2000).

Slowing subsidence and converting drained Delta ecosystems from net C sources to C sinks is key to the long-term sustainability of the Delta and protection of California's water transfer infrastructure. Restoring degraded agriculture systems to flooded land-use types such as rice paddies and restored wetlands has been recognized as a potential management option for the Delta that can prevent further peat oxidation (Hatala *et al.*, 2012b, Miller *et al.*, 2000, Miller *et al.*, 2008). Furthermore, it creates additional benefits such as providing habitat for wildlife. The flooded status of these environments decreases the rate of peat oxidation by physically impeding the transport of oxygen required for most microbial metabolisms into the soil. Consequently, rates of ecosystem respiration (ER) are lower in these flooded environments than in traditional agricultural systems, and the reduction in CO_2 production can help reverse net C loss (Eugster *et al.*, 2010, Hatala *et al.*, 2012b, Hendriks *et al.*, 2007, Herbst *et al.*, 2013, Miller *et al.*, 2000). Earlier investigations in the Delta have confirmed this result through comparison of conventional drained agricultural crops and pastures, which were large C sources, with flooded agricultural systems (i.e. rice) (Deverel & Rojstaczer, 1996, Hatala *et al.*, 2012b). Wetlands are among the most effective terrestrial ecosystems at building soil organic matter and sequestering C (McLeod et al., 2011, Mitsch et al., 2013,

Rocha & Goulden, 2009). Consequently, wetland restoration has been broadly proposed as a way to mitigate fossil fuel emissions (Bernal & Mitsch, 2013, Maljanen et al., 2010, Poffenbarger et al., 2011, Zedler & Kercher, 2005). High C sequestration rates are expected from restored marshes in the Delta since the region has a long and warm growing season with abundant water and sunlight (Brinson et al., 1981, Miller & Fujii, 2010). Miller et al. (2008) investigated the subsidence reversal potential of two restored wetlands in the Delta and found that land-surface elevations increased by an average of 4 cm yr^{-1} in both wetlands over a nine year period.

However, managing the Delta for enhanced CO_2 sequestration is expected to alter the fluxes of other greenhouse gases (GHGs). While the conversion from drained to flooded land-use types will help stop the net emissions of CO_2 due to peat oxidation, flooding is expected to increase the emissions of methane (CH_4) (Hatala *et al.*, 2012b, Herbst *et al.*, 2013, Miller, 2011, Teh *et al.*, 2011), a GHG with a global warming potential (GWP) 25 times greater than CO_2 over a 100 year time scale (Forster *et al.*, 2007). Therefore, even relatively low rates of CH_4 emissions could offset the benefit of CO_2 sequestration in terms of the net GHG effect. This is often observed in natural wetlands, particularly in more northern wetlands (Blais et al., 2005, Bridgham et al., 2006, Whiting & Chanton, 2001), however, overall the CH_4 budgets of wetland ecosystems remain highly uncertain (Bridgham *et al.*, 2006). Despite a growing interest in peatland restoration for C sequestration (Drösler et al., 2008, Maljanen et al., 2010), few studies have measured integrated, near-continuous CO_2 and CH_4 fluxes from restored wetlands (e.g. Hendriks *et al.*, 2007, Herbst *et al.*, 2013, Miller, 2011, Reid *et al.*, 2013, Waddington & Day, 2007, Waddington *et al.*, 2010).

In this study, we measured year-round fluxes of CO_2 and CH_4 from three land-use types in the Delta spanning a range of inundated conditions using the eddy covariance (EC) technique to assess the short-term consequences and tradeoffs of the conversion from drained to flooded land-uses on C capture and GHG emissions. Our study investigated a total of five field sites (Figure 2.1) comprising three representative land-use classes: (1) *Conventional drained agricultural sites*: a drained and grazed degraded peatland pasture and a corn field, (2) *Agricultural wetland site*: a rice paddy, and (3) *Restored wetland sites*: a newly restored wetland (2010) and a long-term restored wetland (1997). The first goal of this study was to compare the annual C balance of the three different land-use types. We hypothesized that the conventional drained agricultural sites would be large net sources of C while the rice paddy and restored wetlands would be net C sinks and thus viable land-use types for stopping or reversing soil subsidence in the Delta. Our second objective was to quantify the impacts of land-use conversion from drained to flooded ecosystems on CH_4 fluxes due the greater GWP of CH_4 relative to CO_2. This has implications for the overall GHG budgets of these sites

and is important for GHG accounting protocols and verification. We hypothesized the higher CH_4 emissions from the flooded sites could result in these ecosystems being net GHG sources despite their potential for C sequestration.

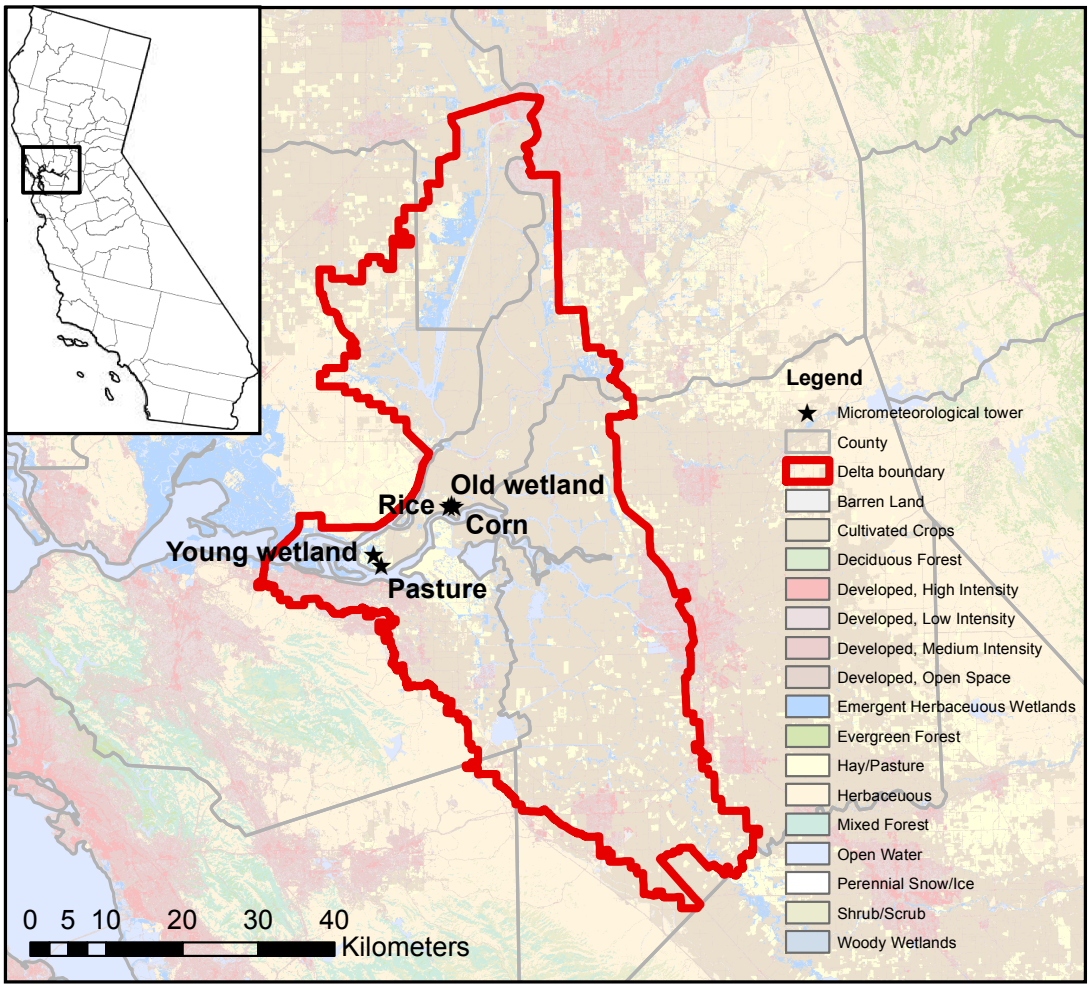

Source: National Land Cover Database 2001; UTM Zone 10, NAD 1983

Figure 2.1. Location of the five Delta sites. All field sites are located in the Sacramento-San Joaquin Delta, inland of San Francisco Bay. Since these sites are all within ~16 km of each other, they share the same basic meteorology, enabling a direct comparison of differences in the carbon and greenhouse gas budgets between sites. Pasture and corn together cover over 60% of the primary Delta, while rice and wetlands each currently cover less than 1% of the Delta.

2.3. Materials and methods

2.3.1. Study sites

The locations and overall characteristics of the five sites in this study are described in Table 2.1. All sites are located in the Sacramento- San Joaquin Delta of California, which is roughly 100 km inland from the Pacific Ocean (Figure 2.1). The region experiences a Mediterranean climate, with hot, dry summers and cool, wet winters. The growing season typically extends from February to November. The 30-year mean air temperature (1981-2010) recorded at a nearby climate station (Antioch, CA) is 16.4 °C and mean annual precipitation is 335 mm.

i) Conventional drained agricultural sites: The two business-as-usual land-use types are a grazed degraded peatland pasture on Sherman Island (Pasture) and a cornfield on Twitchell Island (Corn). Flux measurements at the Pasture began in April 2007. Two invasive plants make up the dominant cover types in the pasture: from December-April the canopy is dominated by mouse barley (*Hordeum murinum* L.), a long-naturalized C_3 grass in this region, and from April-October the canopy is dominated by pepperweed (*Lepidium latifolium* L.), a perennial forb. This site (~0.9 km × ~0.4 km), which has been a pasture for over 20 years, is fenced and grazed year-round by ~100 cattle. The cattle tend to congregate in the far end of the field opposite the flux tower during the day in the summer months, however, they commonly pass by the tower in the evening and during the winter months. Their presence in the flux footprint notably impacts CH_4 fluxes and to a much lesser extent CO_2 fluxes (Baldocchi *et al.*, 2012, Detto *et al.*, 2010). The site is located on degraded peat soil, where the upper 0.6 m of soil is silt loam that overlays a deep peat layer (Hatala *et al.*, 2012b). The water table is largely maintained below the soil surface throughout the year by continual pumping. While the drained portion of the Pasture is a small CH_4 source (Baldocchi *et al.*, 2012), strong sources of CH_4 exist from cattle, flooded depressions in the field and drainage ditches (Baldocchi *et al.*, 2012, Teh *et al.*, 2011). The typical daytime flux footprint is confined to the well-drained portions of the field, but the elongated nighttime flux footprint crosses drainage ditches and wetter portions of the pasture that are hot-spots for CH_4 production (Baldocchi *et al.*, 2012, Detto *et al.*, 2010).

EC measurements at the cornfield were made from May 2012 to May 2013. The site (~1 km × ~1.2 km) is also on degraded peat soil. The water table is kept below the crop-rooting zone by an actively managed drainage network. During this study, the field was planted May 20 – 21, 2012 and was harvested November 1 – 8, 2012. The field remained fallow during winter. The variety of corn planted was ES-7477 hybrid corn commercialized by Eureka seeds, and the field was fertilized once at seeding with 118

Table 2.1. Site characteristics. These sites capture a range of hydrologic conditions within the Delta: the conventional drained agricultural sites are drained year-round, the agricultural wetland is flooded for over half the year but is drained for field preparation and planting, herbicide and fertilizer application and harvest, and the restored wetlands are permanently flooded.

	Conventional drained agricultural sites		*Agriculture wetland site*	*Restored wetland sites*	
	Pasture	Corn	Rice	Young wetland	Old wetland
Location	38.0366°N, 121.7540°W	38.1047°N, 121.6433°W	38.10875°N, 121.6530°W	38.0498°N, 121.7650°W	38.1074°N, 121.6469°W
Elevation (m)	-7	-5	-5	-3	-9
Measurement period considered in this study	1 March 1 2012-1 March 2013	9 May 2012-9 May 2013[b]	1 March 2012-1 March 2013	1 March 2012-1 March 2013	1 August 2012-1 August 2013
Average annual air temperature[a] (°C)	14.9	15.3	14.5	15.0	15.6
Average annual soil temperature[a] (°C)	16.0	16.4	15.8	15.8	12.5
Average peak growing season soil temperature (°C)[c]	22.2	21.9	20.3	19.8	16.6
Annual precipitation[a] (mm)	263	290	390[d]	390[d]	278[d]
Total incoming radiation (MJ m^{-2} yr^{-1})	7001	7140	7050	7050	7137
Mean (min, max) peak growing season water table depth[c] (cm)	-65 (-92, -37)	-82 (-86, -76)	9 (-30, +17)	+107 (+102, +109)	+26 (+6, +32)
Peak PAI	2.2	3.0	4.1	N/A	N/A
Peak aboveground biomass (g DM m^{-2})	N/A	2201	2050	2303[e]	1357[e]
Typical vegetation	*Hordeum murinum* L. *Lepidium latifolium* L.	*Zea mays*	*Oryza sativa*	*Schoenoplectus acutus* *Typha* spp.	*Schoenoplectus acutus* *Typha* spp.

[a]Corresponds to the measurement period considered in this study.

[b]Measurements only began on May 22nd, therefore to complete a full year of measurements, fluxes from May 9th – May 22nd were extrapolated based on the first 13 days of measurement and meteorological variables were either extrapolated

or estimated based on measurements from other sites.
[c]Corresponds to August & September 2012.
[d]Values estimated from a nearby California Irrigation Management Information System (CIMIS) station on Twitchell Island since measurements weren't available at these sites.
[e]From Byrd *et al.* (2014).

kg N ha^{-1} in the form of urea ammonium nitration solution (UAN 32%).

ii) Agricultural wetland site: The rice paddy on Twitchell Island (Rice) represents the agricultural wetland land-use class. Micrometeorological measurements at this site began in April 2009 upon conversion from traditional corn and alfalfa agriculture. The rice site is a pilot project managed by the California Department of Water Resources (CADWR) to assess the potential of growing rice in the Delta. Prior to 1990, rice was not farmed in the Delta due to cool nighttime growing season temperatures. However, with the development of new varietals capable of withstanding these conditions, currently there are ~20 km^2 of rice farmed in the Delta. The field where this site is located is ~0.55 km × 0.7 km. The field was flooded for more than half the year, however, it was drained several times during the year for cultivation and planting, fertilizer and herbicide application, and harvest. Due to late precipitation in winter 2012 the field was plowed, harrowed, and leveled for planting in early May, which is about a month later than previous years (Hatala *et al.*, 2012b). The rice variety M104, a cold weather cultivar, was planted on May 17, 2012. The field was fertilized with 11-52-0 mono-ammonium phosphate fertilizer at a rate of 68 kg $acre^{-1}$ during planting and then again with 30-0-20 ammonium sulfate fertilizer on June 16, 2012 at a rate of 68 kg $acre^{-1}$. The rice field was first treated with herbicide in mid-June (3.65 g $acre^{-1}$ Regiment, 324 g $acre^{-1}$ Prowl, 32 g $acre^{-1}$ SYL-TAC, 324 g $acre^{-1}$ UN-32, and 4.1 g $acre^{-1}$ Sandea), and then again with Propanil Flowable Herbicide (i.e. SuperWham!) in mid-July to control a weed infestation. The crop was harvested November 13-16, 2012. Following harvest of the rice grains, the remaining plant residue was left on top of the soil, and the field was re-flooded for the following winter to provide habitat for migrating birds.

iii) Restored wetland sites: CO_2 and CH_4 fluxes were also measured at a long-term restored wetland (Old wetland) and newly restored wetland (Young wetland). In 1997, the Old wetland (0.028 km^2) was constructed in the central part of Twitchell Island (Miller, 2011, Miller *et al.*, 2008). We began GHG measurements at this site in July 2012. The wetland was built on a former agricultural field by excavating surface soil, which was used to construct berms around the area excavated for the wetland. *Schoenoplectus acutus* (tule) shoots and rhizomes were planted in the eastern portion of the site prior to flooding, and cattails (*Typha latifolia, T. domingensis*, and *T. angustifolia*) from adjacent waterways were allowed to disperse naturally to the pond via windborne seeds. In October 1997, the sites was flooded to a constant water depth of ~25 cm. Following flooding, the site was rapidly colonized by cattails, and presently approximately 100% of the pond is filled with emergent macrophytes. Several floating aquatic plants (*Ludwigia peploides* and *Lemna* sp.) and submerged aquatics are also present in the ponds.

A considerably larger (1.21 km^2) restored wetland was constructed in 2010 on a drained peatland pasture on Sherman Island (Young wetland), with flux measurements initiated shortly after (October, 2010). During wetland construction, a heterogeneous bathymetry was excavated to preserve existing wetland vegetation and generate regions of shallow water (a few centimeters) and adjoining areas of deeper water (up to 2 m). Consequently, this site is spatially heterogeneous, consisting of a mix of open water and vegetation patches, where the abundance and spatial aggregation of the vegetation strongly affect CH_4 fluxes at this site (Matthes *et al.*, 2014). Today, this mixed configuration presents a contrast to the Old wetland, where the site and flux footprint is much more homogenous and dominated entirely by emergent vegetation. Both wetlands support both *Schoenoplectus acutus* and *Typha* spp., but differ in relative dominance between them.

2.3.2. Eddy covariance measurements

We employed the EC method to measure 30-min fluxes of CO_2 (NEE; μmol m^{-2} s^{-1}), CH_4 (nmol m^{-2} s^{-1}), latent heat (LE; W m^{-2}), and sensible heat (H; W m^{-2}). A similar set of EC instrumentation was deployed at each site (Table 2.1). At each tower, a sonic anemometer measured high frequency wind velocity in three coordinates (u, v, w; m s^{-1}) and temperature (T_{sonic}) (Table 2.1). Fluctuations in CO_2 and H_2O molar density (ρ_{CO2} and ρ_{H2O}) were measured with open-path infrared gas analyzers (Table 2.1). Open-path CH_4 sensors, based on wavelength modulation spectroscopy, were used to measure fluctuations in CH_4 molar density (ρ_{CH4}), with the exception of the Pasture, where CH_4 mixing ratio (χ_{CH4}) was measured with a closed-path tunable diode laser fast methane analyzer (FMA). AC power was available at the Pasture, therefore we used a scroll pump (BOC ESDP 30A, Edwards, Tewksbury, MA, USA) which requires 770 W of power and provides a flow rate of ~ 40 L min^{-1} at the FMA cell pressure (19 kPa). Extensive field testing was conducted to evaluate the performance of the FMA sensor at this site (Detto et al., 2010) and comparisons between the magnitude of 30-min fluxes showed good agreement between open-path and closed-path flux systems (Detto *et al.*, 2011). CH_4 fluxes were not measured at the Corn as CH_4 emissions were assumed to be negligible from this site since the water table was well below the soil surface throughout the study. We used either digital dataloggers systems (LI-7550A; LI-COR Biogeosciences, Lincoln NE, USA) or Campbell CR1000 dataloggers (Campbell Scientific, Logan, UT, USA) to record raw turbulence data at 10Hz.

Fluxes were calculated using the 30-min covariance of vertical wind speed (w) and the appropriate scalar after applying a series of standard corrections using in-house software (Detto *et al.*, 2010, Hatala *et al.*, 2012b). First, this software removed artificial spikes in the 10 Hz data and diagnostic instrument values that corresponded with poor

Table 2.2. Description of the eddy covariance flux measurement systems and analysis.

	Conventional drained agricultural sites		*Agriculture wetland site*	*Restored wetland sites*	
	Pasture	Corn	Rice	Young wetland	Old wetland
Eddy covariance height (m)	3.2	5.15	3.25	3.7	4.64
Sonic anemometer,	WMP 1352	WMP 1352	WMP 1352	WM 1590	WM 1590
CO_2 analyzer	LI-7500	LI-7500	LI-7500	LI-7500	LI-7500
and CH_4 analyzer	FMA	N/A	LI-7700	LI-7700	LI-7700
Threshold friction velocity (m s^{-1})	0.15–0.20	0.15	0.15	0.15–0.185	0.20
Filtered wind directions	N/A	180–200° & 355–10°	0–190°	N/A	290–240°
Percentage of observations rejected[a]	26–31%	35–42%	48–52%	24–38%	58–59%
Energy balance closure	0.90	0.76	0.97	0.70	0.84

[a]The % of observation rejected varies depending on which flux measurement is considered.

readings, which were primarily associated with precipitation or fog events. Next, coordinate rotations were used to align the streamlines with the surface of each site resulting in zero mean w and v within each 30-min block. Where open-path sensors were used, the Webb-Pearman-Leuning correction was applied to account for the effect of air density fluctuations (Detto & Katul, 2007, Webb et al., 1980), and the relevant additional spectroscopic corrections for ρ_{CH4} fluctuations measurements with the LI-7700 instrumentation were also applied (McDermitt et al., 2011). For the closed-path sensor, CH_4 measurements were adjusted to eliminate air density variations due only to the effects of water vapor since it is assumed that high frequency temperature fluctuations were dampened when sampling through the tube (Detto et al., 2010, Detto & Katul, 2007). Fluctuations in T_{sonic} were calculated from fluctuations in the speed of sound following crosswind and humidity corrections (Kaimal & Gaynor, 1991, Schotanus et al., 1983). After calculating the fluxes, we filtered flux values with low friction velocity (u^*) to constrain our analysis to turbulent conditions. Friction velocity thresholds (Table 2.1), which varied seasonally, were identified as values above which nighttime NEE no longer varied with increasing u^*. Fluxes were further filtered for spikes in 30-min mean densities, variances and covariances with thresholds varying seasonally and between sites. Lastly, fluxes from wind directions outside the footprint of each site were filtered from the data set and omitted from this analysis (Table 2.1). The percentage of 30-min fluxes excluded from this analysis is given in Table 2.1. Additionally, for the closed-path CH_4 measurements, we used a procedure similar to the one outlined in Aubinet et al. (1999) and Humphreys (2004) in order to correct for the high frequency flux losses resulting from sensor separation and attenuation of fluctuations of χ_{CH4} down the sampling tube. No high frequency corrections were applied to fluxes measured using open-path sensors since flux losses amounted to less than 5%, which is well within the accuracy of an individual flux measurement (Aubinet et al., 1999).

Energy balance closure at these sites, defined as the energy balance ratio (Wilson et al., 2002), ranged between 0.72 and 1.24 (Table 2.1). These values fall within the range generally observed at sites within the FLUXNET network (Stoy et al., 2013, Wilson et al., 2002). At all sites we accounted for radiant energy absorbed in photosynthesis as in Leuning et al. (2012), and we approximated heat storage in the water column at the Rice and Old wetland as in Drexler et al. (2004) since water depth was relatively uniform across these sites. At the Young wetland, an EB closure greater than 100% is likely related to the difficulty in adequately estimating net radiation (R_{net}) and storage terms at this site where the distribution of water and vegetation is spatially heterogeneous.

2.3.3. Gap-filling, NEE partitioning and annual budget computation

The artificial neural network (ANN) technique was used to gap-fill half-hourly fluxes with meteorological variables (Moffat et al., 2007, Papale et al., 2006). The ANN routine was optimized for both representativeness and generalizability. To avoid the ANN being biased towards environmental conditions that typically have better data coverage such as summertime and daytime measurements, the explanatory data were divided into natural data clusters using a k-means clustering algorithm (MATLAB, 2014). Data used to train, test, and validate the ANN were proportionately sampled from these clusters. For generalizability, the simplest ANN architecture with good performance (< 5% gain in model accuracy for additional increases in architecture complexity) was chosen for 20 extractions of the training, test, and validation data. Within each extraction, each tested ANN architecture was re-initialized 10 times, and the initialization with the lowest root-mean-square-error was selected to avoid local minima. When the optimum ANN architecture for each extraction was determined, the resultant prediction was saved. The median of the 20 predictions was used to fill each gap and the spread of the predictions was used to provide a measure of uncertainty resulting for the ANN gap-filling procedure. The only variable that was not gap-filled was CH_4 flux at the Pasture, as extra precaution is needed to interpret eddy flux CH_4 measurements in intensively grazed pastures (Baldocchi et al., 2012). CH_4 fluxes at this site were strongly influenced by the combined effects of CH_4 emissions from cattle, and by the collapsed nocturnal boundary layer and elongation of the flux footprint over CH_4 hot spots (Baldocchi et al., 2012). Rather than integrating all CH_4 flux measurements we used the method described in Baldocchi et al. (2012) to estimate conditional averages, which we used to bound the annual CH_4 budgets. This resulted in a lower bound that is representative of CH_4 emitted from the drained portion of the pasture with less influence from cows, and an upper bound that is representative of CH_4 emissions from the drained and wet portions of the field and includes CH_4 emitted by cows.

The EC method measures the net exchange of CO_2 between the land surface and the atmosphere, which represents the sum of ecosystem photosynthesis (gross ecosystem production; GEP) and ecosystem respiration (ER). NEE can be partitioned into GEP and ER by separately considering the day and night observations, as photosynthesis only occurs during daylight hours. Winds in the Delta are strong even during the night (Hatala *et al.*, 2012b), thereby minimizing the need to account for the uncertainties related to nighttime EC measurements due to atmospheric stratification and stability (Massman & Lee, 2002). Consequently, NEE was partitioned into GEP and ER using a method similar to Reichstein et al. (2005). Briefly, an Arrhenius-type model after Lloyd and Taylor (1994) is used to describe the temperature dependence of nighttime NEE (i.e. ER since GEP is assumed to be zero at night), and this model is then

extrapolated to daytime periods. GEP was then calculated as the difference between NEE and ER.

We computed annual budgets by integrating the gap-filled and partitioned fluxes over the course of a full year. The dates over which the annual sums were calculated are given in Table 2.1 as they are not the same for all sites due to differences in the timing of the deployment of the sites. The net C balance was estimated as the annual sum of NEE after accounting for the loss of C from the system via CH_4 emissions and harvest. As such, the C balance reflects the net ecosystem C balance as opposed to the C balance from an atmospheric perspective as measured by the EC method (Chapin *et al.*, 2006). The net GHG budget was derived from annual sums of CO_2 and CH_4, assuming that 1 g CH_4 is equivalent to 25 g CO_2 with respect to the greenhouse effect over a time horizon of 100 years, and we assumed that C removed from the sites through harvest would eventually be release to the atmosphere as CO_2. The GHG budgets did not account for secondary emissions at the sites such as emissions related to pumping water off the islands or from farming machinery due to the difficulties in constraining these values. To estimate the amount of uncertainty in the ANN gap-filling procedure for the annual budget of each scalar, we calculated the integrated annual budget using the full range of predictions used to fill each gap (i.e. based on the 20 extractions from the ANN), and calculated the 95% confidence interval from the distribution of the 20 annual budgets. In this study, fluxes towards the surface are negative and fluxes away from the surface are positive, therefore negative NEE represents net CO_2 uptake and positive NEE indicates a net CO_2 source.

2.3.4. Supporting measurements

Micrometeorological instrumentation was deployed at each site to accompany EC measurements. Air temperature (T_{air}) and relative humidity were measured with an aspirated and shielded thermistor and capacitance sensor (HMP45C or HMP60; Vaisala, Vantaa, Finland). Precipitation was measured at the Pasture and Corn with a tipping bucket rain gauge (TR-525I or TR-525M; Texas Electronics Inc., Dallas, TX, USA) and water table depth was measured using pressure transducers (CS450 or CS451; Campbell Scientific, Logan, UT, USA or PDCR 1830; GE Druck, Billerica, MA, USA) at all of the sites except the Pasture where measurements were made manually from a well during field visits. R_{net} was measured with a four-component net radiometer (CNR1; Kipp and Zonen, Delft, Netherlands or NR01; Hukseflux, Delft, Netherlands), except at the Rice and Young wetland where it was measured with a double-sided net radiometer (NR Lite; Kipp and Zonen, Delft, Netherlands). Quantum sensors were used to measure incoming and outgoing photosynthetically active radiation (PAR) (PAR-LITE or PQS 1; Kipp and Zonen, Delft, Netherlands). Ground heat flux at the Pasture, Corn and Rice

was measured as the average of three replicate ground heat flux plates (HFP01 or HFP01SC; Huskeflux Thermal Sensors, Delft, Netherlands) buried just below the soil surface at each of these sites. At all sites we measured soil temperature (T_s) at soil depths of -0.02, -0.04, -0.08, -0.16, and -0.32 m with copper constant thermocouples. We report the mean of three sample replicates at each depth. Similarly, water temperatures were measured just above the soil surface at the Rice, 0.02 and 0.04 m at the Young wetland, and 0.04, 0.8, and 0.16 m at the Old wetland. All supporting measurements were sampled every 10 s, and the 30 min average values were stored on CR10X, CR23X or CR1000 dataloggers (Campbell Scientific, Logan, UT, USA).

2.3.5. Vegetation sampling and monitoring

Plant area index (PAI) was measured every 1 to 2 weeks at the Pasture, Corn and Rice sites during the growing season using an LAI-2000 Plant Canopy Analyzer (LI-COR). Measurements were made every 10 m along a 100 m transect. At the Corn and Rice, destructive measurements of aboveground biomass were also made by clipping all vegetation within five randomly sampled 400 cm^2 plots. At all sites, canopy phenology was monitored using digital camera images. Digital cameras were mounted near the top of each flux tower to record images year-round. JPEG images with red, green, and blue channels were recorded every 30 minutes. An analysis of a pre-defined "region of interest" (ROI) in the foreground of each image was conducted using the PhenoCam GUI application available as a pre-compiled MATLAB© program (PhenocamGUI v1.1; http://phenocam.sr.unh.edu/webcam/tools/) to calculate a normalized green channel brightness (% Green) for the ROIs as in Richardson et al. (2007). The % Green index was selected to monitor canopy phenology since it reveals clear seasonal patterns that can be associated with canopy development and senescence and is a good descriptor of NDVI (Migliavacca et al., 2011, Richardson et al., 2007, Westergaard-Nielsen et al., 2013).

2.4. Results

2.4.1. Weather conditions, water table management, and phenology

As a result of the Delta's Mediterranean climate, trends in meteorological variables at the sites followed a strong seasonal cycle (Figure 2.2a,b). Mean annual T_{air} was similar across sites despite somewhat different measurement periods (Table 2.1), and values were just below the 30-year (1981-2010) mean of 16.4 °C from the Antioch Climate Station located 10 km from the Pasture site. Annual precipitation at the sites ranged from 263 to 390 mm (Table 2.1), with a mean of 322 mm across sites that is comparable to the 30-year average of 335 mm. Total incoming radiation ranged

between 7001 and 7140 MJ m^{-2} yr^{-1} with differences between sites attributable to differences in measurement periods. T_s at the flooded sites were lower than at the drained sites, particularly during the peak growing season ($T_{s,grow}$) when the rice and wetland canopies were closed (Table 2.1). T_s and $T_{s,grow}$ were lowest at the Old wetland which was due to the tall, dense, and closed canopy at this site.

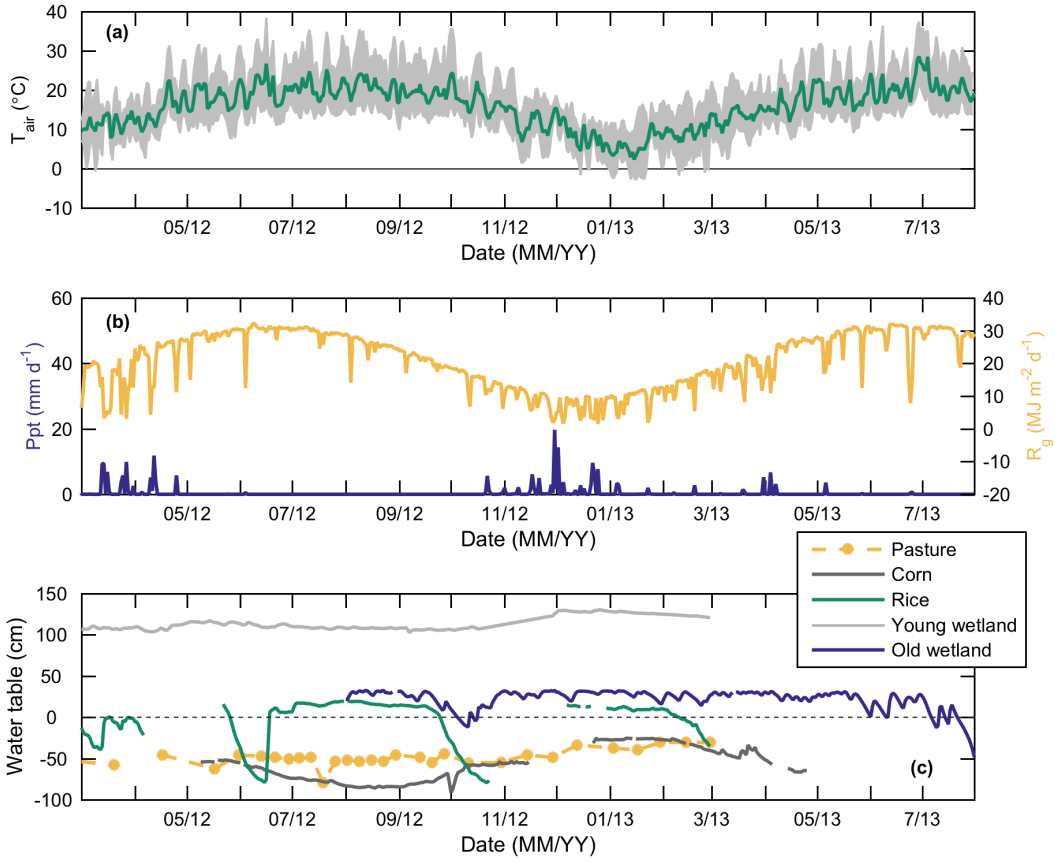

Figure 2.2. Typical pattern of the Mediterranean climate experienced at the sites, which is characterized by warm summers and cool winters (T_{air}) (a), and high incoming radiation (R_g) and low precipitation (Ppt) during the summer months and wet winters (b), and differences in water table management across sites (c). Measurements in (a) and (b) are only plotted for the peatland pasture since the values for the other sites are almost identical. The gray shaded area in (a) bounds the minimum and maximum daily air temperature and the dash-dot line in (c) reflects the fact that measurements were made manually during weekly or bi-weekly field visits.

Water table depth at the Pasture and Corn was maintained below the soil surface throughout the year by continual pumping (Figure 2.2c). Nonetheless, at the Pasture CH_4 is produced within flooded drainage ditches and in zones of saturation in the soil profile (Teh *et al.*, 2011). Water levels at the Rice were regulated to ~0.05 to 0.10 m above the soil surface for just over half the year, but the field was drained for about 80 days (March 1 to May 19, 2012) for cultivation and planting, approximately 20 days (May 28 to June 19, 2012) for fertilizer and herbicide application, about 50 days (September 30 to November 21, 2012) for harvest, and then again for another 20 days when the field was prepared for planting the following spring (February 10 to March 1, 2013) (Figure 2.2c). Water table depth at Young wetland was always well above the soil surface, and while the Old wetland was generally flooded to a depth of ~25 cm, accidental drops in the water table to or below the soil surface occurred periodically due to mechanical problems with the pumps.

As indicated from the % Green index derived from the digital camera images, the restored wetlands had a much longer growing season than the crops (Figure 2.3); the wetlands began greening up as early as mid-March and canopy senescence did not begin until November, whereas the growing season at the Rice and Corn sites only extended from June to October. The secondary peak in % Green at the Corn site in April was due to an invasion by grasses in spring. Peak % Green occurred in the summer months, with the exception of the Pasture where the index decreased during this time as the pepperweed's small white flowers masked the true "greenness" of the site (Sonnentag *et al.*, 2011).

2.4.2. Temporal variability of CO_2 fluxes and annual budgets

The general pattern of NEE at all sites followed a similar seasonal cycle (Figure 2.4) with most photosynthesis occurring in spring and summer when incoming solar radiation was greatest (Figure 2.5). The highest rate of net CO_2 uptake at the Pasture (~ -6 g C-CO_2 m^{-2} d^{-1}) occurred in late spring, corresponding with pepperweed growth. Despite the lack of precipitation and low soil moisture during this period, plant growth was possible since the pepperweed can tap the shallow water table. Low rates of photosynthesis during the rainy season were due to the presence of winter grasses at this site (Figure 2.5), which grow slowly over this time period due to low temperatures. Although peak GEP was greatest at the Corn due to canopy architecture and C_4-type photosynthesis, peak net CO_2 uptake (~ -5 g C-CO_2 m^{-2} d^{-1}) was lower than at the Pasture as a result of higher rates of ER (Figure 2.5). On an annual timescale, GEP at the Pasture was greater than at the Corn, since although the Corn had higher rates of growing season photosynthesis, year-round growth at the Pasture compensated for the lower canopy photosynthetic capacity. The highest rates of net CO_2 release at the drained

sites corresponded to the return of the winter rains, and reached values up to 10 g C-CO_2 m^{-2} d^{-1} during this period. The increase in ER following the start of the rainy season occurs as moisture at the surface reactivates microbial activity resulting in large pulses of CO_2 emissions following the first rains (Huxman *et al.*, 2004, Ma *et al.*, 2012). Although budgets of GEP at the Corn and Pasture were largely comparable to those at the flooded sites, the drained land-use types were net sources of CO_2 to the atmosphere on an annual basis due to high rates of ER (Table 2.3). The Pasture was the largest net source of CO_2 to the atmosphere, releasing 326 g C-CO_2 m^{-2} when integrated over a year, while the Corn was a slightly smaller net CO_2 source (276 g C-CO_2 m^{-2} yr^{-1}).

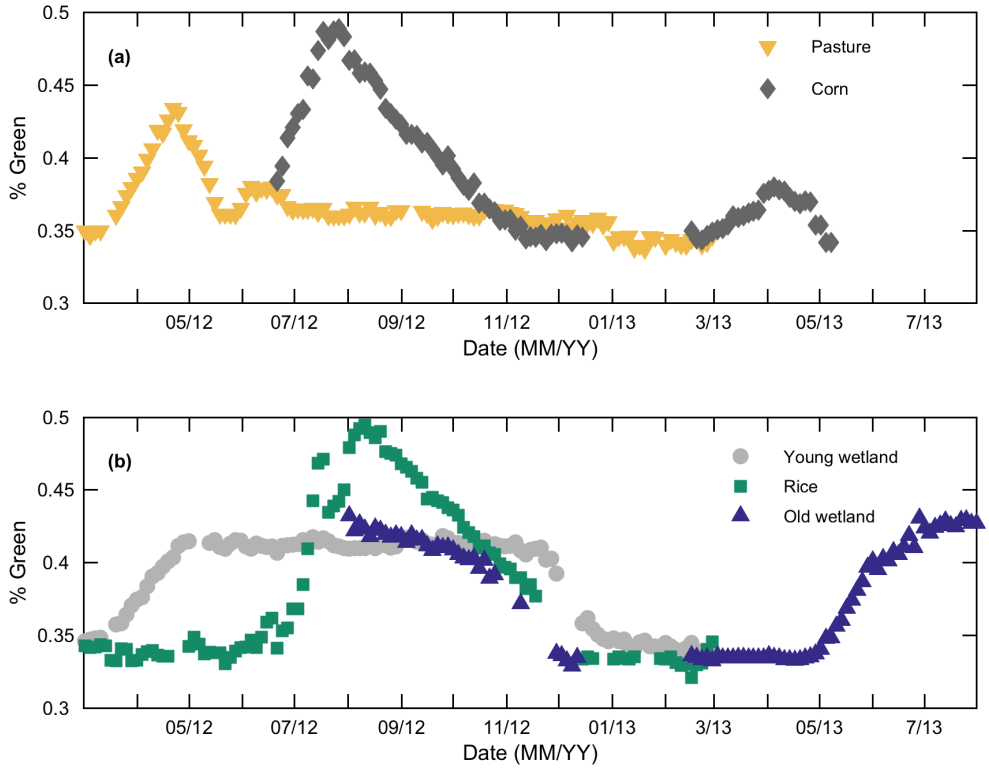

Figure 2.3. Time series of relative green brightness (% Green) for the conventional drained agricultural sites (a), and the agriculture and restored wetland sites (b). The pattern of % Green generally reaches a maximum at all sites during the summer months, except at the Pasture. This index does not appropriately reflect vegetation cover at this site as the greenness index decreases during this time despite high cover, as the pepperweed's small white flowers cause a decrease in site greenness. It is also clear from the seasonality of greenness index that while the crops are highly productive, their growing season is much shorter than that of the restored wetlands.

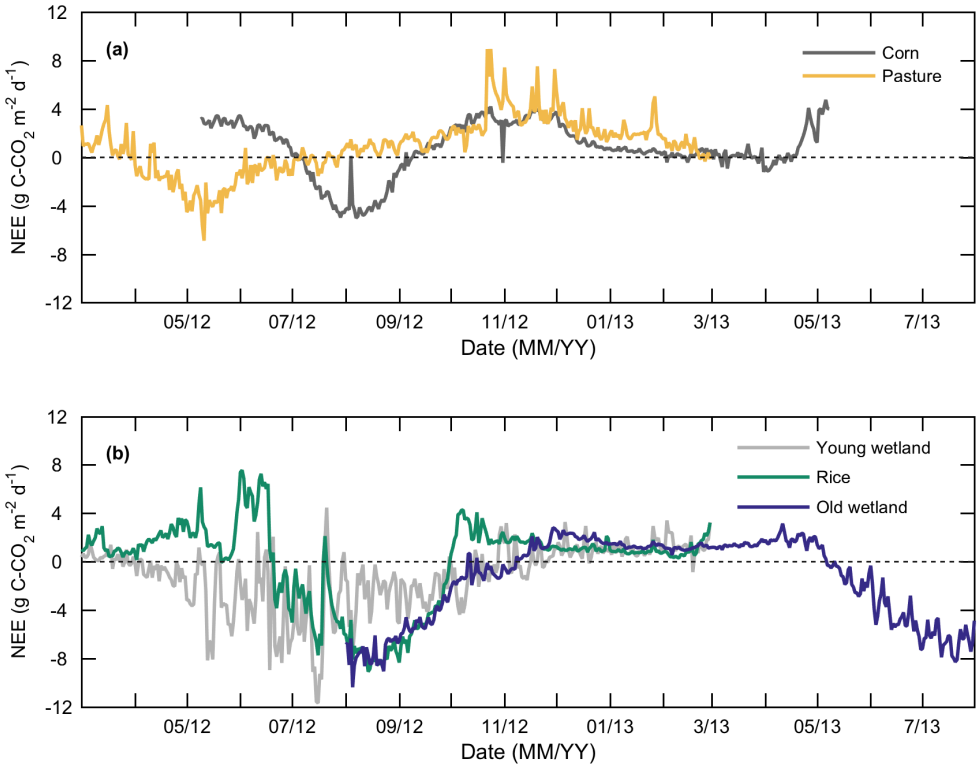

Figure 2.4. Seasonal variability of net ecosystem CO_2 exchange (NEE) for the conventional agricultural sites (a), and the agriculture and restored wetland sites (b). Net ecosystem exchange at all sites follows a similar seasonal cycle with peak carbon uptake in the spring and summer and net carbon emissions in the wintertime.

Growing season NEE at the flooded sites was quite similar with maximum net CO_2 uptake ranging between -10 and -12 g C-CO_2 m^{-2} d^{-1} (Figure 2.4). Wintertime NEE at these sites rarely exceeded 2 g C-CO_2 m^{-2} d^{-1} since flooding and cool temperatures inhibited ER (Figure 2.5). The periods of increased net CO_2 emissions at the Rice in spring and fall coincided with drainage events that resulted in large pulses of CO_2 to the atmosphere, which are attributable a combination of degassing due to reduced hydrostatic pressure and increased ER. On an annual basis the flooded sites ranged from being strong CO_2 sinks to near CO_2 neutral due largely to lower rates of ER (Table 2.3). Flooding resulted in comparably low annual sums of ER at the Rice and Old wetland, but despite similar rates of growing season photosynthesis (Figure 2.5), yearly GEP was considerably greater at the Old wetland due to its longer growing season (Figure 2.3). Consequently, the Old wetland was a much larger annual net CO_2 sink, sequestering 506 g C-CO_2 m^{-2} yr^{-1}, whereas the rice paddy only sequestered 34 g C-CO_2 m^{-2} yr^{-1}. While NEE budgets at the Old and Young wetlands differed somewhat (by 88 g C-CO_2 m^{-2}), the partitioning of NEE into ER and GEP differed notably between sites

(Table 2.3); although the Young wetland captured more CO_2 through photosynthesis than the Old wetland, this was offset much higher rates of ER, leading to only modest differences in CO_2 budgets between these sites. The higher productivity at the Young wetland compared to the Old wetland was likely due to the rapid expansion of new vegetation during the 2012 growing season as the Young wetland continues to fill in over time, and high rates of respiration may be attributable to higher GEP as ecosystem respiration scales with productivity (Janssens *et al.*, 2001).

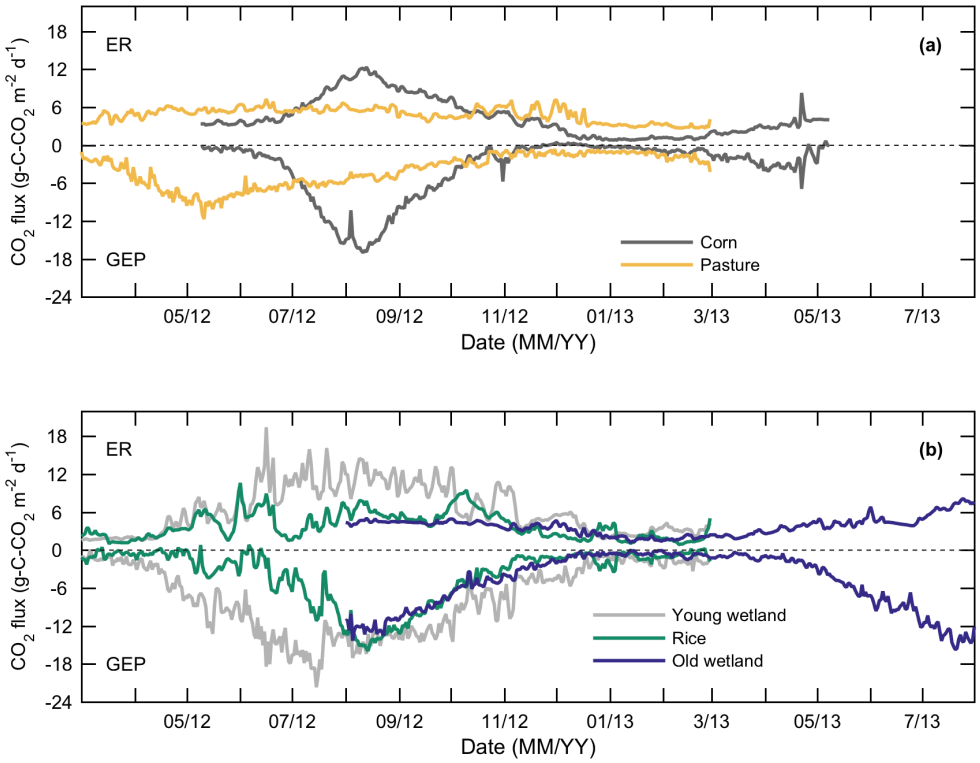

Figure 2.5. Daily partitioned net ecosystem exchange for the conventional agricultural sites (a), and the agriculture and restored wetland sites (b). Peak gross ecosystem production (GEP) occurs during the summer growing season. Flooding and cool temperatures inhibit wintertime ecosystem respiration (ER) at the rice paddy and restored wetlands, whereas autumn rains at the drained sites stimulate ER and drainage at the Rice for planting and harvest cause large pulses of CO_2 to the atmosphere.

Table 2.3. Annual sums of net and partitioned CO_2 fluxes, CH_4 fluxes, harvest, and total ecosystem carbon and greenhouse gas budgets. Error bounds reflect the 95% confidence interval for the gap-filling procedure. Note that there are no error bounds for ecosystem respiration since it is modeled based on the relationship between nighttime net CO_2 exchange and air temperature and is independent of the gap-filling procedure.

	NEE	GEP	ER	CH_4		Harvest	C budget	GHG budget
Site	g C-CO_2 m^{-2}	g C-CO_2 m^{-2}	g C-CO_2 m^{-2}	g C-CH_4 m^{-2}	g CO_2eq m^{-2}	g C m^{-2}	g C m^{-2}	g CO_2eq m^{-2}
Pasture[1]	326 ±68	-1450 ±68	1773	5.85 ±1.51 to 11.4 ±2.64	195 ±50 to 381 ±88	N/A	332 ±70 to 337 ±71	1390 ±300 to 1575 ±337
Corn	276 ±24	-1338 ±23	1614	N/A	N/A	293	569 ±24	2086 ±88
Rice	-34 ±58	-1433 ±58	1400	6.97 ±1.92	233 ±64	162	135 ±60	702 ±276
Young wetland	-418 ±32	-2754 ±32	2335	65.2 ±1.51	2176 ±50	N/A	-353 ±33	644 ±166
Old wetland	-506 ±53	-1874 ±53	1368	43.8 ±2.47	1464 ±83	N/A	-462 ±55	-390 ±276

[1]The upper and lower bounds for the CH_4 budget at the Pasture are representative of different field conditions. Additional details are given in the body of the paper.

2.4.3. *Seasonal course of CH_4 fluxes and annual budgets*

Large differences in both the magnitude and seasonal pattern of CH_4 fluxes were observed across sites (Figure 2.6). CH_4 emissions at the Pasture were a mixture of fluxes from lower CH_4-emitting upland soils, high CH_4-emitting drainage ditches, and CH_4 emitted by cattle (Baldocchi *et al.*, 2012, Teh *et al.*, 2011). CH_4 fluxes during the dry season generally ranged between 0 and 50 mg C-CH_4 m^{-2} d^{-1}. Greater CH_4 effluxes were observed during the rainy period, when daily CH_4 fluxes ranged between 10 and 330 mg C-CH_4 m^{-2} d^{-1}. We constrained the annual CH_4 budget at the Pasture to range between 5.85 and 11.4 g C-CH_4 m^{-2} yr^{-1}, with the lower end representative of the drained portion of the field with little influence from the cows and the upper end comprising both the drained and wet portions of the field and greater influence from the cattle.

The CH_4 fluxes at the Rice were comparable in magnitude to those at the Pasture, but followed a different seasonal pattern (Figure 2.6a); CH_4 emissions at the Rice largely tracked GEP (Figure 2.5), and large pulses of CH_4 to the atmosphere occurred during drainage of the field in late September 2012 and in mid-February 2013 (Figure 2.2c). The release of CH_4 upon drainage can be attributed to a combination of degassing due to reduced hydrostatic pressure and to decreased CH_4 oxidation due to the more rapid transport of CH_4 through the soil profile (Han *et al.*, 2005, Hatala *et al.*, 2012b). Once the field was well drained, CH_4 fluxes were quite low, rarely exceeding 20 mg C-CH_4 m^{-2} d^{-1}. Over the course of a year, the rice paddy released 6.97 g C-CH_4 m^{-2} to the atmosphere.

Growing season CH_4 emissions at the restored wetlands were an order of magnitude greater than those at the Rice or Pasture, with peak emissions of 590 mg C-CH_4 m^{-2} d^{-1} at the Young wetland and 390 mg C-CH_4 m^{-2} d^{-1} at the Old wetland. Again CH_4 emissions followed a seasonal pattern that largely paralleled GEP, with the exception of the pronounced peak in daily CH_4 flux at the Old wetland in early July 2013, which was the result of a sudden water table drawdown (Figure 2.2c). On a yearly basis, the Young wetland released the largest amount of CH_4 to the atmosphere (65.2 g C-CH_4 m^{-2}), while the Old wetland released somewhat less CH_4 (43.8 g C-CH_4 m^{-2}) (Table 2.3).

2.4.4. *Annual C and GHG budgets*

As expected from the high rates of subsidence on Delta islands, conventional agricultural sites were both large net C and GHG sources (Table 2.3). While the Pasture was the largest annual CO_2 source to the atmosphere (Table 2.3), if we account for the fact that 293 g C m^{-2} was removed from the cornfield through harvest, total C loss was greatest at the Corn site (569 g C m^{-2} yr^{-1}). The drained sites were large GHG sources, with emissions ranging between 1390 and 2086 g CO_2eq m^{-2} yr^{-1}, which is considerably

greater than GHG emissions from the flooded land-use types.

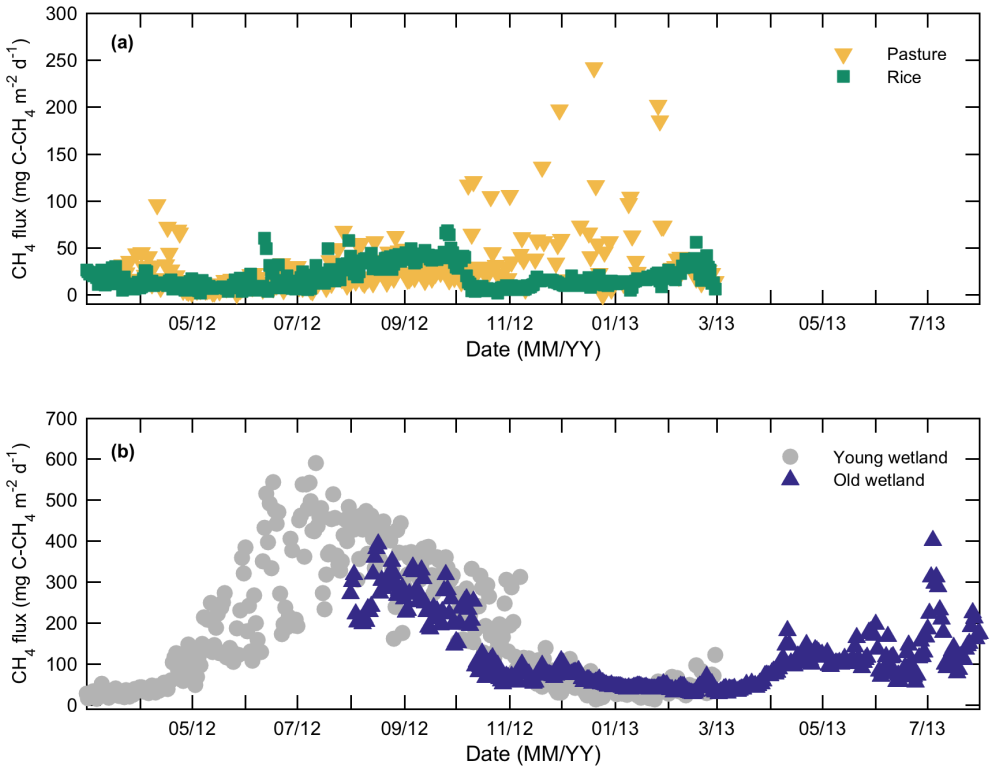

Figure 2.6. Seasonal course of daily integrated CH_4 flux for the drained and flooded agricultural sites (a) and restored wetland sites (b). CH_4 fluxes were generally low at the rice paddy and pasture sites, while fluxes at the restored wetlands were up to an order of magnitude greater (note the difference in the vertical axis in (a) and (b)). With the exception of the pasture, CH_4 emissions largely followed a pattern that was closely related to that of gross ecosystem production. CH_4 emissions were also strongly influenced by water table dynamics. Note that CH_4 fluxes at all sites were gap-filled with the exception of the Pasture, therefore integrated daily CH_4 emissions at this site were only estimated for days when there was a measured flux for at least half of the possible 48 half-hour intervals.

Although the Rice was a small atmospheric sink for CO_2 (Table 2.3), if we consider the amount of C removed from the field through harvest (162 g C m^{-2}) and CH_4 emissions, the rice paddy acted as both a net C and GHG source (135 g C m^{-2} yr^{-1} and 702 g CO_2eq m^{-2} yr^{-1}, respectively). The restored wetlands could be either a GHG source or sink depending on CH_4 emissions: while NEE at the wetlands was roughly comparable, higher CH_4 fluxes at the Young wetland relative to the Old wetland resulted in the former site being a net GHG source (Table 2.3). Regardless of the

differences in GHG flux totals, the restored wetlands were both strong C sinks, sequestering between 353 and 462 g C m^{-2} yr^{-1}.

2.5. Discussion

2.5.1. CO_2 fluxes

Due to high rates of soil subsidence, the practice of drained agriculture in the Delta is unsustainable in the long-term. Like other drained and degraded peatlands (e.g. Hirano *et al.*, 2012, Nieveen *et al.*, 2005, Veenendaal *et al.*, 2007), the Pasture was a large net source of CO_2 to the atmosphere (Table 2.3), as reported for previous years (Hatala *et al.*, 2012b). Corn is generally a C sink or C neutral, even when considering harvest (Bernacchi *et al.*, 2005, Hollinger *et al.*, 2005, Suyker *et al.*, 2004), however, high rates of peat oxidation resulted in the Corn being a large net CO_2 source.

The results of this study showed that converting drained Delta landscapes back to flooded conditions offers a promising intervention to halt C loss and associated subsidence. Rice agriculture is one possible flooded land-use type that can slow subsidence by limiting ER, as the rice paddy was an atmospheric sink for CO_2 (Table 2.3), in agreement with an earlier study at this site (Hatala *et al.*, 2012b). Growing season net CO_2 uptake at the Rice was on the lower range of values reported for other studies (e.g. Alberto *et al.*, 2012, Bhattacharyya *et al.*, 2014, McMillan *et al.*, 2007, Miyata *et al.*, 2005, Saito *et al.*, 2005), which was largely due to higher rates of ER at our site with high soil organic C content as GEP at the Rice typically exceeded values measured elsewhere.

Wetland restoration is the most promising management option for reversing subsidence in the Delta, as the restored marshes were the largest C sinks (Table 2.3). We found that NEE budgets at the Young and Old wetlands were over an order of magnitude greater than values reported for temperate and northern peatlands (e.g. Drewer *et al.*, 2010, Nilsson *et al.*, 2008, Olson *et al.*, 2013, Rinne *et al.*, 2007, Roulet *et al.*, 2007, Saarnio *et al.*, 2007), and nearly twice as large as values reported for other temperate *Typha* marshes (Bernal & Mitsch, 2013, Bonneville *et al.*, 2008, Rocha & Goulden, 2008). In contrast, Whiting and Chanton (2001) reported NEE budgets ranging from -896 to -1139 g C-CO_2 m^{-2} yr^{-1} for *Typha* marshes in the Southeast USA, which exceeds values at the Delta wetlands. However, these rates were estimated from monthly or bi-monthly chamber measurements, and while the chamber method is ideal for assessing the spatial variability of fluxes, EC is more suitable for assessing temporal

variability and up-scaling both spatially and temporally (Hendriks *et al.*, 2010). C sequestration rates in restored Delta marshes were also in the upper range of values reported in the literature for other wetland types (c.f. Table 5 in Bernal & Mitsch, 2012, c.f. Table 2 in Mitsch *et al.*, 2013). High rates of net CO_2 uptake at our sites are attributable to the Delta's long, warm growing season with abundant water and sunlight (Brinson *et al.*, 1981). A handful of studies have measured C budgets at other created or restored wetlands and reported net CO_2 uptake rates lower (Bernal & Mitsch, 2013, Herbst *et al.*, 2013, Waddington *et al.*, 2010) or within the range (Badiou *et al.*, 2011, Hendriks *et al.*, 2007) observed in this study.

2.5.2. CH_4 fluxes

While flooding is an effective means of sequestering C, it also has secondary effects on GHG budgets through increased CH_4 production. CH_4 emissions at the Pasture were low relative to CH_4 fluxes at the restored wetlands (Table 2.3), but comparable to fluxes measured at other drained peatlands (Kroon *et al.*, 2010, Schrier-Uijl *et al.*, 2010). Despite the rice paddy being flooded for more than half the year, less CH_4 was emitted annually than at the Pasture (Table 2.3). Furthermore, CH_4 fluxes at the Rice were considerably lower than values measured from rice paddies elsewhere in California (Cicerone & Shetter, 1981, Cicerone *et al.*, 1983, McMillan *et al.*, 2007), and by other studies of CH_4 emissions from rice agriculture around the world (Bhattacharyya *et al.*, 2014, Ding *et al.*, 1999b, Holzapfel-Pschorn & Seiler, 1986, Huang *et al.*, 1997a, Meijide *et al.*, 2011, Seiler *et al.*, 1983). Lower CH_4 emissions in our study could be related to the presence of oxidizing agents, notably ferric iron at this site (Ye *et al.*, 2015), the fact that these soils contain a large abundance of lignin and other aromatics, lipid, and aliphatics, which are not readily decomposable due to their chemical recalcitrance under anoxic conditions [*Ye et al.*, 2016], cooler soil temperatures relative to tropical or subtropical sites (Conrad, 2002, Schütz *et al.*, 1990), differences in rice cultivar (Huang *et al.*, 1997a), and the relatively recent conversion of this site to rice agriculture which influences the amount of labile soil organic C, redox dynamics, and microbial community changes (Eusufzai *et al.*, 2010).

Numerous studies have shown a strong relationship between NEE or plant productivity and CH_4 flux, as vegetation is the primary source of C substrate for methanogenic metabolism (Chanton *et al.*, 1993, Hatala *et al.*, 2012a, Whalen, 2005, Whiting & Chanton, 1993). Since annual NEE at the restored wetlands was in the upper range of values reported in the literature, it follows that CH_4 emissions from these sites were also higher than values reported in other studies, particularly for more northern wetlands (e.g. Drewer *et al.*, 2010, Jackowicz-Korczyński *et al.*, 2010, Olson *et al.*, 2013, Rinne *et al.*, 2007, Roulet *et al.*, 2007, Shurpali & Verma, 1998, Sun *et al.*, 2013,

Turetsky *et al.*, 2014, Wille *et al.*, 2008). Annual CH_4 budgets at a number of temperate and tropical wetlands exceeded values reported in this study, including emissions from marshes in the Midwestern USA (~60 g C-CH_4 m^{-2} yr^{-1}) (Kim *et al.*, 1999, Nahlik & Mitsch, 2010), marshes in the Southwestern USA (up to 130 g C-CH_4 m^{-2} yr^{-1}) (Whiting & Chanton, 2001), and tropical wetlands in Costa Rica (220 to 263 g C-CH_4 m^{-2} yr^{-1}) (Nahlik & Mitsch, 2010). However, with the exception of the study by Kim *et al.* (1999), these emissions were estimated from chamber measurements taken at most once per month. Few studies have quantified CH_4 emissions from restored wetlands: mean annual CH_4 emissions ranged between 68 and 17 g C-CH_4 m^{-2} yr^{-1} for two long-term created marshes in Ohio, USA (Nahlik & Mitsch, 2010), between 31.3 and 32.3 g C-CH_4 m^{-2} yr^{-1} for a restored peatland in the Netherlands (Hendriks *et al.*, 2007), and between 9 and 13 g C-CH_4 m^{-2} yr^{-1} from a restored wetland in Denmark (Herbst *et al.*, 2013).

2.5.3. Impacts of land-use change on C sequestration and GHG budgets

While the restoration of drained wetlands is often suggested as a means to sequester C (Drösler *et al.*, 2008, Maljanen *et al.*, 2010), there are few comprehensive studies that quantify the effects of restoration activities on C and GHG budgets. This study corroborates the findings of the few recent investigations that also found that while managed peatlands are large sources of C, re-wetting can convert these ecosystems back to C sinks (Schrier-Uijl *et al.*, 2013, Waddington *et al.*, 2010). Although the Rice was a net C source from an ecosystem perspective, it lost 434 to 237 g C m^{-2} yr^{-1} less than the Corn and Pasture, respectively. Therefore, while rice agriculture in the Delta does not reverse subsidence, it does experience subsidence rates up to an order of magnitude lower than rates for conventional drained agriculture (Hatala *et al.*, 2012b). Restored wetlands are the land-use type with the greatest potential to capture C (Table 2.3) and reverse subsidence (Miller *et al.*, 2008). Therefore, restoring drained and degraded peatlands to natural wetlands may be critical to ensuring the long-term sustainability of the Delta and other heavily subsided regions throughout the world (Armentano, 1980, Syvitski *et al.*, 2009).

In addition to stopping the degradation of peat soils and reversing subsidence, another goal of drained to flooded land-use change in the Delta is to reduce GHG emissions. This is part of a growing interest in California and elsewhere in wetland restoration and management for C sequestration and possible inclusion in C finance markets (Emmert-Mattox *et al.*, 2010, Murray *et al.*, 2011). In addition to being large sources of C, the drained agricultural sites were significant GHG sources (Table 2.3). GHG balances for these sites represent conservative estimates as the budget of nitrogen GHGs was unaccounted for, and N_2O emissions at the Corn have been found exceed 400 g CO_2eq m^{-2} yr^{-1} (Morris, 2014) while even larger N_2O fluxes have been measured at

the Pasture (Teh *et al.*, 2011). In all cases, flooding reduced GHG emissions (Table 2.3), even when factoring in N_2O emissions from the Rice, which are comparable to those at the Corn (Morris, 2014). Wetland restoration provides the most benefit from both a subsidence and GHG standpoint, with the potential of converting drained peatlands from GHG sources to GHG sinks (Table 2.3). Furthermore, N_2O emissions from natural wetlands are generally low compared with terrestrial soil environments due to the low rates of N_2O production (Page & Dalal, 2011). Additional benefits from wetland restoration include flood protection and the provision of key habitat for many species. While the EC method is a valuable tool to monitor trace gas fluxes from a range of land-use types (Baldocchi *et al.*, 2001), this study is unique in assessing the impacts of restoring drained and subsided agricultural peatlands to flooded ecosystems on CO_2 and CH_4 fluxes. With a growing global interest in peatland rewetting for C sequestration (Couwenberg *et al.*, 2010, Maljanen *et al.*, 2010), there is a strong need for further research on the short and long-term effects of restoration activities on C and GHG exchange, particularly since restored and natural wetlands can exhibit large interannual variability (Chu *et al.*, 2015, Herbst *et al.*, 2013, Strachan *et al.*, 2015).

Chapter 3: Biophysical controls on interannual variability in ecosystem scale CO_2 and CH_4 exchange in a California rice paddy

3.3. Abstract

We present six and a half years of eddy covariance measurements of fluxes of methane (F_{CH4}) and carbon dioxide (F_{CO2}) from a flooded rice paddy in Northern California, USA. A pronounced warming trend throughout the study associated with drought and record high temperatures strongly influenced carbon (C) budgets and provided insights into biophysical controls of F_{CO2} and F_{CH4}. Wavelet analysis indicated that photosynthesis (GEP) induced the diel pattern in F_{CH4}, but soil temperature (T_s) modulated its amplitude. Forward stepwise linear models and neural networking modeling were used to assess the variables regulating seasonal F_{CH4}. As expected due to their competence in modeling non-linear relationships, neural network models explained considerably more of the variance in daily average F_{CH4} than linear models. During the growing season, GEP and water levels typically explained most of the variance in daily average F_{CH4}. However, T_s explained much of the interannual variability in annual and growing season CH_4 sums. Higher T_s also increased the annual and growing season ratio of F_{CH4} to GEP. The observation that the F_{CH4} to GEP ratio scales predictably with T_s may help improve global estimates of F_{CH4} from rice agriculture. Additionally, T_s strongly influenced ecosystem respiration, resulting in large interannual variability in the net C budget at the paddy, emphasizing the need for long-term measurements particularly under changing climatic conditions.

3.4. Introduction

Wetland rice paddies are a major source of atmospheric methane (CH_4) (Reeburgh, 2003, Whalen, 2005), the second most important greenhouse gas (GHG) following carbon dioxide (CO_2) (Myhre *et al.*, 2013). Numerous studies over the past decades have measured CH_4 emissions from rice fields throughout the world (cf. Aulakh *et al.*, 2001, Yan *et al.*, 2005). Previous studies have identified a number of factors and processes controlling CH_4 emissions, including soil properties (Huang *et al.*, 1997a, Neue & Sass, 1994, Sass *et al.*, 1994, Yagi & Minami, 1990), agricultural practices such as floodwater management (Alberto *et al.*, 2014, Corton *et al.*, 2000, Linquist *et al.*, 2015, Wassmann *et al.*, 2000a, Yagi *et al.*, 1996) and fertilizer application (Bronson *et al.*, 1997, Cicerone *et al.*, 1992, Corton *et al.*, 2000, Lindau *et al.*, 1991, Naser *et al.*, 2007, Sass *et al.*, 1991a, Schütz *et al.*, 1989a, Wassmann *et al.*, 2000a, Yagi & Minami, 1990), cultivar selection (Ding *et al.*, 1999a, Huang *et al.*, 1997a, Wassmann & Aulakh, 2000), grain to

biomass ratios (Denier van der Gon *et al.*, 2002), and climate (Neue & Sass, 1994, Sass *et al.*, 1991b, Schütz *et al.*, 1990, Wassmann *et al.*, 2000b, Yan *et al.*, 2005). In addition, CH_4 is strongly regulated by the ecological function of rice plants since they are the primary transport mechanism of CH_4 from the soil to the atmosphere with diffusion being the dominant mechanism for gas exchange in rice (Chanton *et al.*, 1997, Den van der Gon & Van Breemen, 1993, Wassmann & Aulakh, 2000). Rice plants also promote CH_4 oxidation via transport of atmospheric oxygen through aerenchyma, and they are an important source of carbon (C) substrates for methanogenic metabolism (Cicerone *et al.*, 1992, Hatala *et al.*, 2012a, Huang *et al.*, 1997b, Wassmann & Aulakh, 2000). Even in wetland ecosystems, where soil organic carbon can exceed 90%, there is strong evidence to suggest that CH_4 production is fueled by recent plant photosynthates in the form of exudates in the rhizosphere with limited contributions from recalcitrant soil organic matter (Bridgham *et al.*, 2013, Ström *et al.*, 2003). However, considerable uncertainty remains regarding the quantitative relationships between CH_4 emissions from rice paddies and the biophysical processes driving these fluxes (Huang *et al.*, 1997a), which contributes to the large uncertainty (25 to 300 Tg CH_4 yr^{-1}, with a median value of 53 Tg CH_4 yr^{-1}) in global CH_4 budgets from rice agriculture (Bridgham *et al.*, 2013).

Methane emissions from rice fields have predominantly been measured using the closed chamber technique (cf. Aulakh *et al.*, 2001). While chambers are advantageous for assessing spatial variability and treatment effects on fluxes, are easy to manipulate, and relatively inexpensive, placing a chamber over the plant-soil environment can introduce a number of potential biases due to direct interaction with the near-surface environment (Baldocchi, 2003, Chanton *et al.*, 1997, Meijide *et al.*, 2011). Furthermore, measurements are performed over a limited area and are often discrete in time, which provides challenges for estimating robust annual budgets since CH_4 emissions from rice show large spatio-temporal variability (Holzapfel-Pschorn & Seiler, 1986, Khalil & Butenhoff, 2008, Schütz *et al.*, 1989a). In recent years, the eddy covariance technique has emerged as an alternative means of measuring trace gas exchange since it provides quasi-continuous measurements at the ecosystem scale without interfering with the processes of gas exchange between the surface and the atmosphere (Baldocchi, 2003). While the eddy covariance method has largely been used to measure CO_2, water, and energy fluxes, the development of open-path sensors suitable for remote and fast CH_4 measurements (Detto *et al.*, 2011, McDermitt *et al.*, 2011) has allowed a growing number of studies to measure CH_4 fluxes using this method (e.g. Baldocchi *et al.*, 2012, Chu *et al.*, 2014, Hatala *et al.*, 2012b, Hendriks *et al.*, 2010, Hendriks *et al.*, 2007, Herbst *et al.*, 2013, Knox *et al.*, 2015, Koebsch *et al.*, 2015, Kroon *et al.*, 2010, Matthes *et al.*, 2014, Petrescu *et al.*, 2015, Rinne *et al.*, 2007, Sturtevant & Oechel, 2013, Sturtevant *et al.*, 2012). However, to date few studies have used this method to measure CH_4 emissions from flooded rice paddies on seasonal or annual

time scales (Alberto *et al.*, 2014, Bhattacharyya *et al.*, 2014, Hatala *et al.*, 2012a, Hatala *et al.*, 2012b, Knox *et al.*, 2015, Meijide *et al.*, 2011).

Concurrent near-continuous measurements of CH_4, CO_2 and water vapor, along with ancillary physical variables (e.g. temperature, water depth, radiation) can improve our understanding of the major controlling factors of CH_4 emission across a spectrum of timescales (hours to years) (Baldocchi, 2014, Chu *et al.*, 2014, Koebsch *et al.*, 2015). Considerable insight can be gained by exploring which of these variables are strongly correlated with CH_4 exchange and under what conditions, even if these variables, such as ecosystem respiration of CO_2 or ecosystem photosynthesis and evapotranspiration, may not represent direct drivers of CH_4 production, oxidation or transport processes (Morin *et al.*, 2014, Sturtevant *et al.*, 2016). For examples, previous studies observed tight couplings between rice photosynthesis and CH_4 exchange across periods of hours (Hatala *et al.*, 2012a) to seasons (Chanton *et al.*, 1997, Huang *et al.*, 1997b, Sass *et al.*, 1990), highlighting the connection between recent photosynthates and CH_4 production and/or the influence of stomatal conductance on CH_4 transport. Additionally, exploring the relationship between evapotranspiration and CH_4 flux can provide insight into the influence of plant activity and vegetation dynamics on CH_4 transport (Morin *et al.*, 2014, Sturtevant *et al.*, 2016), including the role of transpiration in driving diel variations in CH_4 emission (Chanton *et al.*, 1997). Ecosystem respiration has also been found to be an important predictor of CH_4 flux, improving the prediction of CH_4 emissions beyond the contribution of other direct environmental drivers alone, highlighting the complex and non-linear relationships of these environmental drivers on metabolic processes across the microbial community (Morin *et al.*, 2014). Simultaneous measurements of CO_2 and CH_4 fluxes from rice fields over annual time periods also allow the quantification of CO_2 to CH_4 ratios that can be used to assess the potential of estimating the flux of one gas from the other (McMillan *et al.*, 2007, Stallard, 1998, Whiting & Chanton, 1993) and the extent to which net CO_2 uptake can offset the radiative effect of CH_4 emissions, which currently remain uncertain since only a limited number of studies have simultaneously quantified annual budgets of both CH_4 and CO_2 from rice agriculture (Bhattacharyya *et al.*, 2014, Hatala *et al.*, 2012b, McMillan *et al.*, 2007).

In this paper we present results from a six and a half year study of simultaneous measurements of CH_4, CO_2 and water fluxes from a flooded rice field in Northern California using the eddy covariance method. To our knowledge, this is the longest and most comprehensive dataset of eddy covariance measurements of wetland rice greenhouse gas fluxes in the world. Our objectives were to investigate factors affecting CH_4 fluxes across diel to interannual timescales and quantify interannual variability in CO_2 and CH_4 budgets. Specifically, we addressed the following questions: 1) How do CH_4 fluxes at the rice paddy vary across diel, seasonal and interannual timescales? 2)

What is the net C balance and CO_2 to CH_4 ratio of the site and how does this vary from year to year? and 3) What biophysical factors are important for predicting CH_4 fluxes and how do these factors vary across timescales? The severe drought and associated record high temperatures experienced in California during the latter half of the study produced strong variability in environmental drivers, which provided a broad range of conditions to investigate the biophysical regulators of CO_2 and CH_4 exchange in wetland rice systems.

3.5. Materials and methods

3.3.1. Study site and crop management

Our study site is located on Twitchell Island in the Sacramento-San Joaquin Delta, California, USA (referred to hereafter as the Delta) (Figure 3.1), which is located approximately 100 km inland from the Pacific Ocean. The region experiences a Mediterranean-type climate characterized by hot, dry summers and cool, wet winters. The 18-year average temperature (1998-2015) recorded at a nearby weather station located ~1 km northwest of our site on Twitchell Island is 15.1 °C and mean annual precipitation is 326 mm. The Delta exists as a network of islands that maintain a water table below sea level through an extensive levee network and pumping (Deverel & Leighton, 2010, Mount & Twiss, 2005) following the drainage of the Delta's tidal marshes over a century ago. Agricultural cultivation since drainage has caused high rates of peat soil oxidation, where today the land surface in the Delta lies up to 8 m below sea level (Deverel & Rojstaczer, 1996, Drexler *et al.*, 2009b).

Prior to 1990 rice was not farmed in the Delta due to the lack of appropriate cultivars for the cool nighttime growing season temperatures. However, with the development of new varietals and the potential for rice agriculture to slow subsidence in the Delta by lowering rates of ecosystem respiration under flooded conditions (Hatala *et al.*, 2012b, Knox *et al.*, 2015), today there are about 20 km^2 of rice farmed in the region. The Twitchell Island rice paddy is a pilot project managed by the California Department of Water Resources, and the land was converted from traditional drained corn and alfalfa to rice (*Oryza sativa*) in 2009. Figure 3.1 shows the progressive increase in the size of flooded rice agriculture and wetlands on Twitchell Island throughout the study. During the first year, the east-west fetch was less than 500 m, however, by 2014 rice covered 2.44 km^2 of land and the total area of flooded vegetation was 5.7 km^2 (Figure 3.1). As described by Baldocchi *et al.* (2016), during the first few years of the study, the small and relatively isolated extent of flooded rice promoted an 'oasis effect'

that enabled warm dry air to be entrained across the top of the planetary boundary layer. However, by the sixth year of the study, the area of the flooded rice and wetlands approached a horizontal scale that appeared to inhibit the 'oasis effect'. As suggested from co-spectral analysis and analysis with a coupled surface energy balance-planetary boundary model, this likely resulted in water and heat advection in the earlier years of the study (Baldocchi *et al.*, 2016). However, the co-spectral densities for $\overline{w'c'}$ and $\overline{w'm'}$ overlapped one another during 2009 (when there was an 'oasis effect') and 2014 (when there was no evidence for an 'oasis effect'), suggesting that there was likely no CO_2 or CH_4 advection and therefore minimal influence on CO_2 and CH_4 fluxes and budgets.

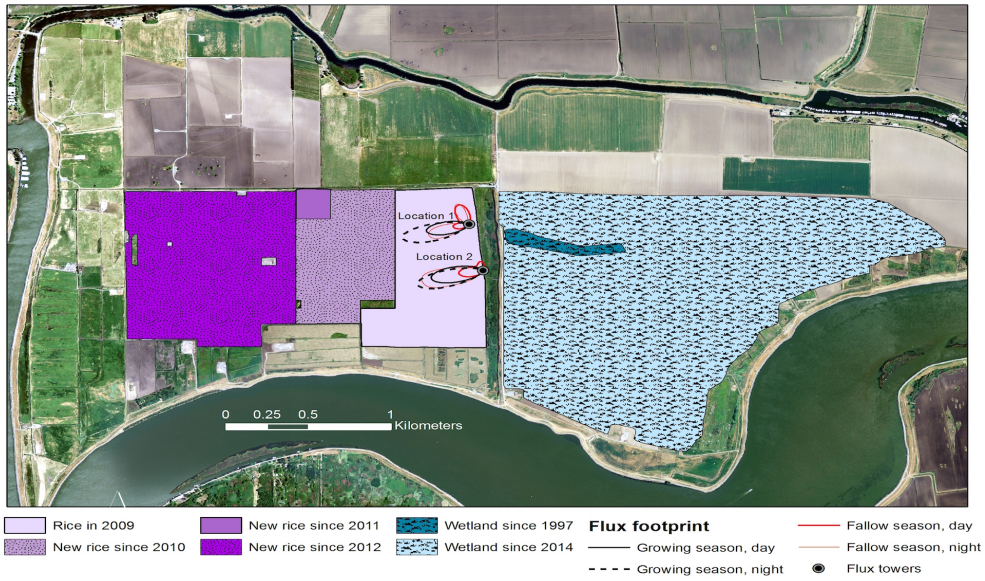

Figure 3.1. Flux tower location, climatological footprint, and extent of flooded rice and wetlands on Twitchell Island, CA, USA throughout the study period. The tower was primarily located at Location 1 throughout the study (38.10875°N, 121.6530°W), except from July 22, 2009 to November 17, 2010 when it was moved 300 m to the south (Location 2; 38.105530°N, -121.652097°W). For the climatological footprint, data are separated by season (growing season vs. fallow season), and day and night status and contours represent the 85% flux footprints. The extent of rice on the island varied throughout the study, and by 2014 the area of flooded rice and wetlands on the island approached 6 km^2.

The rice paddy lies ~5 m below sea level and is located on degraded peat soil with the top-most layer consisting of a silt loam which overlays a deep peat layer. The soil is characterized by low bulk density (0.65 and 0.57 g cm^{-3} at a depth of 0-30 cm and 30-45 cm below the soil surface, respectively) and high C content (15% and 31% at a depth of 0-30 cm and 30-45 cm below the soil surface, respectively) (Hatala *et al.*, 2012b).

Crop management practices are summarized in Table 3.1, and varied somewhat from 2009 to 2015 as changes were made in attempts to improve yields. The field was typically disced once or twice and ring rolled for planting in late-March to mid-April, with the exception of the 2012 growing season when planting was delayed until mid-May due to late rainy season precipitation. Rice varieties M104 or M206, both semi-dwarf, cold weather cultivars were planted at a density of 14 – 17 g m^{-2}. Between 2009 and 2012 the field was fertilized both at planting and just before flooding, however, from 2013 onward fertilizer was only applied once shortly before flooding (Table 3.1). The site was treated with herbicide one to three times throughout the growing season depending on weed infestations (Table 3.1). The field was flooded throughout the growing season, and harvested between late September and late October. With the exception of 2014, the rice straw was chopped and left on the field after harvesting of the grain. The paddy was re-flooded throughout the winter to provide habitat for migrating birds and reduce rates of peat soil oxidation. Few plants grew within the field during the flooded winter period, and therefore wintertime photosynthesis represented typically < 10% of annual gross photosynthetic uptake.

3.3.2. Eddy covariance measurements

We used the eddy covariance method to measure 30-min average fluxes of CH_4 (F_{CH4}; nmol m^{-2} s^{-1}), CO_2 (F_{CO2}; μmol m^{-2} s^{-1}), latent heat (LE; W m^{-2}), and sensible heat (H; W m^{-2}) (Baldocchi *et al.*, 1988). The EC instrumentation was mounted on a tower at an average height of 3.15 m. The tower was primarily located near the northeastern portion of the field (Location 1), except from July 22, 2009 to November 17, 2010 when it was moved 300 m to the south (Location 2). As the field is homogeneous, the location of the tower is likely to have minimal influence on ecosystem-scale F_{CO2} and F_{CH4}. High frequency three dimensional wind speed (u,v,w; m s^{-1}) and temperature (T_{sonic}) were measured with a sonic anemometer (Gill WindMaster or WindMaster Pro; Gill Instruments Ltd, Lymington, Hampshire, England). Fluctuations in CO_2 and H_2O molar density were measured with an open-path infrared gas analyzer (LI-7500; LI-COR Biogeosciences, Lincoln, NE, USA). Prior to January 17, 2012, CH_4 mixing ratio (χ_{CH_4}) was measured with a closed-path tunable diode laser CH_4 analyzer (Los Gatos Research (LGR), Mountain View, CA, USA). Two types of LGR analyzers were used; a fast greenhouse gas analyzer (FGGA) that simultaneously measures concentrations of CO_2, CH_4, and H_2O (June 4, 2009 to August 17, 2010), and a fast methane analyzer

Table 3.1. Cultivars planted, planting, harvest, fertilizer and herbicide application dates, peak plant area index (PAI), yield at 14% moisture content, and grain carbon.

	2009-2010	2010-2011	2011-2012	2012-2013	2013-2014	2014-2015	2015-2016
Variety	M104	M206	M104	M104	M206	M206	M206
Plant date	15 Apr	16 Apr	22 Apr	17 May	2 Apr	28 Apr	16 Apr
Harvest date	20-25 Oct	28-29 Oct	12-14 Oct	13-15 Nov	20 Sep	2 Oct	23 Sep
Fertilizer application	**15 Apr** 100 lb ac^{-1} of 11-52-0 **23-24 May** 150 lb ac^{-1} of 30-0-20	**16 Apr** 100 lb ac^{-1} of 11-52-0 **5-9 Jun** 150 lb ac^{-1} of 30-0-20	**22 Apr** 100 lb ac^{-1} of 11-52-0 **14 Jun** 200 lb ac^{-1} of 30-0-20	**17 May** 100 lb ac^{-1} of 11-52-0 **16 Jun** 200 lb ac^{-1} of 30-0-20	**2 May** 100 lb ac^{-1} of 15-15-15	**5 Jun** 150 lb ac^{-1} of 15-15-15	**31 May** 100 lb ac^{-1} of 15-15-15
Herbicide application	**22 May** Bispyribac sodium & Pendimethalin	**8 Feb** Alecto, Mist Control, Sharl EW **3 Jun** Regiment, Prowl, Syl-Tac Uan-32, Sandea	**10 Jun** Regiment, Prowl, Syl-Tac Uan-32, Sandea **5 Jul** Sprayed for water grass from helicopter	**31 May** Regiment, Prowl, Syl-Tac Uan-32, Sandea **6 Jun** Clincher CA, Mor-Act Adjuvant, Tri-Fol **19 Jul** SuperWham	**1 May** Regiment, Prowl, Syl-Tac Uan-32, Sandea	**4 Jun** Regiment, Prowl, Syl-Tac Uan-32, Sandea	**1 Jun** Regiment, Prowl, Syl-Tac Uan-32, Sandea **25 Jun** SuperWham
Peak PAI	6.7	7	4.6	4.1	4.6	5	3.5
Yield (t ha^{-1})	4.7	4.5	6.0	5.6	7.3	5.7	7.4
Grain carbon[a] (g C m^{-2})	172	163	220	205	266	208	269

[a]Calculated from yields as in Hollinger *et al.* (2005) assuming the fraction of carbon in the grain is 0.43 based on measurements

(FMA) (August 17, 2010 to January 17, 2012). Following January 17, 2012 an open-path CH_4 analyzer, based on wavelength modulation spectroscopy, was used to measure fluctuations in CH_4 molar density (LI-7700; LI-COR Biogeosciences, Lincoln, NE, USA). The specifications and details of the external pump required to operate the closed-path system are given in Detto *et al.* (2011) and Hatala *et al.* (2012b). Extensive field-testing was done to evaluate the performance of the closed-path CH_4 sensors at this site (Detto *et al.*, 2010), and good agreement was observed in the magnitude of 30-min fluxes between the open-path and closed-path flux systems (Detto *et al.*, 2011). Raw turbulence data was initially recorded with a Campbell CR1000 datalogger (Campbell Scientific, Logan, UT, USA), and following May 7, 2012 using a digital datalogger system (LI-7550A; LI-COR Biogeosciences, Lincoln NE, USA). Prior to July 27, 2013 anemometer readings and trace gas densities were recorded at 10 Hz intervals, but thereafter the data was collected at 20 Hz since it resulted in slightly less high frequency attenuation.

Fluxes were calculated using the 30-min covariance of vertical wind speed (w) and scalars of interest after applying a series of standard corrections using in-house software (Detto *et al.*, 2010, Hatala *et al.*, 2012b) as outlined in Knox *et al.* (2015). Briefly these included despiking high frequency data, applying coordinate rotations, correcting for effects of air density fluctuations, filtering fluxes with low friction velocity (0.12 to 0.15 m s^{-1}, varying somewhat seasonally) and spikes in 30-min mean densities, variances and covariances, and rejecting fluxes from winds between 0°–190° for Location 1 and outside of 200°–350° for Location 2, which was estimated based on the relationship between wind direction and fluxes, and the flux footprint calculated a 2-D footprint model (Table 3.1). Unlike previous versions of the in-house software that used a default time lag between w and scalars defined by the user, a variable lag was calculated based on a maximum cross-correlation method. The software was also updated to filter fluxes with large vertical rotation angles (> ±7°) and flagged fluxes using the stationarity test of Foken and Wichura (1996). The percentage of 30-min fluxes excluded annually from this analysis, including periods of power loss and sensor malfunction, ranged between 43 and 54% for F_{CO2}, and 44 and 61% for F_{CH4} with the exception of the first year of measurement when 82% of the data was excluded due to the late deployment of the CH_4 analyzer (June), and generator outages and sensor malfunction. However, much less data was excluded during the growing season (13-32% for F_{CO2} and 13-38% for F_{CH4} again with the exception of 2009 when 77% of the data was excluded) due to the prevalence of clear sunny days and robust and persistent winds that flow through the Carquinez Strait between the cool coast and the warm interior valley (Table 3.1).

No high frequency corrections were applied to fluxes computed using open-path sensors since co-spectral analysis indicated that flux losses were less than 5% (Knox *et*

al., 2015), which is well within the accuracy of individual eddy covariance flux measurements and of the correction algorithms (Aubinet *et al.*, 1999, Massman & Lee, 2002, Moore, 1986). However, corrections for the closed-path CH_4 measurements were applied to account for the high frequency flux losses due to sensor separation and attenuation of χ_{CH_4} fluctuations down the sampling tube. When the FGGA was present, corrections were calculated as in Detto *et al.* (2011) by taking advantage of the additional CO_2 channel. When the FMA sensor was present and we couldn't take advantage of the additional CO_2 channel, we used a procedure similar to the one outlined in Aubinet *et al.* (1999) and Humphreys (2004) as described in Knox *et al.* (2015). F_{CH4} corrected for spectral loss agreed to within about 3% with CH_4 emissions measured using an open path sensor for periods when both systems were present for comparison (August 17, 2010 to September 21, 2010 and January 17, 2012 to April 25, 2012).

Energy balance closure, defined as the slope between daily net radiation and the residual of the energy balance (Wilson *et al.*, 2002), was 0.84 for the entire study period, and ranged between 0.81 and 0.89 when calculated for individual years. In addition to the ground heat flux, storage terms included radiation energy absorbed in photosynthesis calculated as in Leuning *et al.* (2012) and heat storage in the water column approximated as in Drexler *et al.* (2004). Energy balance closure reported in this study falls within the range typically observed at sites within the FLUXNET network (Stoy *et al.*, 2013, Wilson *et al.*, 2002), and on the upper end of values reported for wetland sites (Malone *et al.*, 2014, Stoy *et al.*, 2013), where lower closure is typically observed due to the difficulties in estimating storage terms (Malone *et al.*, 2014).

3.3.3. Gap-filling, flux partitioning, and budget estimations

Half-hourly fluxes were gap-filled using an artificial neural network (ANN) method (Baldocchi & Sturtevant, 2015, Dengel *et al.*, 2013, Knox *et al.*, 2015, Moffat *et al.*, 2007, Morin *et al.*, 2014, Papale *et al.*, 2006). To facilitate representativeness, explanatory data were divided into a maximum of 20 natural data clusters using the k-means method. To avoid biasing towards conditions with better flux data coverage, data used to train, test, and validate the ANN were proportionately sampled from these clusters. Several architectures of increasing complexity were tested to facilitate generalizability of the neural network. The architecture of each neural network was initialized ten times with random starting weights, and the initialization resulting in the lowest mean sampling error was used. The simplest architecture, whereby additional increases in complexity resulted in < 5% reduction in mean square error, was selected and the prediction saved. This procedure was replicated with twenty re-samplings of the data, and the median prediction was used to fill missing half-hours.

While ecosystem photosynthesis (gross ecosystem production; GEP) and respiration (ER) are not directly measured via the eddy covariance method, net CO_2 fluxes (F_{CO2}) can be partitioned into GEP and ER by separately considering daytime and nighttime observations because photosynthesis only occurs during daylight hours. Since winds in the Delta are strong even at night (Baldocchi & Sturtevant, 2015, Hatala *et al.*, 2012b, Knox *et al.*, 2015), uncertainties in nighttime eddy covariance measurements due to atmospheric stratification and stability are minimized (Massman & Lee, 2002). F_{CO2} was gap-filled separately for daytime and nighttime observations. Predictions from the ANN resulting from the nighttime gap-filling were used to model ER for all data (daytime and nighttime values) and GEP was calculated by subtracting gap-filled F_{CO2} from modeled respiration (F_{CO2} = ER - GEP) (Baldocchi & Sturtevant, 2015). In this study, negative F_{CO2} values indicated net CO_2 uptake while positive values indicate net CO_2 release, while both GEP and ER are presented with positive signs.

For half hourly fluxes, the entire observation period was used to train, test, and validate the ANNs. Explanatory variables used to gap-fill daytime F_{CO2} included air temperature (T_a), photosynthetically active radiation (PAR), vapor pressure deficit (VPD), water table depth (WTD), friction velocity (u_*), decimal day of year since the start of the study, and sine and cosine functions to represent seasonal changes. Explanatory variables used to gap-fill nighttime F_{CO2} and partition ER included the same variables as daytime F_{CO2} with the exception of PAR and VPD. Unlike F_{CO2}, LE and F_{CH4} were not gap-filled separately for daytime and nighttime data. Explanatory variables used to gap-fill LE were the same as daytime F_{CO2}, and variables used to gap-fill F_{CH4} included soil temperature (T_s) at 2 cm depth, WTD, u_*, GEP, ER, LE, decimal day of year, and sine and cosine functions, which represent the main environmental drivers of CH_4 emissions or variables that strongly covary with F_{CH4} (Chu *et al.*, 2014, Morin *et al.*, 2014, Sturtevant *et al.*, 2016, Treat *et al.*, 2007). The optimal neural network for both daytime and nighttime F_{CO2} gap-filling included 2 hidden layers with 15 and 8 hidden nodes, respectively, while most often the optimal neural network for F_{CH4} gap-filling included 2 hidden layers with 10 and 5 hidden layers, respectively.

Gap-filling and partitioning routines performed very well; daytime (nighttime) neural network predictions for F_{CO2} gave a model r^2 of 0.95 (0.76) with a RMSE of 2.4 (1.5) μmol m^{-2} s^{-1}, for F_{CH4} model r^2 was 0.79 with a RMSE of 30 nmol m^{-2} s^{-1}, and for LE model r^2 was 0.93 with a RMSE of 0.82 mmol m^{-2} s^{-1}. We also tested the Reichstein *et al.* (2005) algorithm to estimate ER and found negligible differences in the results presented below while annual budgets of GEP and ER differed on average < 10% between the two flux partitioning methods.

Annual and seasonal sums of F_{CO2}, GEP, ER, and F_{CH4} were calculated by

integrating gap-filled and partitioned fluxes over time. For annual budgets, half hourly fluxes were integrated from April 1 to April 1 of the following year. For figures, labels refer to the year that includes the growing season (e.g. 2009 is used as the label for 2009-2010). Growing season budgets were calculated by integrating fluxes from planting to harvest of a given year, while fallow season budgets were calculated from harvest of one year to planting of the following year. To estimate the amount of uncertainty in the ANN gap-filling procedure for the annual and seasonal budgets, we calculated the integrated budget using the full range of predictions used to fill each gap (i.e. based on the 20 extractions from the ANN), and calculated the 95% confidence interval from the distribution of the 20 annual or seasonal budgets (Knox *et al.*, 2015).

3.3.4. Footprint model

To model the spatial origin of the flux measurements, we used an analytical two-dimensional footprint model (Detto *et al.*, 2006, Hsieh *et al.*, 2000). The flux tower footprint shows the spatial portion of the landscape represented by each half hourly eddy covariance flux measurement. The footprint model uses wind speed and direction, roughness length (z_o; m), displacement height (d; m), boundary layer stability, and turbulence data to trace the probability that a certain air parcel measured at the tower at the level of the eddy covariance instrumentation originated from any particular point within the landscape. We used the method of Pennypacker and Baldocchi (2015) to derive continuous estimates of canopy height, z_o and d. We show the 85% analytical footprint (i.e. the areal extent from which 85% of the measured flux originated), because as the analytical footprint approaches 100%, the area of the footprint expands rapidly, although there is only a small contribution to the measured flux from this extensive area (Matthes *et al.*, 2014). The climatological footprints in Figure 1 clearly indicate that at both the diel and annual scale, measured fluxes predominantly originated from the rice paddy, and illustrate that the diel patterns we observe are in fact true biological signals and not an artifact of differences in wind direction and hence flux footprint between night and day.

3.3.5. Meteorological and vegetation measurements

Meteorological conditions including T_a, relative humidity, WTD, incoming solar radiation, net radiation (R_{net}), PAR, ground heat flux, T_s at depths of -0.02, -0.04, -0.08, -0.16, and -0.32 m below the ground surface, and water temperature (T_w) were characterized with a standard set of sensors as described in Knox *et al.* (2015). Gaps in T_a were filled using data from a nearby weather station on Twitchell Island while gaps in other meteorological variables were filled with a 2-D interpolator that conserves the mean diurnal variation. There were few gaps in meteorological measurements (e.g. < 1% for PAR for the entire observation period), however, ground sensors were removed

from the soil for approximately two weeks to a month for each planting and harvesting event.

Plant area index (PAI) was measured approximately weekly or bi-weekly during the growing season. Measurements were made using a LAI-2000 Plant Canopy Analyzer (LI-COR Biogeosciences, Lincoln, NE, USA). Measurements were recorded every 10 m along a 100 m transect extending west, the predominant wind direction at the site. The fraction of photosynthetically active radiation (FPAR) absorbed by the canopy was calculated from PAI using the Beer-Lambert law (Ruimy *et al.*, 1999) assuming a light extinction coefficient of 0.6 (Monteith, 1969). FPAR was then multiplied by PAR to estimate absorbed PAR (APAR). Canopy phenology and crop management were monitored with a digital camera (Richardson *et al.*, 2007).

3.3.6. Data analysis

We used a combination of linear regression models, neural network modeling and time series analysis to investigate the biophysical controls on F_{CH4} from the rice paddy. Different data analysis techniques were used for each timescale of interest, taking advantage of the analysis technique most suitable to each timescale.

3.3.6.1. Interannual and seasonal timescales

Due to the limited number of data points (n = 6 or 7 years or growing seasons, respectively), pairwise linear regression models were used to explore the factors predicting CH_4 fluxes at the interannual scale. At the seasonal scale, we took advantage of the significantly larger number of daily average flux and environmental variables to explore neural network models (Dengel *et al.*, 2013, Knox *et al.*, 2015, Morin *et al.*, 2014), in addition to linear models, for daily average F_{CH4} (referenced simply as 'daily F_{CH4}' hereafter). We used a statistical model selection process similar to Morin *et al.* (2014) to assess the effectiveness of T_a, T_s, WTD, u^*, GEP, ER, LE in predicting daily F_{CH4} since these are the primary variables regulating or covarying with F_{CH4} (Chu *et al.*, 2014, Koebsch *et al.*, 2015, Morin *et al.*, 2014, Sturtevant *et al.*, 2016, Treat *et al.*, 2007). Both environmental variables and fluxes of carbon and water were included as potential drivers of F_{CH4} because they can represent strongly shared mechanisms between F_{CH4} and other environmental or flux variables even if they are not directly linked by causality, and thus their inclusion can provide empirical predictive power for F_{CH4} (Morin *et al.*, 2014).

We divided daily F_{CH4} into growing season and fallow season periods to capture differences in processes. Models were developed across years for both the growing and fallow seasons, and for each individual growing season (excluding 2009 due to the

limited sample size). Individual fallow periods were not modeled due to the lack of flux coverage in winter; on average there were 153 measurements of daily F_{CH4} during the growing season (excluding 2009) and only 58 measurements in the winter period.

First we created multivariate linear regression models to investigate the relationships between environmental and flux drivers and daily F_{CH4}. Daily F_{CH4} was estimated by taking the mean of quality controlled half-hourly fluxes for days with gaps of less than 8 hours, and values were log-transformed before being fit with linear models (Chu *et al.*, 2014, Treat *et al.*, 2007, Yan *et al.*, 2005). We used a forward stepwise approach, where driving variables were ranked based on their pairwise correlation with F_{CH4} and additional variables were included in the model if: 1) there was a significant pairwise correlation, 2) their effect in the model was significant, 3) they improved the overall R^2 of the model, and 4) their inclusion resulted in an AIC reduction (Morin *et al.*, 2014). The order in which the variables were added to successive multiple regression models was assessed by minimizing the AIC score of the model, and the model was expanded in a stepwise hierarchical manner to include variables until the addition of variables resulted in an increase in the AIC score, suggesting an overparameterized model.

Once we found the optimal linear model, a similar stepwise approach was used for the ANNs, where the variables from the linear model were used one by one and the incremental increase in R^2 and AIC values were calculated. To decrease processing time, rather than testing all potential variable orders, we included variables in the same order in the ANNs as in the linear models (Morin *et al.*, 2014). Following the addition of all variables identified as significant in the linear models, we also tried including those that weren't identified as significant since neural networks can better capture non-linear relationships. However, in the majority of cases if a variable was rejected from the linear models it was also rejected from the ANNs, with the notable exception of WTD in neural network of fallow season F_{CH4}. Slight modifications to the ANN were made to account for a decrease in sample size when using daily F_{CH4} rather than half hourly fluxes. Unlike the ANN gap-filling procedure described above, explanatory data were not divided into clusters and the fraction of the random samples going to the training, validation, and testing subsamples was 50%, 30%, and 20%, respectively. In addition, the complexity of the neural network architecture was decreased, ranging from one hidden layer with 3 nodes to 2 hidden layers with 5 and 3 nodes, respectively. In this case, for each added variable, we ran the ANN for one neural network architecture at a time (again with 20 extractions), and then chose the best architecture based on the calculated AIC value.

3.3.6.2. Diel timescale

Due to their near-continuous nature, eddy covariance flux observations are also well suited for time series analysis (Hatala *et al.*, 2012a, Koebsch *et al.*, 2015, Novick *et al.*, 2015, Stoy *et al.*, 2005, Torrence & Compo, 1998). We used the continuous wavelet transform (CWT) with the Morlet mother wavelet to explore the correlation and time lag between F_{CH4} and biophysical factors at the diel scale. Relative to Fourier analysis, wavelet transforms are much better suited for spectral analysis of nonstationary time series such as eddy covariance data (Katul *et al.*, 1998, Stoy *et al.*, 2005, Torrence & Compo, 1998). The wavelet coherence spectrum represents the local correlation between two signals in time-frequency space from which a phase angle can be calculated and used to establish potential causal relationships (Grinsted *et al.*, 2004). The statistical significance of wavelet power was tested against the null hypothesis of a red noise first order autoregressive process with lag-1 autocorrelation (Grinsted *et al.*, 2004). For diel time periods with significant wavelet coherence, the phase angle was used to calculate the time lag between the two signals. To avoid spurious correlations between F_{CH4} and driving variables, we did not use gap-filled data, and instead replaced missing values with the median for the whole growing season (Hatala *et al.*, 2012a), and time series were standardized to have a zero mean and unit variance (Hatala *et al.*, 2012a, Stoy *et al.*, 2005). All analyses described above were performed using MATLAB (MathWorks Inc., 2015, version 8.6.0).

3.6. Results

3.4.1. Weather conditions and water table management

Due to the severe drought and record high temperatures experienced in California from 2012 to 2015 (Griffin & Anchukaitis, 2014), climatic variability was greater than expected, and there was an increasing trend in temperature over the course of the study (Table 3.2; Figure 3.2a,b). Mean annual T_a was coolest in 2010-2011 (14.0 °C), with largely negative deviations in mean monthly T_a, while 2014-2015 was the warmest year of the study (15.8 °C), with predominantly positive deviations in T_a (Figure 3.2a). Soil temperatures showed a similar pattern as T_a (Figure 3.2b), however, the range in mean annual and seasonal T_s (> 3.0 °C) was larger than that of T_a (> 1.8 °C) (Table 3.2) since rice management (e.g. PAI and water regulation) in addition to T_a played a role in modulating T_s.

Water table depth at the paddy was actively managed throughout the study and the drought did not result in water restrictions at the site. The field was typically

flooded 45 to 60 days after planting and drained 30 to 45 days before harvest (Figure 3.2d). Therefore, over the course of the growing season there was standing water on the field between 64 and 112 days, with water levels generally maintained at 10 to 20 cm above the soil surface. In addition, the field was flooded for about 65 to 135 days during the fallow winter period.

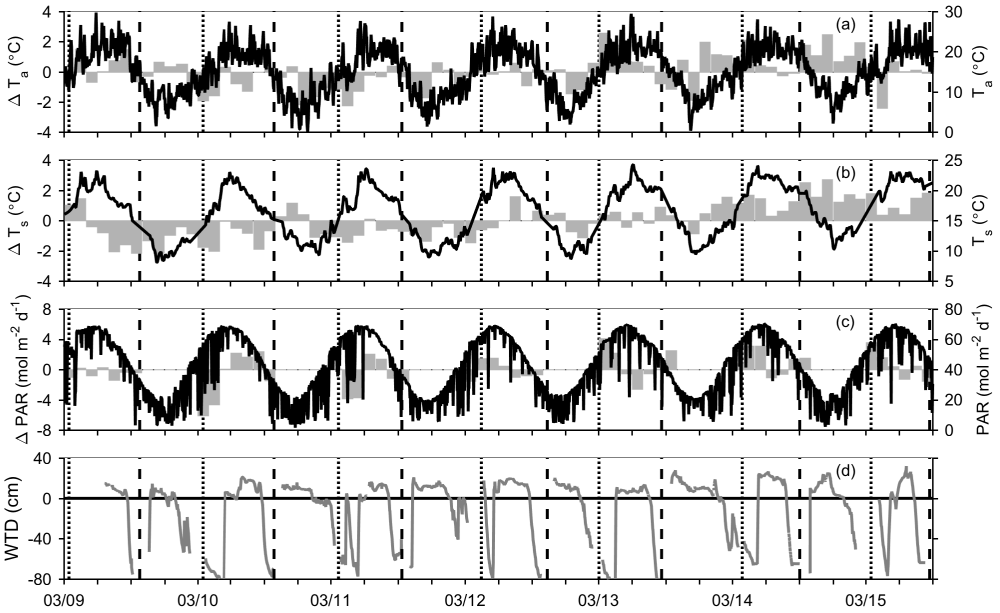

Figure 3.2. Monthly anomaly (grey bars) and time series of daily micrometeorological variables (solid lines), including (a) air temperature (T_a), (b) soil temperature at 32 cm depth (T_s), (c) photosynthetically active radiation (PAR), and (d) water table depth (WTD). Dotted and dashed lines indicate planting and harvest dates, respectively.

3.4.2. CO_2 fluxes

While the rice paddy was generally a net CO_2 sink during the growing season, large interannual differences were observed, with the site ranging from a large net CO_2 sink in the 2010 growing season (-607 g C-CO_2 m^{-2}) to near CO_2-neutral in 2015 (8 g C-CO_2 m^{-2}) (Table 3.2; Figure 3.3). Large interannual variability was also observed in growing season GEP and ER (Figure 3.3); GEP budgets differed by more than 500 g C-CO_2 m^{-2} yr^{-1} over the 7 growing seasons, while cumulative growing season ER ranged from 782 to 1152 g C-CO_2 m^{-2} (Table 3.2). Interannual variability in growing season ER was strongly related to mean growing season T_s (Figure 3.8b). In addition, early drainage (i.e. a month earlier than the average drainage date) of the rice paddy in the 2015 growing season (Figure 3.2d), coupled with warm late-summer temperatures (Figure 3.2b), resulted in high rates of respiration and positive F_{CO2} in the later part of the growing season (Figure 3.3d,c), contributing to the near neutral net CO_2 budget that season.

Table 3.2. Annual, growing and fallow season mean air (T_a) and soil temperature (T_s) at 2 cm depth, and sums of photosynthetically active radiation (PAR), net CO_2 flux (F_{CO2}), gross ecosystem production (GEP), ecosystem respiration (ER), CH_4 flux (F_{CH4}), and annual carbon (C) budget. The annual carbon budget includes the amount of C lost as CH_4 and removed from the field through harvest. Error bounds indicate the 95% confidence interval for the gap-filling procedure.

	Annual	Growing Season	Fallow Season		Annual	Growing Season	Fallow Season
T_a (°C)				GEP (g C-CO_2 m^{-2})			
2009-2010	15.0	19.6	9.7	2009-2010	1340 ± 152	1268 ± 73	67 ± 134
2010-2011	14.0	18.6	9.0	2010-2011	1648 ± 74	1535 ± 59	97 ± 59
2011-2012	14.0	18.7	10.7	2011-2012	1328 ± 94	1182 ± 60	195 ± 78
2012-2013	14.7	19.0	8.8	2012-2013	1304 ± 130	1198 ± 85	69 ± 70
2013-2014	15.4	20.2	11.6	2013-2014	1555 ± 96	1431 ± 70	146 ± 66
2014-2015	15.8	20.5	12.0	2014-2015	1445 ± 107	1343 ± 86	89 ± 80
T_s (°C)	--	19.4	--			1014 ± 75	
				ER (g C-CO_2 m^{-2})			
2009-2010	14.6	18.4	10.1	2009-2010	1173 ± 124	782 ± 29	406 ± 107
2010-2011	15.1	18.7	11.0	2010-2011	1252 ± 54	928 ± 32	362 ± 42
2011-2012	15.0	19.6	11.3	2011-2012	1361 ± 66	921 ± 21	502 ± 64
2012-2013	15.8	19.8	11.1	2012-2013	1336 ± 76	904 ± 39	296 ± 54
2013-2014	16.5	20.9	13.3	2013-2014	1601 ± 60	1095 ± 12	600 ± 55
2014-2015	17.6	22.0	13.7	2014-2015	1761 ± 60	1152 ± 18	567 ± 58
2015-2016	--	21.4	--	2015-2016	--	1022 ± 25	--
PAR (mol m^{-2})				F_{CH4} (g C-CH_4 m^{-2})			
2009-2010	14427	10427	4044	2009-2010	6.4 ± 4.3	2.5 ± 2.5	4.0 ± 2.0
2010-2011	14423	10533	4331	2010-2011	12.1 ± 2.0	6.2 ± 0.7	7.0 ± 2.1
2011-2012	14636	9506	6426	2011-2012	7.8 ± 1.0	4.0 ± 0.4	3.0 ± 1.0
2012-2013	15249	9337	3625	2012-2013	6.7 ± 1.8	4.1 ± 0.3	2.1 ± 1.4
2013-2014	15273	9960	6619	2013-2014	13.7 ± 2.0	8.9 ± 0.2	5.0 ± 2.0
2014-2015	15332	9281	5449	2014-2015	19.3 ± 1.4	11.1 ± 0.2	8.1 ± 1.4
2015-2016	--	9436	--	2015-2016	--	9.3 ± 0.4	--
F_{CO2} (g C-CO_2 m^{-2})				C budget			
2009-2010	-167 ± 96	-486 ± 26	339 ± 91	2009-2010	5 ± 96	--	--
2010-2011	-396 ± 46	-607 ± 19	264 ± 47	2010-2011	-232 ± 46	--	--

2011-2012	-33 ± 49	-261 ± 28	307 ± 39	2011-2012	253 ± 49	--	--
2012-2013	32 ± 65	-294 ± 36	227 ± 49	2012-2013	237 ± 65	--	--
2013-2014	46 ± 34	-335 ± 10	455 ± 33	2013-2014	312 ± 34	--	--
2014-2015	316 ± 50	-192 ± 10	478 ± 51	2014-2015	524 ± 50	--	--
2015-2016		8 ± 15			--	--	--

When including the fallow season, the site ranged from being a strong net sink of CO_2 in 2010-2011 (-396 g C-CO_2 m^{-2} yr^{-1}) to a considerable net source in 2014-2015 (316 g C-CO_2 m^{-2} yr^{-1}) (Table 3.2). Annual F_{CO2} was significantly related to annual ER ($p < 0.05$, $r^2 = 0.67$), but not GEP ($p = 0.43$, $r^2 = 0.16$), suggesting that interannual variability in F_{CO2} at the paddy was driven more by changes in ER than GEP. Similar to growing season ER, interannual variability in annual ER was strongly related to mean annual T_s (Figure 3.8a), which explains why the rice paddy was a net CO_2 sink in the earlier, cooler years, and a net CO_2 source in the later, warmer years (Table 3.2).

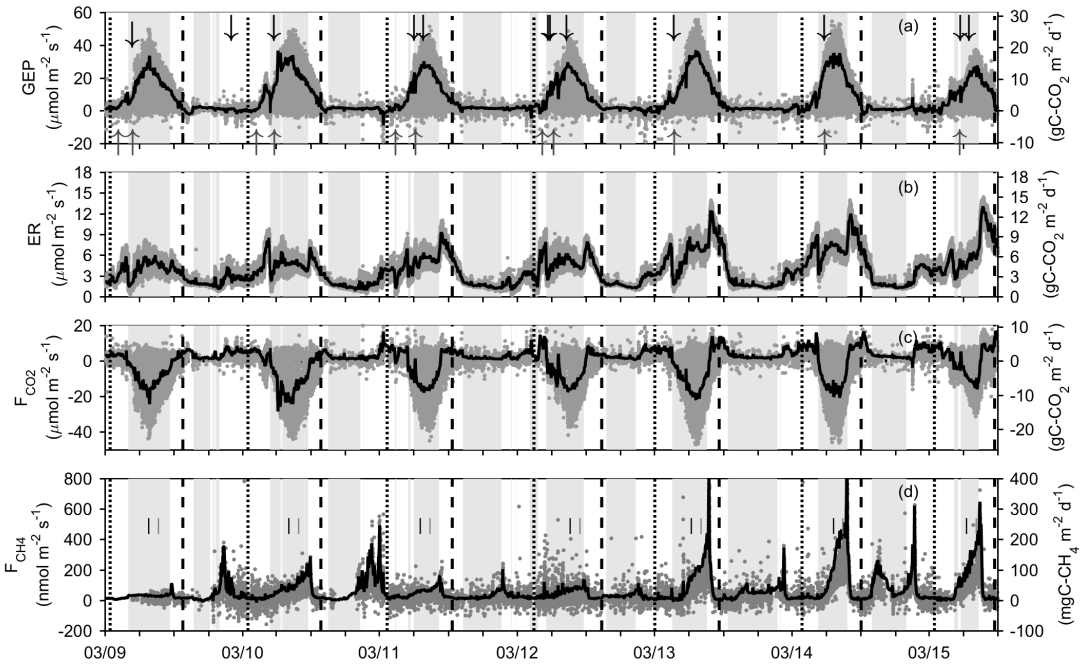

Figure 3.3. Times series of half-hourly (grey circles) and daily (solid lines) (a) gross ecosystem production (GEP), (b) ecosystem respiration (ER), (c) net ecosystem CO_2 exchange (F_{CO2}), and (d) net ecosystem CH_4 exchange (F_{CH4}). Half-hourly fluxes were not gap-filled and daily data were integrated from gap-filled half-hourly data using the artificial neural network method. Shaded grey areas in the background of all panels indicate periods when the field was flooded. Dotted and dashed lines indicate planting and harvest dates, respectively. Herbicide application dates are indicated by the black downward pointing arrows and fertilizer application dates are indicated by the upward facing grey arrows in (a). Panicle initiation and heading dates are indicated in (d) by black and grey dashes, respectively.

3.4.3. Temporal variability in CH_4 fluxes and annual budgets

Daily F_{CH4} increased throughout the growing season, reaching a maximum toward grain ripening, with a large pulse of CH_4 to the atmosphere following drainage

of the field for harvest (Figure 3.3d). Although the overall seasonal pattern of F_{CH4} was similar between years, the magnitude of the fluxes varied by an order of magnitude (Figure 3.3d). Lowest daily F_{CH4} was observed in the 2009 summer period when, prior to drainage, emissions were < 20 mg C-CH_4 m^{-2} d^{-1}. In contrast, daily F_{CH4} during the growing season of 2014 exceeded 200 mg C-CH_4 m^{-2} d^{-1} prior to the drop in WTD for harvest. Emissions during the fallow season were generally low (~10 to 30 mg C-CH_4 m^{-2} d^{-1}) except when the field was drained for planting, which caused a large release of stored CH_4 (Figure 3.3d).

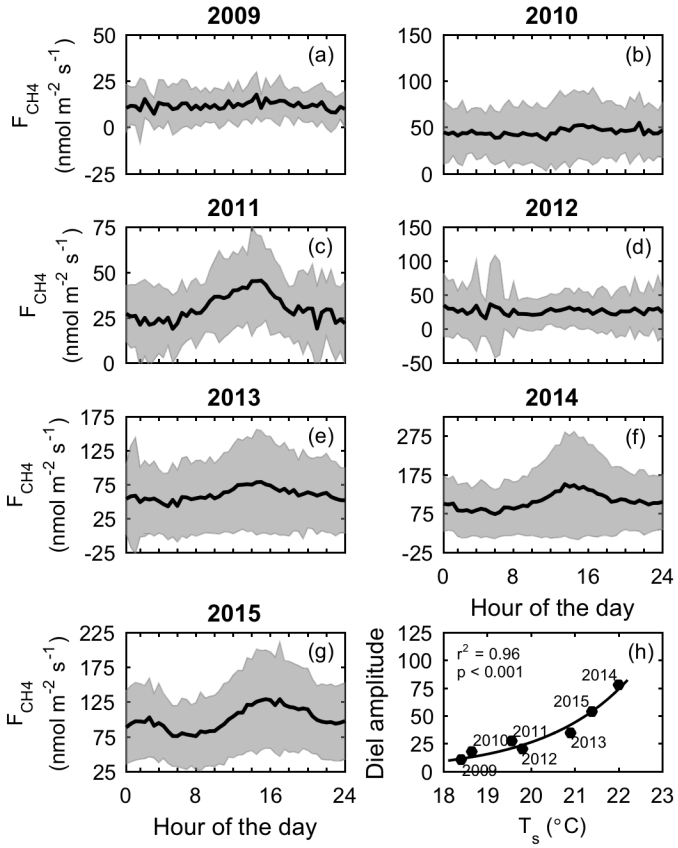

Figure 3.4. (a) – (g) Mean diel variation in CH_4 flux (F_{CH4}) during the growing season when the field was flooded, and (h) amplitude of the mean diel variation in F_{CH4} as a function of mean growing season soil temperature (T_s) at 2 cm. The shaded area in (a) – (g) indicates the standard deviation. Note the difference in the vertical axes.

Strong diel variation in F_{CH4} was observed during the growing seasons of 2011, 2013, 2014, and 2015 while weak or no consistent diel patterns were observed in other years (Figure 3.4; Figure 3.5 to Figure 3.7). In years with strong daily variation in F_{CH4}, the diel peak in F_{CH4} occurred in mid-afternoon between 14:00 and 15:30 hours. Furthermore, in addition to large differences in the magnitude of the fluxes, the

amplitude of the diel cycle varied strongly between years, increasing exponentially with mean growing season T_s (Figure 3.4h). No diel patterns were observed when the field was flooded during the winter months.

Annual CH_4 budgets varied considerably throughout the study, with over three times more CH_4 emitted in 2014-2015 than in 2009-2010 (Table 3.2). Growing season CH_4 emissions ranged from 2.5 to 9.3 g C-CH_4 m^{-2} in 2009 and 2014, respectively, and wintertime F_{CH4} was greatest in 2014-2015 (8.1 g C-CH_4 m^{-2}) and considerably less CH_4 was released over the 2012-2013 fallow period (2.3 g C-CH_4 m^{-2}).

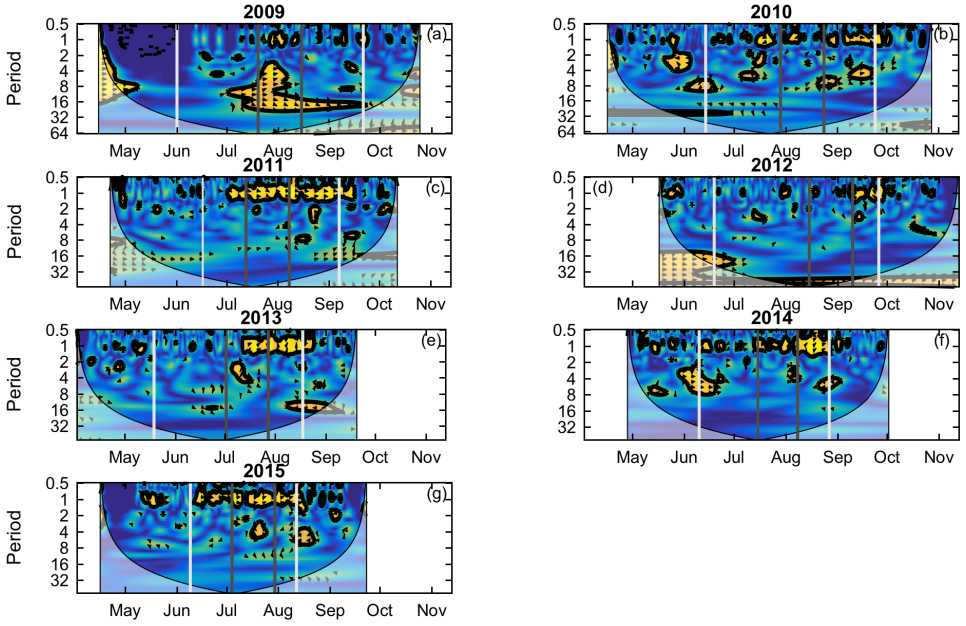

Figure 3.5. Wavelet coherence between soil temperature (T_s) and CH_4 flux (F_{CH4}) for the rice paddy during each growing season. Significant coherency (at the 5% level with 500 Monte Carlo simulations of AR-1 autocorrelation) is outlined by the black lines. The direction of the arrows show the phase angle between the two time series, where an arrow to the right with no inclination indicates no lag between the time series. The cone of influence represents the limit where wavelet power drops to e^{-2} of the edge values. The solid vertical light gray lines indicate when the field when the field was fully flooded (ranging from mid-May to mid-June) and drained (ranging from mid-August to late September). The solid vertical dark gray lines show the approximate dates of panicle initiation (ranging from early July to mid-August) and heading (ranging from late July to early September).

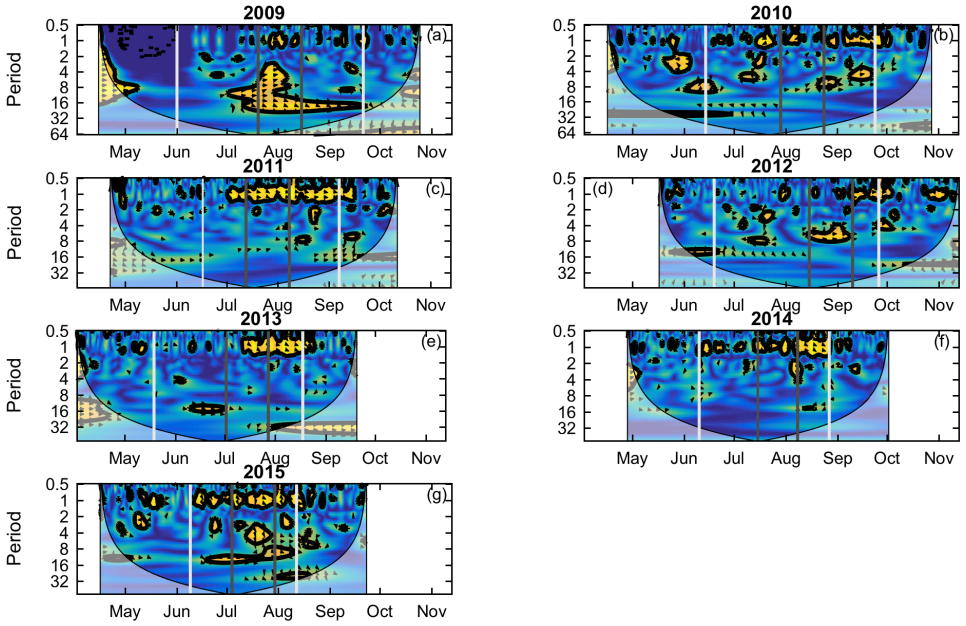

Figure 3.6. Wavelet coherence between ecosystem photosynthesis (GEP) and CH_4 flux (F_{CH4}) for the rice paddy during each growing season. Significant coherency (at the 5% level with 500 Monte Carlo simulations of AR-1 autocorrelation) is outlined by the black lines. The direction of the arrows show the phase angle between the two time series, where an arrow to the right with no inclination indicates no lag between the series. The cone of influence represents the limit where wavelet power drops to e^{-2} of the edge values. The solid vertical light gray lines indicate when the field when the field was fully flooded (ranging from mid-May to mid-June) and drained (ranging from mid-August to late September). The solid vertical dark gray lines show the approximate dates of panicle initiation (ranging from early July to mid-August) and heading (ranging from late July to early September).

3.4.4. CH_4 emission predictors

3.4.4.1. Interannual scale

Interannual differences in annual and growing season CH_4 emissions were not significantly correlated with annual or growing season GEP ($p > 0.24$), F_{CO2} ($p > 0.24$), or the number of drained or flooded days ($p > 0.14$). However, like ER (Figure 3.8a and 3.8b), annual and growing season F_{CH4} were significantly correlated with mean annual or growing season T_s, respectively (Figure 3.8d,e). Over the full year, F_{CH4} was most strongly related to T_s at intermediate depths (8 and 16 cm) since warmest T_s and presumably greatest CH_4 production were observed near the soil surface in the summer and deeper in the soil profile in winter, while during the growing season F_{CH4} was most

significantly correlated with T_s at 2 cm. As expected from these observations, there was a strong relationship between annual or growing season ER and F_{CH4} ($p = 0.029$, $r^2 = 0.74$ and $p = 0.0011$, $r^2 = 0.90$, respectively). Increasing T_s also resulted in a significant increase in the annual or growing season CH_4 to GEP ratio (Figure 3.8g,h). Over the whole year, the ratio of F_{CH4} (g C-CH_4 m^{-2} yr^{-1}) to GEP (g C-CO_2 m^{-2} yr^{-1}) ranged from 0.5% in 2009-2010 to 1.4% in 2014-2015 (Figure 3.8g), while during the growing season this ratio varied between 0.2% in 2009 and 0.9% in 2015 (Figure 3.8h). No variables were found that were significantly correlated with interannual differences in cumulative fallow season F_{CH4}, including T_s (Figure 3.8f) or fallow season ER ($p = 0.42$).

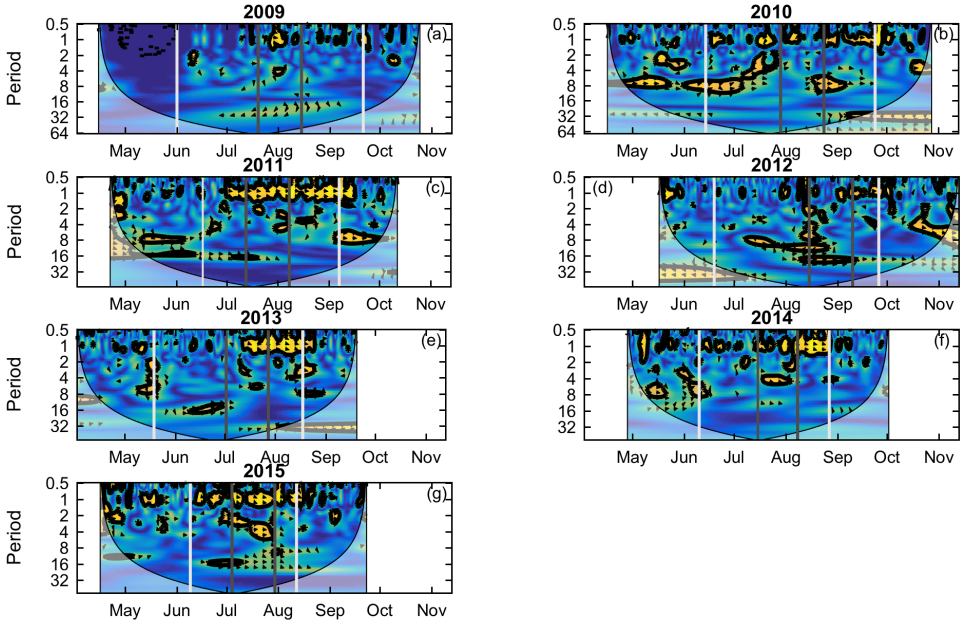

Figure 3.7. Wavelet coherence between latent heat flux (LE) and CH_4 flux (F_{CH4}) for the rice paddy during each growing season. Significant coherency (at the 5% level with 500 Monte Carlo simulations of AR-1 autocorrelation) is outlined by the black lines. The direction of the arrows show the phase angle between the two time series, where an arrow to the right with no inclination indicates no lag between the series. The cone of influence represents the limit where wavelet power drops to e^{-2} of the edge values. The solid vertical light gray lines indicate when the field when the field was fully flooded (ranging from mid-May to mid-June) and drained (ranging from mid-August to late September). The solid vertical dark gray lines show the approximate dates of panicle initiation (ranging from early July to mid-August) and heading (ranging from late July to early September).

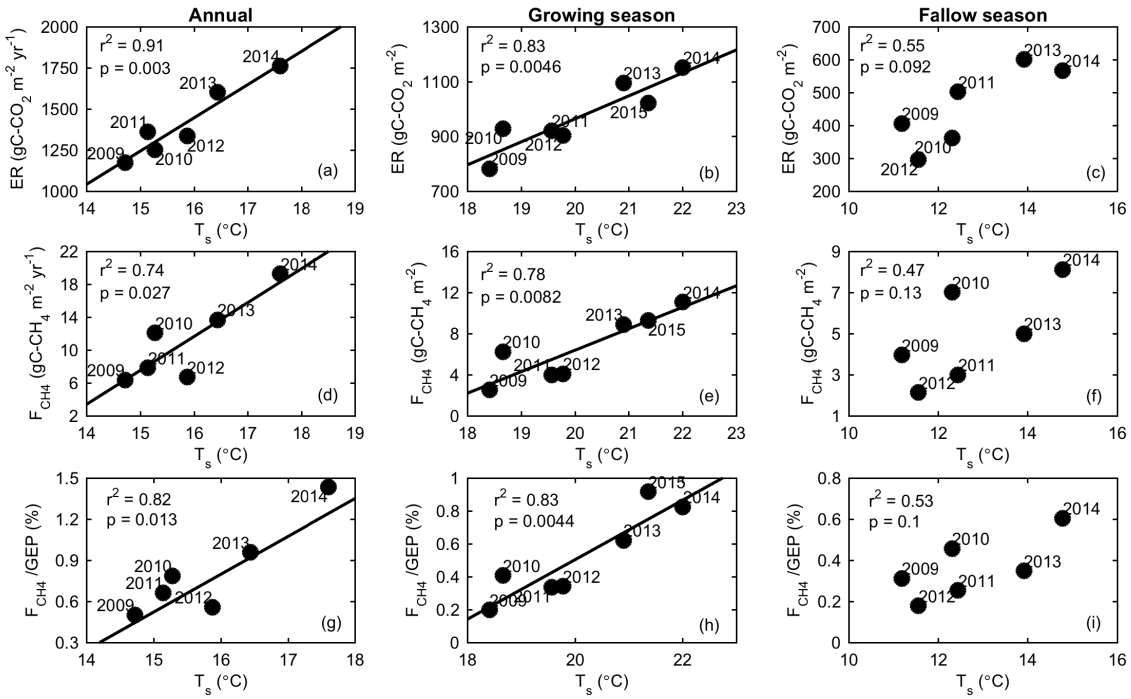

Figure 3.8. (a) Cumulative annual ecosystem respiration (ER) as a function of mean annual soil temperature (T_s) at 8 cm, (b) growing season ER as a function of mean growing season T_s at 2 cm, (c) fallow season ER as a function of mean fallow season T_s at 32 cm, (d) annual CH_4 emissions (F_{CH4}) as a function of mean annual soil temperature (T_s) at 8 cm, (e) growing season F_{CH4} as a function of mean growing season T_s at 2 cm, (f) fallow season F_{CH4} as a function of mean fallow season T_s at 32 cm, (g) ratio of annual F_{CH4} (g C-CH_4 m^{-2} yr^{-1}) to GEP (g C-CO_2 m^{-2} yr^{-1}) as a function of mean annual T_s at 8 cm, (h) ratio of growing season F_{CH4} (g C-CH_4 m^{-2}) to GEP (g C-CO_2 m^{-2}) as a function of mean growing season T_s at 2 cm, and (i) ratio of fallow season of F_{CH4} (g C-CH_4 m^{-2}) to growing season GEP (g C-CO_2 m^{-2}) as a function of mean fallow season T_s at 32 cm.

3.4.4.2. Seasonal scale

Unsurprisingly, the neural network models consistently resulted in overall higher R^2 values than the multiple linear models (Table 3.3). Across all growing seasons and within individual growing seasons, GEP and WTD were typically selected as the top two variables in the models. Both daily GEP and WTD were positively correlated with daily F_{CH4}, but exhibited non-linear relationships with daily F_{CH4}. WTD acted primarily as an 'on-off switch' for F_{CH4}, with the exception of drainage of the field for harvest when large pulses of CH_4 were released to the atmosphere, comprising between ~20-26% of the total CH_4 released throughout the growing season (Figure 3.3d). During the flooded summer period (excluding the end-of-season CH_4 pulse), daily F_{CH4} was strongly related to daily GEP (Figure 3.9). Analysis of covariance indicated that the

Table 3.3. Statistical tests (correlation coefficient (R), coefficient of determination (R^2), and Akaike Information Criterion (AIC)) for the significance of biophysical drivers in the models of daily methane flux (F_{CH4}), including pairwise linear[a,b], stepwise multivariate linear[b], and hierarchical neural network models.

		Pairwise	Stepwise Linear		Neural Network	
		R	R^2	AIC	R^2	AIC
Growing season						
2009-2015	GEP	0.622	0.386	2853	0.258	7704
	WTD	0.575	0.424	2793	0.462	7431
	ER	0.168	0.458	2737	0.713	6853
	LE	0.452	0.469	2718	0.751	6716
	u_*	0.147	0.470	2718	0.765	6671
	T_a	0.309	0.471	2717	0.814	6462
	T_s	0.195	0.474	2712	0.825	6420
2015	WTD	0.716	0.509	456	0.310	1248
	GEP	0.620	0.671	402	0.930	931
	T_s	0.307	0.682	398	0.943	914
	LE	0.631	0.697	392	0.954	898
	ER	-0.168	0.704	391	0.964	839
	u_*	0.348	0.702	*393	–	–
	T_a	0.275	0.702	*393	0.976	830
2014	GEP	0.729	0.528	454	0.396	1321
	WTD	0.704	0.557	445	0.942	981
	LE	0.569	0.588	435	0.947	980
	T_a	0.216	0.605	430	0.945	*1004
	u_*	*0.059*	–	–	–	–
	T_s	*-0.057*	–	–	–	–
	ER	*-0.009*	–	–	0.973	935

2013	GEP	0.731	0.532	507	0.474	1322
	ER	0.499	0.580	491	0.944	1000
	WTD	0.493	0.594	486	0.957	968
	LE	0.448	0.656	461	0.962	961
	T_s	0.282	0.657	461	0.984	787
	T_a	0.410	0.663	460	0.986	*790
	u*	*0.102*	–	–	–	–
2012	GEP	0.551	0.299	391	0.289	811
	T_a	0.359	0.344	382	0.379	800
	LE	0.238	0.348	382	0.725	709
	WTD	0.469	0.399	371	0.731	691
	T_s	0.319	0.397	*373	–	–
	ER	*0.148*	–	–	–	–
	u*	*0.042*	–	–	–	–
2011	GEP	0.731	0.531	224	0.539	733
	WTD	0.722	0.574	212	0.642	706
	ER	0.296	0.649	185	0.781	642
	T_a	0.413	0.656	183	0.792	642
	LE	0.608	0.654	*185	–	–
	u*	*0.111*	–	–	–	–
	T_s	*0.103*	–	–	–	–
2010	WTD	0.69	0.472	387	0.708	853
	GEP	0.609	0.481	386	0.877	731
	LE	0.466	0.488	385	0.905	720
	T_a	0.318	0.496	384	0.910	*735

	ER	*0.133*	–	–	–	–
	u_*	*0.071*	–	–	–	–
	T_s	*-0.07*	–	–	–	–
Fallow season						
2009-2014	ER	-0.39	0.15	1079	0.089	2649
	LE	0.237	0.201	1060	0.303	2566
	T_s	-0.38	0.215	1055	0.444	2500
	WTD	0.301	0.216	*1056	0.617	2442
	T_a	-0.345	0.216	*1057	–	–
	u_*	*0.062*	–	–	–	–

[a]Pairwise relationships indicate the direct (i.e. not incremental) correlation of each variable with daily F_{CH4}

[b]Daily F_{CH4} values were log-transformed before being fit with linear models

*Indicates that this variable was rejected from the model

Note: italic p-values indicate that the pairwise relationships were not significant and therefore not included in the stepwise linear models. Also, variables rejected from the stepwise linear models were tested in the neural network models and the results were only presented if the addition of the variable improved the overall R^2 of the model, and was justified by a reduction in the AIC of the model

parameters of the linear regression model of log-transformed daily F_{CH4} against daily GEP differed significantly between years, while pairwise comparisons of the slopes using Bonferroni critical values showed that regression coefficients were clustered into two groups, where slopes in 2009 to 2012 were significantly different from those 2013 to 2015 (Figure 3.9). Regression coefficients appeared to be strongly influenced by mean growing season T_s, with smaller slopes observed in cooler years (2009 to 2012), and significantly larger slopes observed in warmer years (2013 to 2015) (Table 3.2), explaining the increasingly non-linear relationship observed between daily GEP and F_{CH4} in the latter years of the study (Figure 3.9). Within more than half the individual growing seasons, ANNs using just GEP and WTD as input variables were able to explain more than 90% of the variance in daily F_{CH4} (Table 3.3), accurately capturing the non-linear relationships associated with CH_4 emissions. However, across all growing seasons, GEP and WTD together only accounted for 46% of the variance in daily F_{CH4}, indicating that additional variables are needed to account for the interannual variability in CH_4 emissions.

While mean growing season T_s was a significant factor explaining interannual differences in cumulative growing season F_{CH4} (Figure 3.8e), across all growing seasons ER rather than temperature appeared as the third variable in the ANN model, strongly increasing model R^2 (Table 3.3). The overall positive correlation between ER and CH_4 emissions indicates that ER and F_{CH4}, both products of microbial metabolism, were similarly affected by environmental regulators across years. The fact that ER improved the model beyond the contribution of other direct environmental drivers, including temperature, suggests that the common effects of these environmental drivers on soil respiration and F_{CH4} are complex and non-linear.

While ER strongly informed the model across all growing seasons, within individual years, there was frequently no significant relationship between ER or T_s and F_{CH4}. Since rice paddies are managed ecosystems, the timing of planting and flooding had a strong influence on the relationship between T_s and F_{CH4}, whereby planting in mid-April to mid-May followed by flooding a month of more later resulted in a decoupling between T_s and F_{CH4}; during the period of active rice growth daily F_{CH4} increased while daily mean T_s typically decreased of remained near constant (Figure 3.2b and Figure 3.3d). Consequently, even when there was a significant relationship between these variables, ER or T_s (or T_a) were typically only added as one of the later variables, resulting in only minor increases in model R^2.

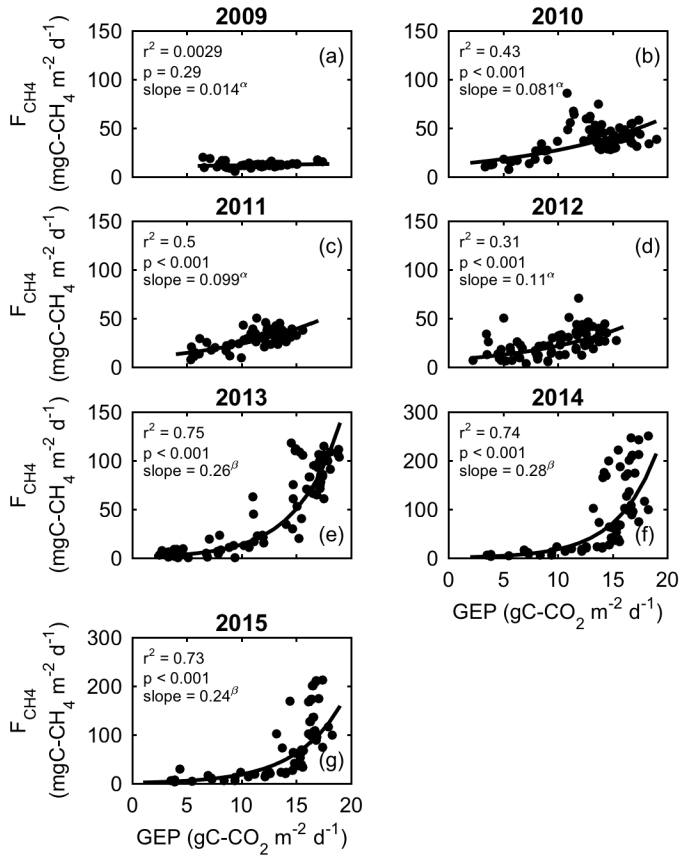

Figure 3.9. Linear regression models of log-transformed daily CH_4 emission (F_{CH4}) against daily gross photosynthesis (GEP) during the growing season from the time when the field was flooded to when water levels began to drop in preparation for harvest. Separate model parameters are fitted for each year. The lack of a significant relationship in 2009 is likely due to the larger amount of data that was excluded in that year (c.f. *Materials and methods*). Greek letters indicate statistically separate regression coefficients (i.e. slopes). Note the difference in the vertical axis in (f) and (g).

Within most years there was no significant relationship between u^* and F_{CH4}, and across all years, u^* was only selected at the fifth variable in the model, explaining only minor variations in daily F_{CH4}. LE was typically the third or fourth variable added to the models, but generally also only resulted in relatively small increases in model R^2.

During the fallow season, across all years (and within years; data not shown) daily F_{CH4} was negatively correlated with T_s and ER (Table 3.3). Conversely, across all years there was a significant positive relationship between fallow season T_s and ER ($r = 0.75$, $p < 0.001$). The overall negative correlation between daily ER and F_{CH4} during the fallow season suggests that during this period, their response to environmental drivers differed. LE was added as the second variable in the ANN model of fallow season daily

F_{CH4}, explaining an additional 21% of the variance in daily F_{CH4}. Although WTD wasn't a significant predictor of fallow season F_{CH4} in the stepwise linear model, the ANN was able to model the non-linear interaction between daily F_{CH4} and WTD, which is important for capturing the pulse of CH_4 to the atmosphere following water table drawdown in spring, as these CH_4 pulses accounted for on average > 50% of the total CH_4 emitted during the fallow period.

3.4.4.3. Diel scale

The diel pattern in F_{CH4} from rice paddies has often been attributed to diel variation in T_s (Khalil *et al.*, 1998, Meijide *et al.*, 2011, Schütz *et al.*, 1989a), which would be confirmed by the diel peak in T_s is temporally leading or coinciding with the peak in F_{CH4} (Hatala *et al.*, 2012a). However, in all years with a pronounced and consistent diel pattern in growing season F_{CH4} (2011, 2013, 2014, and 2015), T_s lagged F_{CH4} between 1.3 ± 0.04 hours (2015) and 5.2 ± 0.06 hours (2011) (Figure 3.10e,f,i,j,k,l,m). In contrast, the peak in GEP led that of F_{CH4} with a mean time lag varying between 1.6 ± 0.03 hours in 2011 and 4.4 ± 0.04 hours in 2015 (Figure 3.10e,f,i,j,k,l,m). While the time series of both growing season T_s and F_{CH4} and GEP and F_{CH4} were strongly coherent at the diel timescale (Figure 3.5 and Figure 3.6), the time lag between GEP and F_{CH4} in combination with phase-locked behavior (as indicated by the unimodal distribution of the phase angle; Figure 3.10f,j,l,n) provides strong support that GEP and not T_s likely caused the diurnal pattern in F_{CH4}. Although there is limited direct evidence for a link between stomatal conductance and CH_4 flux for rice plants, as stomata do not appear to be the major release site of CH_4 from rice plants (Nouchi & Mariko, 1993) (rather most CH_4 is released from the culm and both the abaxial epidermis of the lower portion of leaf sheath and near the junction of the nodal region and leaf sheath), we also investigated the hypothesis that canopy stomatal conductance (G_s) regulated CH_4 flux. G_s was calculated for the rice growing season by inverting the Penman-Montheith equation for LE, where the available energy was approximated using the sum of H+LE (Humphreys *et al.*, 2006). Figure 3.11 shows that G_s increased following sunrise and then began to decrease around noon each day. Although G_s led the diurnal peak of CH_4 flux (Figure 3.11), if G_s were driving F_{CH4}, we would expect to see a corresponding increase in F_{CH4} much earlier, with peak CH_4 emissions when stomatal conductance is greatest. Hatala *et al.* (2012a) found similar results for the 2011 growing season at the rice paddy, and further analysis using Granger causality showed that there was no direct causal link between G_s and F_{CH4}. This differs from other wetland plant species that also diffusively transport oxygen to roots (e.g. *Scheonoplectus acutus*), where stomatal aperture was found to regulate CH_4 emissions, with greatest CH_4 flux observed during peak light availability when stomatal aperture was largest (Sturtevant *et al.*, 2016, Van Der Nat *et al.*, 1998).

Although gas transport in rice plants occurs primarily through molecular diffusion (Chanton *et al.*, 1997, Den van der Gon & Van Breemen, 1993), a minor component may be due to transpiration-induced bulk flow as suggested from isotopic evidence and peak diel F_{CH4} coinciding with maximum daily transpiration rates (Chanton *et al.*, 1997). In this study, LE and F_{CH4} were also significantly coherent at the daily period (Figure 3.7), and varied nearly in phase (Figure 3.10f,j,l,n), indicating that the diel variation in F_{CH4} could also in part be associated with transpiration.

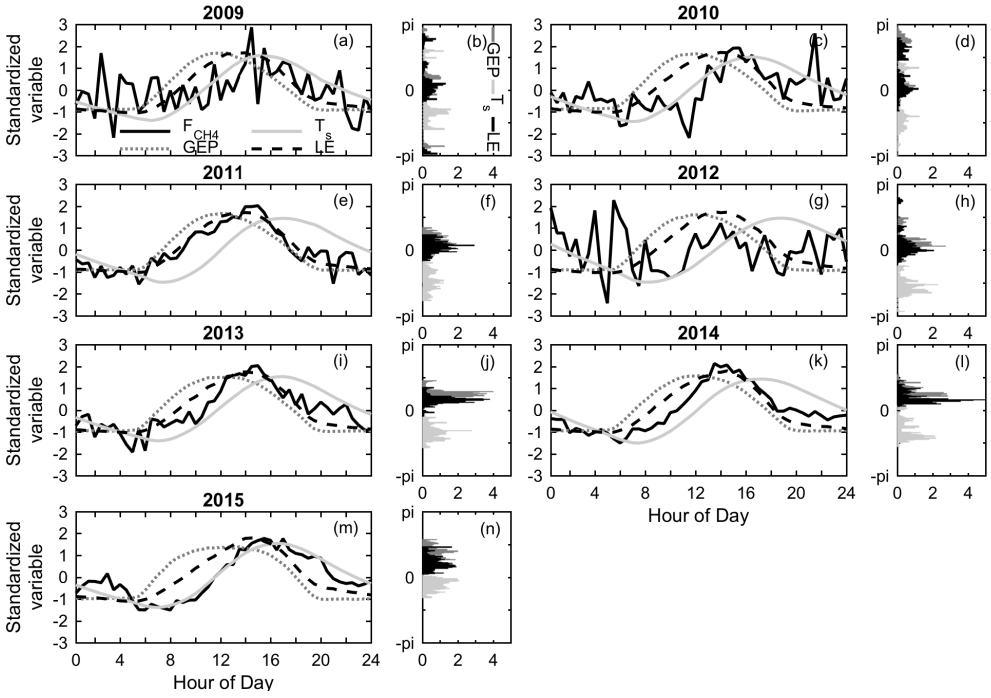

Figure 3.10. (a,c,e,g,i,k,m) Standardized (i.e. zero mean and unit variance) mean diurnal variation in CH_4 flux (F_{CH4}) (black line), photosynthesis (GEP) (dotted line), soil temperature (T_s) at 2 cm (gray line), and latent heat flux (LE) (dashed line) during the growing season averaged over the same period as Figure 3.4, and (b,d,f,h,j,l,n) distribution of the phase angles between F_{CH4} and GEP (dark gray bars), T_s (light gray bars), or LE (black bars) at the daily timescale for periods when there was significant coherence.

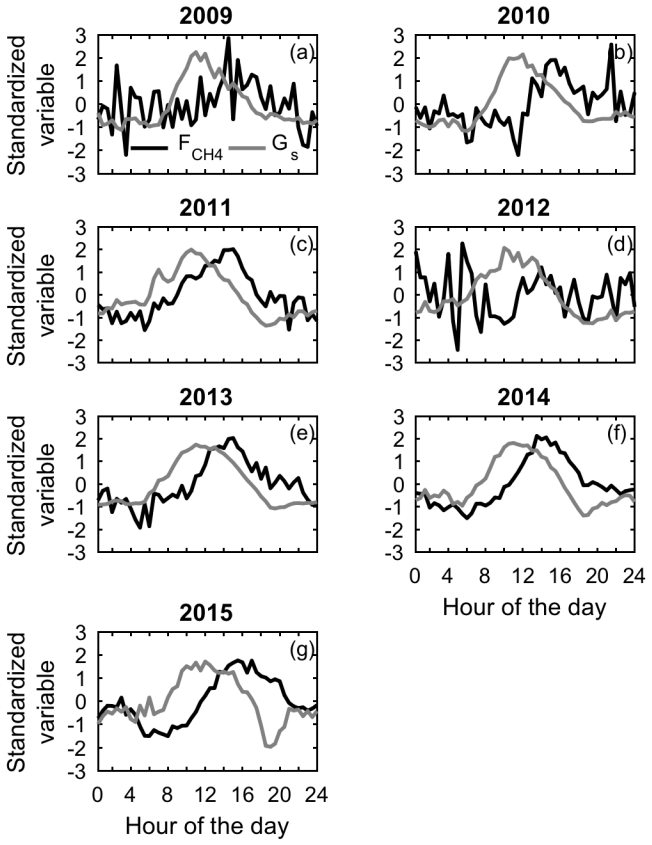

Figure 3.11. Standardized (i.e. zero mean and unit variance) mean diel variation in CH_4 flux (F_{CH4}) (black line) and stomatal conductance (G_s) (gray line) during the growing season when the field was flooded.

3.7. Discussion

3.5.1. Interannual variability in F_{CH4}

Soil temperature, which experienced large variability throughout the study due to record high temperatures experienced during this period (Griffin & Anchukaitis, 2014), explained much of the interannual variability in annual and growing season ER and F_{CH4}. This likely results from increased microbial activity with higher soil temperatures (Conrad, 2007, Yvon-Durocher *et al.*, 2014) and in the case of F_{CH4}, stronger temperature effects on CH_4 production than consumption, which is consistent with greater temperature sensitivity of methanogenesis than methanotrophy (Le Mer & Roger, 2001). This is also supported by the positive correlation between annual or growing season ER and F_{CH4}; increased overall microbial activity (i.e. enhanced ER) resulted in greater CH_4 emissions, suggesting higher temperatures disproportionately

influenced CH_4 production over CH_4 consumption (Morin *et al.*, 2014).

While several studies found that wetland net ecosystem production (NEP, where NEP = $-F_{CO2}$) or plant biomass were positively correlated with F_{CH4} (Bellisario *et al.*, 1999, Chanton *et al.*, 1997, Huang *et al.*, 1997b, Sass *et al.*, 1990, Whiting & Chanton, 1993), in this study, the growing season F_{CH4} to GEP ratio varied considerably from year-to-year, and GEP was not significant predictor of F_{CH4}. However, the ratio of annual or growing season F_{CH4} to GEP was significantly correlated with mean T_s, which is consistent and expected from the considerably higher temperature dependence of ecosystem-level CH_4 emissions relative to photosynthesis (Yvon-Durocher *et al.*, 2014), and follows the findings of Yvon-Durocher *et al.* (2014) who observed an increase in the CH_4 to CO_2 ratio with seasonal increases in temperature across a range of wetland sites. Our observation of an increase in the ratio of CH_4 to GEP with increasing temperature has implications for upscaling F_{CH4} from both rice paddies and wetland ecosystems.

Using the relationship between F_{CH4} and rice productivity, several studies have estimated CH_4 emissions from rice paddies at regional to global scales assuming that a constant fraction of net primary productivity (NPP) is released as CH_4 (Aselmann & Crutzen, 1989, Bachelet *et al.*, 1995, Bachelet & Neue, 1993, Taylor *et al.*, 1991). However, given the large interannual variability in the ratio of F_{CH4} to photosynthesis, upscaling CH_4 fluxes by estimating emissions as a constant fraction of NPP ignores an important source of variability (Cao *et al.*, 1995, Denier van der Gon *et al.*, 2000). Our results suggest that instead of estimating F_{CH4} as a constant fraction of productivity, F_{CH4} can be estimated as a variable fraction of GEP, which changes linearly with T_s. This relationship can potentially be used to help improve global estimates of CH_4 emissions from rice paddies. However, whether this relationship holds across or within other sites remains to be tested since few studies have made simultaneous measurements of CO_2 and CH_4 fluxes from rice paddies over the course of a full growing season or year. Based on a limited number of studies, the ratios of F_{CH4} to GEP reported for other rice paddies are slightly higher than the values measured in this study, which is consistent with warmer temperatures at these locations (Table 3.4). The F_{CH4} to GEP ratio may also be influenced by other factors known to influence CH_4 emissions. For instance, Huang *et al.* (1997a) found that the carbon ratio of seasonal CH_4 emission to NPP (deduced from grain yield) varied from 1.2% to 5.4%, with an average value of 2.8%, and that this ratio was soil and variety dependent. Additional variables that could influence this correlation include fertilizer type and application rate (Cicerone *et al.*, 1992, Lindau *et al.*, 1991, Naser *et al.*, 2007, Schütz *et al.*, 1989a, Yagi & Minami, 1990, Yan *et al.*, 2005), grain to biomass ratio (Denier van der Gon *et al.*, 2002) and floodwater management (Alberto *et al.*, 2014, Linquist *et al.*, 2015, Wassmann *et al.*, 2000a, Yagi *et al.*, 1996).

Table 3.4. Growing season mean air temperature (T_a), net CO_2 flux (F_{CO2}), CH_4 emissions (F_{CH4}) and ratio of CH_4 flux (F_{CH4}) to GEP from the literature as compared to the values reported in this study.

Location	Growing season	Mean T_a[c] (°C)	F_{CO2} (g C-CO_2 m^{-2})	F_{CH4} (g C-CH_4 m^{-2})	F_{CH4}/GEP (%)	Reference
California, USA	2009	19.6	-486	2.5	0.2	This study
California, USA	2010	18.6	-607	6.2	0.4	This study
California, USA	2011	18.7	-261	4.0	0.3	This study
California, USA	2012	19.0	-294	4.1	0.3	This study
California, USA	2013	20.2	-335	8.9	0.6	This study
California, USA	2014	20.5	-192	11.1	0.8.	This study
	2015	19.4	8	9.3	0.9	This study
	Average	19.4	-310	6.6	0.5	This study
Laguna, Philippines	2008 DS[a]	27.2	-241			*Alberto et al.* [2012]
Laguna, Philippines	2008 WS[b]	27.7	-375			*Alberto et al.* [2012]
Laguna, Philippines	2009 DS	27.2	-402			*Alberto et al.* [2012]
Laguna, Philippines	2009 WS	27.7	-293			*Alberto et al.* [2012]
Laguna, Philippines	2010 DS	27.2	-311			*Alberto et al.* [2012]
Odisha, India	2012 WS	31	-355	8.4	1.3	*Bhattacharyya et al.* [2014]
Odisha, India	2012-2013 DS	23.4	-341	12.9	2	*Bhattacharyya et al.* [2014]
Ibaraki, Japan	2002	20.7	-400			*Saito et al.* [2005]
Ibaraki, Japan	2003	23	-354	9.3	1.3	*Miyata et al.* [2005]
Okayama, Japan	2003	20	-438			*Miyata et al.* [2005]
Texas, USA	1994 & 1995	25.2			1.4[d]	*Huang et al.* [1997a]
California, USA	2002		-789			*McMillan et al.* [2007]

[a]DS - Dry season

[b]WS – Wet season

[c]Note that air temperature (T_a) was reported instead of soil temperature (T_s) since most studies did not report T_s

[d]Based on the mean carbon ratio of CH_4 to NPP of 2.8% and assuming NPP = 0.5GPP

Cumulative growing season F_{CH4}, which ranged from 2.5 to 11.1 g C m^{-2} (or 13 to 71 mg C-CH_4 m^{-2} d^{-1}), was low compared to other rice systems (cf. Table 4-9 IPCC, 1997, Yan *et al.*, 2005). For continuously flooded rice without organic amendment, CH_4 emissions are estimated to average 135 mg C-CH_4 m^{-2} d^{-1} (Yan *et al.*, 2005). Low CH_4 production in some peatlands has been attributed the fact that these soils have large amounts of high molecular weight organic compounds that can be very resistant to microbial degradation (Bridgham *et al.*, 2013), which is in agreement with a recent study at our site that showed the highly organic soil contained a large abundance of lignin and other aromatics, lipid, and aliphatics, which are likely not readily decomposable due to their chemical recalcitrance under anoxic conditions and can also be highly inhibitory to soil microorganisms (Ye *et al.*, 2016). Cooler soil temperatures at our site (typically in the range of 4 ± 2 °C cooler; c.f. Table 2 Huang *et al.* (1998)) compared to tropical or subtropical sites may also explain lower CH_4 fluxes (Neue & Sass, 1994, Wassmann *et al.*, 2000b). Additional factors potentially contributing to low F_{CH4} at our site may be differences in rice cultivar (Ding *et al.*, 1999a, Huang *et al.*, 1997a, Wassmann & Aulakh, 2000), soil properties (Aulakh *et al.*, 2001, Bachelet & Neue, 1993, Sass *et al.*, 1994) including the presence of electron acceptors, particularly ferric iron at this site (Ye *et al.*, 2015), and the relatively recent conversion of this site to rice agriculture which influences the amount of labile soil organic C, redox dynamics, and microbial community changes (Eusufzai *et al.*, 2010). Seasonal CH_4 totals lower than the ones reported in this study are generally observed in rice paddies with little or no organic amendments and/or mid-season or intermittent drainage (e.g. Alberto *et al.*, 2014, Bossio *et al.*, 1999, Bronson *et al.*, 1997, Cicerone *et al.*, 1992, Ding *et al.*, 1999a, Eusufzai *et al.*, 2010, Linquist *et al.*, 2015, Nishimura *et al.*, 2004, Yagi & Minami, 1990, Yagi *et al.*, 1996). Despite high C content soils and prolonged flooding periods, rice in the Delta emits less CH_4 relative to rice crops in warmer climates while also reducing the loss of soil through peat oxidation.

3.5.2. Seasonal variability in F_{CH4}

While daily F_{CH4} in natural wetlands has been found to be strongly explained by T_s (Chu *et al.*, 2014, Herbst *et al.*, 2013, Sturtevant *et al.*, 2016), the lack of a relationship between growing season F_{CH4} and T_s is commonly reported in the literature (Cicerone *et al.*, 1983, Huang *et al.*, 1997b, Huang *et al.*, 1998, Neue & Sass, 1994, Sass *et al.*, 1990, Schütz *et al.*, 1990), since the timing of management decisions can mask the relationship between F_{CH4} and soil temperature. Instead the seasonal variability in F_{CH4} may be due to the influence of other overriding factors such as plant growth and development (Le Mer & Roger, 2001, Sass *et al.*, 2000). The relationship between plant productivity and F_{CH4} is well established (Chanton *et al.*, 1997, Hatala *et al.*, 2012b, Huang *et al.*, 1997b, Whiting & Chanton, 1993), and similarly we observed a strong relationship between

daily F_{CH4} and GEP throughout the growing season, with GEP being an important predictor of daily F_{CH4}. Increased productivity can enhance CH_4 emissions by providing a greater number and larger diameter conduits from the reducing soil to the atmosphere and by providing C substrates for CH_4 production (Chanton *et al.*, 1997, Le Mer & Roger, 2001). Another possible effect of increased plant activity would be an increased supply of oxygen to the rhizosphere stimulating CH_4 oxidation, however, the results from this study suggest a net stimulation of CH_4 production by rice plants. Although variations in F_{CH4} during the crop cycle were not attributed to temperature variations, T_s did appear to have a strong influence on the amount of fixed C respired as CH_4, as indicated from the significantly larger slopes and increasingly non-linear relationship between daily GEP and F_{CH4} in the warmer, latter years of the study.

Water table depth was also a major controlling factor of seasonal F_{CH4}, both during the growing season and fallow period. WTD plays a key role in regulating the balance between CH_4 production and oxidation by influencing the depth of anaerobic and aerobic zones in the soil (Whalen, 2005). Fluctuations in water levels were also associated with large pulses of CH_4 to the atmosphere. As expected, ANNs better captured the non-linear influence of WTD on F_{CH4}.

Friction velocity and LE had considerably less influence on daily F_{CH4} than GEP and WTD over the course of the growing season. Increased turbulent mixing (i.e. higher u_*) can enhance CH_4 transport, although turbulent mixing has typically been found to be more important in regulating shorter-term (e.g. hourly) CH_4 fluxes (Chu *et al.*, 2014, Koebsch *et al.*, 2015). LE has been observed to be an important driver of F_{CH4} in wetlands across multiple timescales, as increased evaporation can enhance convective mixing at the water surface enhancing CH_4 transport, and CH_4 exchange and transpiration are linked through the mechanism of internal gas transport in wetland plants (Morin *et al.*, 2014, Sturtevant *et al.*, 2016). However, the weaker dependence of daily F_{CH4} on LE observed in this study can be explained by the fact that that transpiration likely dominated LE for most of the growing season and that plant-mediated gas transport in rice plants appears to be independent (Neue *et al.*, 1997, Seiler *et al.*, 1983) or only weakly dependent on transpiration rates (Chanton *et al.*, 1997). However, during the fallow period, LE was an important driver of F_{CH4}, potentially reflecting enhanced convective mixing and CH_4 transport with increased evaporation.

As observed by Morin *et al.* (2014), ER was an important variable for explaining CH_4 emissions. Across growing seasons, ER likely represented the end result of complex non-linear processes that similarly influenced CH_4 exchange, in particular the influence of T_s since it was a significant driver of year-to-year differences in CH_4 emissions. Incorporating ER in gap-filling models for CH_4 can therefore inform more

about CH_4 fluxes than models using only direct drivers (Morin *et al.*, 2014). While there was a positive relationship between ER and F_{CH4} across growing seasons, a negative relationship was observed across fallow seasons. This negative relationship likely reflects differences in the transport pathways between CO_2 and CH_4 during this time, due in large part to solubility differences. CO_2 is highly soluble in water, and many lakes (similar to our flooded and fallow rice field), are oversaturated with CO_2 and therefore there is a high rate of diffusive loss of CO_2 at the air-water interface, particularly in the winter when productivity is low (Casper *et al.*, 2000). Conversely, CH_4 is much less soluble, with lower concentrations predicted in the surface water as a consequence of oxidation at the oxic/anoxic boundary, and therefore CH_4 is more transport limited, with ebullition expected to be the dominant pathway of CH_4 emission to the atmosphere (Casper *et al.*, 2000). As a result of these differences in transport pathways, ER and T_s were positively correlated, while F_{CH4} was negatively correlated with ER and T_s during the fallow season.

3.5.3. Diel variability in F_{CH4}

Understanding drivers of diel variations in F_{CH4} has important implications for improving mechanistic models of CH_4 flux and for daily and seasonal extrapolation of studies that only measure daytime F_{CH4} (Hatala *et al.*, 2012a). While some studies report a diel pattern in CH_4 emissions from rice paddies (e.g. Bronson *et al.*, 1997, Chanton *et al.*, 1997, Ding *et al.*, 1999a, Satpathy *et al.*, 1997, Schütz *et al.*, 1989a, Yagi & Minami, 1993), others found none (Cicerone *et al.*, 1983, Yagi & Minami, 1990). Diel variations have often attributed to daily fluctuations in temperature (Den van der Gon & Van Breemen, 1993, Holzapfel-Pschorn & Seiler, 1986, Khalil *et al.*, 1998), however, several studies found no or poor correlations among these variables (Aulakh *et al.*, 2001). Using wavelet coherence (Grinsted *et al.*, 2004, Torrence & Compo, 1998) we showed the diurnal pattern in F_{CH4} can largely be attributed to GEP and not T_s, consistent with an earlier study at this site that reported on the diel pattern for the 2011 growing season (Hatala *et al.*, 2012a). Additional support for this finding comes from the fact that no diel fluctuation in F_{CH4} was observed during the fallow season although T_s showed a distinct diel variation, and from stable isotope labeling studies that showed a strong transient link between rice photosynthesis and F_{CH4}, with time lags between CO_2 assimilation and CH_4 emission from about 2 hours to 3 days (Dannenberg & Conrad, 1999, Minoda & Kimura, 1994, Minoda *et al.*, 1996). Although GEP appeared to induce the diel pattern in F_{CH4}, we found that mean T_s significantly influenced the amplitude of diel CH_4 fluctuations, again suggesting that the amount of photosynthetic C respired as CH_4 is strongly dependent on T_s. Temperature can also influence CH_4 transport through rice plants with conductance for CH_4 increasing with temperature (Le Mer & Roger, 2001). The increase in the amplitude of diel CH_4 variations with temperature

also helps explain why diel patterns were observed in some years but not others.

Our results also suggest that, in addition to photosynthesis, diel variations in F_{CH4} may in part be linked with transpiration, as a minor component of gas transport in rice may be due to transpiration-induced bulk flow (Chanton *et al.*, 1997). However, since diel patterns were only observed in some years, while transpiration-induced bulk flow is expected to occur in all years, it is unclear whether daily fluctuations are linked with transpiration. Furthermore, other studies have found that plant-mediated gas transport is independent of transpiration rate (Neue *et al.*, 1997, Seiler *et al.*, 1983). Similar to previous studies, we also ruled out the role of stomatal conductance in driving diel F_{CH4} (Chanton *et al.*, 1997, Hatala *et al.*, 2012a, Nouchi & Mariko, 1993) since F_{CH4} appears to be independent of stomatal opening as CH_4 is released to the atmosphere from various parts of the rice plant including from the culm and both the abaxial epidermis of the lower portion of leaf sheath and near the junction of the nodal region and leaf sheath (Nouchi & Mariko, 1993), with the development of nodes providing the major release pathway of CH_4 to the atmosphere at later growth stages (Wang *et al.*, 1997). Although this study strongly suggests that photosynthesis primarily caused the diel variation in F_{CH4}, more studies are needed to explicitly understand the role of temperature, photosynthesis, transpiration, and other factors (e.g. methane oxidation and transport, pH, microbial community changes) (Satpathy *et al.*, 1997, Schütz *et al.*, 1989b) in driving diel CH_4 patterns.

3.5.4. Interannual variability in net C budgets

By monitoring the rice field for seven growing seasons, we observed large variability in seasonal and annual net CO_2 and C budgets. Net CO_2 uptake at the site generally fell within the range of values reported for other irrigated rice paddies around the world, with the exception of 2014 and 2015, when uptake was reduced or the site was near-CO_2 neutral, respectively (Table 3.4). Considering the full annual C budget, including the amount of C lost as CH_4 and removed from the field through harvest, the site was on average a net C source, but showed considerable interannual variability with values ranging between -232 to 524 g C m^{-2} yr^{-1} (Table 3.2). Variability in net CO_2 budgets was strongly linked to the variability in ER, which is perhaps not unexpected as ER is a year-round process (Strachan *et al.*, 2015), with higher ER and a shift towards a positive C balance under warmer conditions. This is similar to studies of temperate freshwater marshes where interannual climatic variability caused marsh C budgets to vary considerably among years as a result of warmer temperatures enhancing ER and F_{CH4} (Chu *et al.*, 2015, Strachan *et al.*, 2015). As observed in natural and restored wetlands (e.g. Helfter *et al.*, 2015, Herbst *et al.*, 2013, Rocha & Goulden, 2008, Roulet *et al.*, 2007), we show that wetlands converted to agricultural land, a widespread practice

due to the economic benefit of the fertile soil (Kramer & Shabman, 1993), can exhibit strong interannual variability in CO_2 and CH_4 budgets. This highlights the need for more long-term flux measurements from both natural and managed wetlands under a range of climate conditions, since a warming climate is likely to have a strong influence on the net greenhouse gas balance and radiative forcing of these complex ecosystems (Petrescu *et al.*, 2015).

3.8. Conclusion

In this paper, we present six and a half years of eddy covariance measurements of CO_2 and CH_4 exchange from an irrigated rice paddy located in Northern California, and investigate the factors affecting CH_4 emissions across diel to interannual scales by using time series analysis and empirical modeling. Improved understanding of the environmental drivers of CH_4 emissions is critical for improving our ability to adequately model whole-ecosystem CH_4 emissions (Bridgham *et al.*, 2013). Based on wavelet analysis we showed that photosynthesis and not soil temperature was the dominant factor influencing the diel pattern in CH_4 flux, although soil temperature significantly influenced the amplitude of diel CH_4 fluctuations. Linear and neural network models indicated that during the growing season, photosynthesis and water levels explained much of the variance in daily average F_{CH4}. This differs from natural wetlands where soil temperature has frequently been observed to be an important factor regulating seasonal CH_4 fluxes due to the strong impact of the timing of rice planting and flooding on relationships with temperature. However, temperature strongly influenced the amount of photosynthetic carbon respired as CH_4. LE and u^* generally only explained minor variations in daily F_{CH4} during the growing season. Unsurprisingly, ANNs explained much more of the variance in daily F_{CH4} than the linear models. ANNs were able to capture between 73% and 98% of the variance in daily growing season CH_4 exchange and 62% of the variance in fallow season fluxes. Differences in R^2 values between years and the percentage of unexplained variance may be attributable to management as no management variables were included in the models. Future work could focus on explicitly incorporating management variables (e.g. fertilizer and herbicide application rates and timing, planting density, cultivar type, straw residue, etc.) into empirical models of F_{CH4}.

Soil temperature was a significant driver of interannual differences in annual and growing season CH_4 sums. Temperature also had a strong influence on the annual and growing season ratio of CH_4 flux to productivity, with this ratio increasing significantly with mean soil temperature. While previous studies have upscaled CH_4 emissions from

rice by simply relating them to primary production, our results suggest that the relationship between the carbon ratio of CH_4 to photosynthesis and soil temperature may help improve global estimates of CH_4 flux from rice paddies. More studies, however, are needed to assess if this relationship holds across or within other rice paddies and wetlands in general. The pronounced variation in temperature observed throughout the study also had a strong influence on ecosystem respiration, which resulted in large interannual variability in net carbon budgets at the paddy, highlighting the need for long-term measurements particularly under changing climatic conditions.

Chapter 4: Using digital camera and Landsat imagery with eddy covariance data to model gross primary production in restored wetlands

4.1. Abstract

Wetlands have the ability to accumulate large amounts of carbon (C), and therefore wetland restoration has been proposed as a means of sequestering atmospheric carbon dioxide (CO_2) to help mitigate climate change. There is a growing interest in using the C services of wetlands to help reduce habitat loss and finance restoration projects. However, including wetlands in C markets worldwide requires a better understanding of CO_2 and methane exchange in these systems and models that can accurately and cheaply predict these fluxes. Remote sensing technology, including both near-surface and satellite instruments/approaches, is an effective tool for modeling C fluxes including gross primary productivity (GPP) from site to global scales. In this study, we evaluate the potential of using digital cameras as simple and cost-effective means of estimating GPP in restored wetland ecosystems, and assess the suitability of using Landsat data to model GPP in these environments for regional upscaling. Our research focused on restored temperate freshwater marshes due to the high C sequestration potential of these systems.

As observed in other ecosystems, daily GPP was strongly correlated with site greenness derived from camera imagery (GCC_{cam}). Based on this, we show the potential of using GCC_{cam} and eddy covariance data to develop and parameterize a light use efficiency (LUE) model to predict daily GPP. The LUE model combining GCC_{cam} and meteorological data was able to explain up to 91% of the variation in daily GPP at the restored marshes, and predict annual GPP budgets within 0% to 20% of observed budgets. However, model performance decreased with increasing site complexity, highlighting the need to explicitly consider spatial heterogeneity in LUE models. We also tested a similar model using Landsat-derived indices, and found that although model performance was high at a homogeneous wetland dominated by emergent vegetation, data-model agreement decreased at a site comprised of a mixture of open water and vegetation, reflecting limitations of Landsat data. Nonetheless, we show that digital camera and Landsat imagery can be used to model photosynthesis in restored wetlands, providing low-cost methods for monitoring carbon cycling in these systems that can be used in C market-funded wetland conservation and restoration.

4.2. Introduction

Wetlands play an important role in global carbon (C) dynamics due to their large soil C pools, high methane (CH_4) fluxes, and potential for C sequestration in soils and biomass (Mitra et al. 2005, Bridgham et al. 2006). For example, although wetlands cover only 2 to 6 % of the earth's land surface, they store a considerable proportion of the C in terrestrial soil reservoirs (~15×10^2 Pg) (Kayranli et al. 2009). Much of this C resides in peatlands, defined as wetland environments with > 40 cm of surface organic matter, which contain 16-33 % of the global soil C pool (Bridgham et al. 2006).

Due to their ability to accumulate large amounts of C, as a result of limited decomposition rates in anaerobic soils and potential for high productivity, there has been a growing interest in the greenhouse gas mitigation potential of wetland restoration (Merrill et al. 2010, Mack et al. 2012, Hiraishi et al. 2014). Wetland restoration and conservation projects can play an important role in managing atmospheric C (Pendleton et al. 2012), provided conditions are optimized to minimize CH_4 emissions. Freshwater marshes are especially productive ecosystems with a large capacity to sequester CO_2, as rates of net primary productivity can be comparable to that of tropical forests and intensive agricultural ecosystems (Rocha and Goulden 2009, Miller and Fujii 2010). In addition to C sequestration, wetlands offer numerous environmental co-benefits and ecosystem services, including wildlife habitat, improved water quality, and flood protection (Costanza et al. 1997, Zedler and Kercher 2005). Wetland destruction and degradation is widespread, with over 50 % lost globally (Zedler and Kercher 2005). Consequently, there is broad interest in using greenhouse gas offset programs and markets to help reduce habitat loss and finance restoration project (Emmett-Mattox et al. 2011, McLeod et al. 2011). However, including wetlands in C markets worldwide requires a better understanding of C cycling in these systems and models that can accurately and cheaply predict C fluxes.

Remote sensing technology is an effective tool for modeling C fluxes including gross primary productivity (GPP) and net primary productivity (NPP) from site to global scales (Ruimy et al. 1999, Running et al. 2004, Xiao et al. 2004, Hilker et al. 2008). Greenness indices from digital repeat photography, a form of near-surface remote sensing, has recently been shown to be strongly correlated with canopy-scale photosynthesis in deciduous broadleaf forests, evergreen needleleaf forests, grasslands, croplands (Ahrends et al. 2009, Rossini et al. 2010, Migliavacca et al. 2011, Keenan et al. 2014, Toomey et al. 2015), however, whether camera-derived greenness can predict canopy-scale photosynthesis in wetland ecosystems is largely unexplored (e.g. Westergaard-Nielsen et al. 2013). Spaceborn remote sensing has traditionally been used to provide regional and global estimates of GPP (Running et al. 2000, Heinsch et al.

2006, Kalfas et al. 2011, Ryu et al. 2011). Current satellite remote sensing-based GPP models have largely been developed and validated for forest, crop, and grassland ecosystems (e.g. Heinsch et al. 2006, Sims et al. 2008, Sjöström et al. 2011, Gitelson et al. 2012), with a limited number of studies focused on wetland ecosystems (Kang et al. 2014, Wu et al. 2015). Most of these satellite-based studies have used the light use efficiency (LUE) approach to estimate GPP (Xiao et al. 2004), which is based on the work by Monteith (1972) and Monteith and Moss (1977) relating gross photosynthesis to the amount of photosynthetically active radiation absorbed by photosynthetic biomass and the radiation use conversion efficiency of the vegetation (Heinsch et al. 2006).

Since 1999, the National Aeronautics and Space Administration (NASA) has provided GPP estimates for the entire globe based on the Moderate Resolution Imaging Spectroradiometer (MODIS) 1 km products (e.g. Running et al. 2000, Running et al. 2004). While the MODIS GPP algorithm provides reasonable spatio-temporal patterns and variability across a diverse range of biomes and climate types (Heinsch et al. 2006), it has been shown to underestimate GPP in natural wetlands (Kang et al. 2014) and flooded rice agriculture (Xin et al. 2016), which has been attributed to the climate data, pixel heterogeneity, and the light use efficiency parameter used in the model. Furthermore, for some wetland types, the deciduousness of these systems and the presence of standing litter can complicate estimation of the fraction of radiation absorbed by photosynthetically active elements of plants (Rocha et al. 2008). The coarse spatial resolution (1 km) of MODIS can also be problematic for estimating wetland GPP as these ecosystems can be small in size, and highly distributed, fragmented or disconnected from other habitat types (Byrd et al. 2014). Possible alternatives to MODIS are the Landsat Thematic Mapper (TM), Landsat Enhanced Thematic Mapper (ETM), and Landsat Operational Land Imager (OLI) products, which have considerably finer spatial resolution (30 m pixel), spectral sensitivity in electromagnetic regions characteristic of vegetation function and are available at no cost. Landsat data may therefore provide useful information to facilitate the analysis of CO_2 fluxes in wetland ecosystems. With the opening of Landsat archives to free and web-based access, the use of the sensor data with much greater spatial resolution may be well suited to accurately estimating GPP in natural and restored wetland ecosystems.

Based on the broad interest of including wetlands in greenhouse gas offset programs and markets, our aim is to provide accurate and inexpensive means of modeling wetland GPP that is relevant to C market-funded wetland restoration, thereby advancing the opportunity to counteract the widespread degradation of wetlands worldwide. Specifically, the objectives of this study were to: 1) Evaluate the potential use of digital cameras as a simple and low-cost means of estimating GPP in wetland ecosystems, and 2) Assess the suitability of using Landsat data to model GPP in these

environments. We combine eddy covariance CO_2 fluxes measurements, flux footprint analysis, and near-surface or satellite remote sensing data to investigate the potential of using the light use efficiency approach to accurately and cost-effectively estimate GPP in wetland systems.

4.3. Materials and methods

4.4.1. Study sites

We focus on two freshwater marshes in the Sacramento-San Joaquin River Delta, California, USA (hereafter, the Delta). This study was designed to help inform methodologies to quantify greenhouse gas emission reductions from wetland restoration, including the methodology currently being developed specifically for the Sacramento-San Joaquin Delta (Deverel et al. 2016, Oikawa et al. 2016). Wetland restoration in the Delta offers large C removal potential. Since drainage of the wetlands in this region for agriculture around 1850, islands in the Delta have subsided between 3 and 8 m below sea level due largely to peat soil oxidation (Rojstaczer and Deverel 1993, Deverel and Leighton 2010). This peat soil oxidation corresponds to roughly 200 Tg of C lost since drainage, making it a large atmospheric C source (Oikawa et al. 2016). Restoring drained and degraded peatlands in the Delta back to wetlands can help recover soil C and reverse soil subsidence as these ecosystems can sequester over 350 g C-CO_2 m^{-2} yr^{-1} (Knox et al. 2014). Previous studies in the Delta have shown that converting a corn field to a wetland can have a greenhouse gas benefit up to 2.5 kg CO_2eq m^{-2} yr^{-1} after accounting for CH_4 emissions with a global warming potential of 32-45 times greater than CO_2 over a 100 year time horizon (Knox et al. 2014, Neubauer and Megonigal 2015).

Field measurements were collected at two restored wetland sites in the Delta: West Pond wetland and Mayberry wetland (Figure 4.1). The West Pond site (38.0498°N, 121.7650°W) is a 7 acre wetland that was built in 1997 (Miller et al. 2008, Miller and Fujii 2010). The site is permanently flooded to a depth of ~25 cm, and contains virtually no areas of open water. The wetland is narrow, only about 75 m wide, and characterized by a high intermixing of emergent marsh species, including *Schoenoplectus acutus* and *Typha* species. A dense layer of dead *S. acutus* stems 1 to 2 m tall mixed with other plant litter has accumulated at this site. We began eddy covariance measurements of CO_2, CH_4, water and energy at this location in July 2012.

The Mayberry site is a considerably larger restored wetland (300 acres) that was

constructed in 2010. Flux measurements at this site were initiated shortly after construction (October 2010). Unlike the West Pond wetland, a heterogeneous bathymetry was excavated to generate regions of shallow water (a few centimeters) and adjoining areas of deeper water (1 – 2 m deep). As a result, these wetlands are spatially heterogeneous, consisting of a mix of open water and vegetation patches (Figure 4.1), also comprised of *Typha* sp. and *Schoenoplectus acutus*. Vegetation dynamics at the site are controlled by in-filling of vegetation following flooding in 2010, with percent cover of emergent vegetation increasing from 0 to 63 % from 2010 to 2012, and changing very little thereafter (Matthes et al. 2014). Plant litter only began accumulating at the site following the 2012 growing season. Similar to the West Pond site, this wetland is permanently flooded to maximize peat accretion and C sequestration.

Figure 4.1. Flux tower locations and climatological footprints for the two restored wetlands. For the climatological footprints, data were separated by year at the Mayberry wetland since vegetation height and percent cover along with tower height changed throughout the study. Data were not separated by year at West Pond since tower height remained the same throughout the study and vegetation cover and height was roughly similar between years. At both wetland sites, the contours represent the 85% flux footprints.

4.4.2. Eddy covariance flux measurements and micrometeorological data

Biosphere-atmosphere exchange of CO_2 (NEE), CH_4, water and energy were measured using the eddy covariance technique (Baldocchi *et al.*, 1988) as described in Knox *et al.* (2015). A suite of meteorological measurements including air temperature (T_a), relative humidity, water table depth, incoming and outgoing shortwave and longwave radiation, incoming and reflected photosynthetically active radiation (PAR), and soil and water temperature accompanied flux measurements, with details given in Knox *et al.* (2015). High-frequency 3-D wind speed components and virtual temperature were measured with a sonic anemometer (Windmaster, Gill Instruments

Ltd., Lymington, Hampshire, UK) at 4.6 m, and between 3.7 and 5.7 m above the typical water surface at the West Pond and Mayberry wetlands, respectively. The variable sensor height at Mayberry reflects the fact that the tower was raised as the vegetation increased in height over time. At all sites, open-path gas analyzers measured molar concentrations of CO_2, H_2O (LI-7500A, LI-COR Biosciences Inc., Lincoln, NE, USA), and CH_4 (LI-7700, LI-COR Biosciences Inc., Lincoln, NE, USA). Raw flux measurements were recorded at 10 Hz and eventually at 20 Hz on an analyzer interface unit (LI-7550, LI-COR Biosciences Inc., Lincoln, NE, USA), and half hourly fluxes were calculated using in-house MATLAB software (Mathworks Inc., Natick, MA, USA) (Detto *et al.*, 2011, Hatala *et al.*, 2012b, Knox *et al.*, 2015). Accompanying micrometeorological measurements were recorded as 30-minute averages on a datalogger.

As outlined in other studies at these sites (Knox *et al.*, 2015, Sturtevant *et al.*, 2016), flux measurements were gap-filled using an artificial neural network (ANN) approach. F_{CO2} was gap-filled with two separate ANNs, with one for daytime and another for nighttime conditions. Ecosystem respiration (ER) was estimated by extrapolating the ANN trained for nighttime F_{CO2} to the entire day, and GPP was calculated by subtracting gap-filled F_{CO2} from modeled respiration (i.e. NEE = ER – GPP).

4.4.3. Flux footprint modeling

We used an analytical two-dimensional footprint model to model the spatial origin of the flux measurements (Detto *et al.*, 2006, Hsieh *et al.*, 2000). The eddy covariance flux footprint indicates the spatial portion of the landscape represented by each half hourly eddy covariance flux measurement. The footprint model uses wind speed and direction, roughness length (z_o; m), displacement height (d; m), turbulence data and boundary layer stability to trace the probability that a certain air parcel measured by the eddy covariance sensors originated from any particular point within the landscape. This model has been tested against several data sets, and overall has been shown to succeed at reproducing the source region for flux measurements at eddy covariance towers in spatially heterogeneous ecosystems (Matthes *et al.*, 2014). The method of Pennypacker and Baldocchi (2015) was used to derive continuous estimates of canopy height, z_o and d. For the climatological footprints, data were separated by year at the Mayberry wetland since vegetation height and percent cover along with tower height changed throughout the study, resulting in considerable year-to-year differences in the integrated cumulative flux footprint (Figure 4.1). Data were not separated by year at the West Pond wetland since the tower height remained the same throughout the study and dynamics of vegetation cover and height were roughly the same between years. Here we show the 85% analytical footprint (i.e. the areal extent

from which 85% of the measured flux originated), because as the analytical footprint approaches 100%, the area of the footprint expands rapidly, although there is only a small contribution to the measured flux from this extensive area (Matthes *et al.*, 2014).

4.4.4. Digital camera set-up and image analysis

On both eddy covariance towers, a digital camera (i.e. 'phenocam') was installed in a fixed position, leveled with the horizon, with a view across the top of the canopy. Cameras were pointed toward the West, which corresponds to the dominant wind direction (Figure 4.1), and enclosed in waterproof housings. At both sites, Canon Powershot Series A provided JPEG images (image resolution of 10 MP, with three color channels of 8-bit RGB color information, i.e. digital numbers (DN) ranging from 0 to 255) at 30-minute intervals for 12 hours per day. With the exception of automatic exposure, all automatic camera settings were turned off (Richardson *et al.*, 2009).

Time series were first visually inspected for camera shifts and changes in field of view (FOV). The FOV remained largely unchanged at the West Pond wetland, however, larger shifts in the FOV were observed at the Mayberry wetland as the positioning of the camera changed a few times throughout the study (Figure 4.2). Noting these changes, images were processed to extract regions of interest (ROI) encompassing all portions of the wetland within the foreground (Figure 4.2).

To quantify canopy greenness, we calculated the green chromatic coordinate (GCC_{cam}), which is widely used to monitor canopy development and has been shown to be strongly related to GPP (Ahrends *et al.*, 2009, Migliavacca *et al.*, 2011, Richardson *et al.*, 2007, Sonnentag *et al.*, 2012, Toomey *et al.*, 2015)

$$GCC_{cam} = \frac{DN_G}{DN_R + DN_G + DN_B} \quad (1)$$

where DN is the digital number and R, G, and B indicate the red, green, and blue channels, respectively. We also computed another color index, the excess green (ExG_{cam}) index

$$ExG_{cam} = 2DN_G - \left(DN_R + DN_B\right) \quad (2)$$

which can be less noisy than GCC_{cam} in some ecosystems, although GCC_{cam} is generally more effective than ExG_{cam} in suppressing the effects of changes in scene illumination (Sonnentag *et al.*, 2012).

Color indices were calculated for the selected ROI for each image, and computed for images recorded between 1300 to 1500, although images with underexposed ROIs (defined as <15% color saturation) were excluded. Daily GCC_{cam} and ExG_{cam} values were calculated using a three-day running median filter. This reduced some of the

unwanted variability in the GCC_{cam} and ExG_{cam} due to changes in scene illumination compared to simply calculating a daily mean or median value. Sonnentag *et al.* (2012) suggest using a moving window approach that assigns the 90th percentile of all daytime values (0600 to 1800) within a three-day window to the centered day, resulting in three-day ExG_{cam} and GCC_{cam}. We also tested this method but found that it did not significantly increase correlations between camera-derived indices and daily GPP. Furthermore, here we calculate a daily GCC_{cam} value and reduced the computation time by only selecting images for a subset of the day.

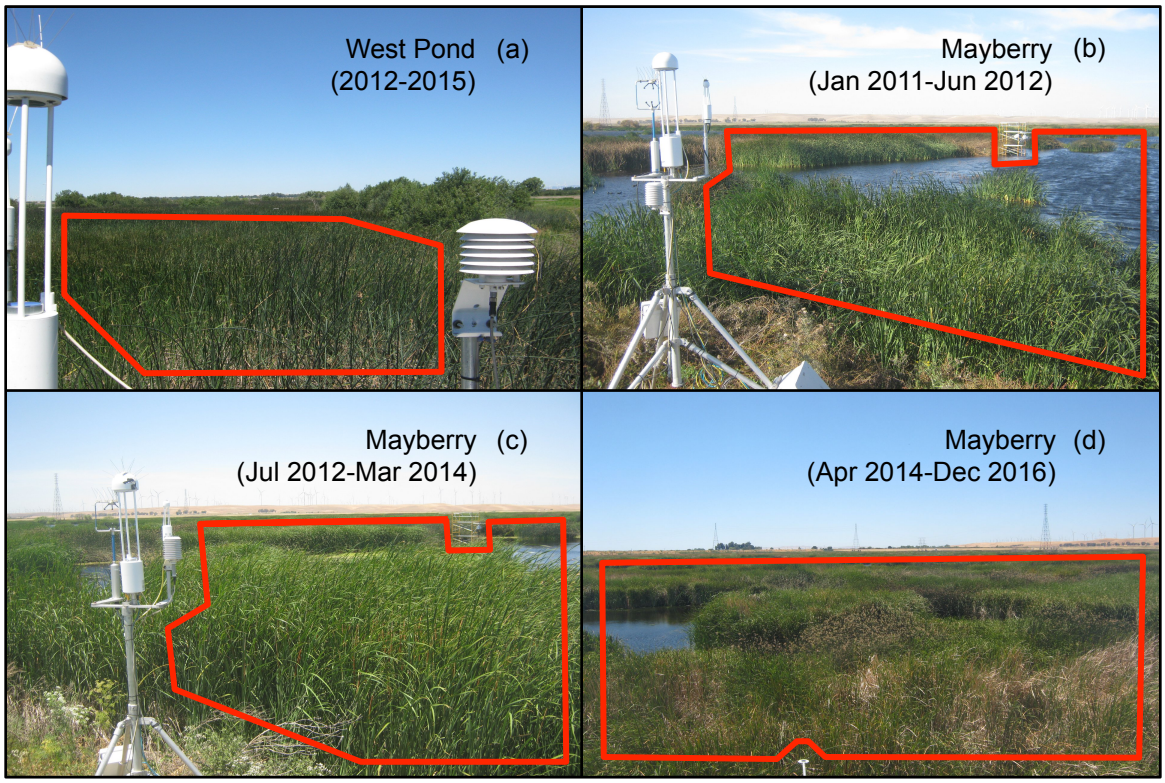

Figure 4.2. Examples of the digital camera images for West Pond (a) and Mayberry (b)-(d). As noted in the above, the field of view (FOV) changed a number of times throughout the study at the Mayberry wetland. Panels (b)-(d) show the major changes in the FOV at Mayberry. Polygons indicated the region of interest (ROI) for extracting image greenness.

Although the sites weren't equipped with a reference panel (Richardson *et al.*, 2007), we assessed the overall quality of the retrieved signal and the day-to-day stability of the imagery color balance by extracting a ROI from the white CH_4 analyzer (LI-7700) at the Mayberry wetland. The coefficient of variation of the GCC_{cam} calculated for this ROI was 0.23% during the 2013 growing season, which is over an order of magnitude smaller than the GCC_{cam} calculated for the primary ROI, giving us confidence in the quality of the retrieved signal (Migliavacca *et al.*, 2011).

4.4.5. Landsat data and vegetation indices

Spectral vegetation indices (VIs) were quantified from the archive of Landsat satellite imagery: Landsat 5 TM for 2010-2011, Landsat 7 ETM+ for 2012 and Landsat 8 OLI for 2013-2015. For each year, the images representing cloud-free conditions over the study area were selected as geo-registered, terrain-corrected Level 1T product converted to surface reflectance with Landsat Ecosystem Disturbance Adaptive Processing System (LEDAPS; Masek et al. 2006). Five of the Landsat spectral bands with 30 m spatial resolution were used in this study: blue (band 1: 450 – 520 nm for Landsat 5 and 7 and band 2: 450 – 510 nm for Landsat 8), green (band 2: 520 – 600 nm for Landsat 5 and 7 and band 3: 530 – 590 nm for Landsat 8), red (band 3: 630 – 690 nm for Landsat 5 and 7 and band 4: 640 – 670 nm for Landsat 8), near-infrared (band 4: 760 – 900 nm for Landsat 5, band 4: 770 – 900 nm for Landsat 7 and band 5: 850 – 880 for Landsat 8), and shortwave-infrared (band 5: 1550 – 1750 nm for Landsat 7 and band 6: 1570 – 1650 nm for Landsat 8). Using Google Earth Engine, a cloud-based geospatial data processing platform (https://earthengine.google.com/), Landsat pixels falling within the 85% climatological footprint of EC towers (Figure 4.1) were selected for subsequent analysis. Using their band reflectance values, seven VIs were quantified (Table 4.1) and summarized as footprint averages for the GPP estimation.

In addition to Landsat-retrieved normalized difference vegetation index ($NDVI_L$), we also calculated broadband NDVI from radiometric measurements at West Pond ($NDVI_{tower}$) as described in Richardson *et al.* (2007) since this site was equipped with both a four-component net radiometer and quantum sensors. Although broadband NDVI could not be estimated at the Mayberry wetland since this site only had a double-sided net radiometer, unlike West Pond, this tower was equipped with a spectral reflectance sensor, built in-house with light emitting diodes, allowing us to compute narrowband NDVI ($NDVI_{tower}$) as outlined in Ryu *et al.* (2010).

Table 4.1. Landsat-derived vegetation indices used in this study.

Vegetation index	Formula	Reference
Enhanced vegetation index (EVI_L)	$G\times(\rho_{NIR}-\rho_{red})/(\rho_{NIR}+C1\times\rho_{red}-C2\times\rho_{blue}+L)$	Huete *et al.* (2002)
Normalized difference vegetation index ($NDVI_L$)	$(\rho_{NIR}-\rho_{red})/(\rho_{NIR}+\rho_{red})$	Kriegler *et al.* (1969), Rouse *et al.* (1974)
Green NDVI ($GNDVI_L$)	$(\rho_{NIR}-\rho_{green})/(\rho_{NIR}+\rho_{green})$	Gitelson and Merzlyak (1997)
Soil enhanced vegetation index ($SAVI_L$)	$(\rho_{NIR}-\rho_{red}+L)/(\rho_{NIR}+\rho_{red})\times(1+L)$	Huete (1988)
Land surface water index ($LSWI_L$)	$(\rho_{NIR}-\rho_{SWIR})/(\rho_{NIR}+\rho_{SWIR})$	Xiao *et al.* (2004)
Green chromatic coordinate (GCC_L)	$\rho_{green}/(\rho_{green}+\rho_{red}+\rho_{blue})$	Woebbecke *et al.* (1995)
Excess green index (ExG_L)	$2\times\rho_{green}-(\rho_{red}+\rho_{blue})$	Woebbecke *et al.* (1995), Meyer *et al.* (1998)

4.4.6. Light use efficiency models

We used a light use efficiency (LUE) approach to estimate GPP

$$GPP = \varepsilon \times fAPAR \times PAR \quad (3)$$

where PAR is incident photosynthetically active radiation, ε is light use efficiency, and fAPAR is the fraction of PAR absorbed by the canopy, which was estimated as (Rossini *et al.*, 2010, Xiao *et al.*, 2004)

$$fAPAR = a_0 + a_1 VI \quad (4)$$

where a_0 and a_1 are the coefficients relating VI, retrieved from either tower measurements (i.e. GCC_{cam}, ExG_{cam}, $NDVI_{tower}$) or Landsat data (c.f. Table 4.1), and fAPAR, and were estimated against observed GPP.

Light use efficiency (ε) is affected by temperature and water stress (Kang *et al.*, 2014, Xiao *et al.*, 2004)

$$\varepsilon = \varepsilon_0 \times T_{scalar} \times W_{scalar} \quad (5)$$

where ε_0 is the apparent quantum yield or maximum LUE and T_{scalar} and W_{scalar} are the scalars for the effects of temperature and water on canopy light use efficiency. In this study, we used the down-regulation scalars from the satellite-based Vegetation Photosynthesis Model (VPM) (Xiao *et al.*, 2004).

ε_0 values vary with vegetation type, and in this study ε_0 was estimated from eddy covariance measurements by fitting a non-linear (i.e. rectangular hyperbola) model to the relationship between GPP and PAR, based on data collected during peak growing season (mid-July to mid-August) (Frolking *et al.*, 1998, Kang *et al.*, 2014)

$$NEE = \frac{\varepsilon_0 \times PAR \times GPP_{\max}}{\varepsilon_0 \times PAR + GPP_{\max}} + ER \quad (6)$$

where GPP_{max} is the maximum gross productivity. We used nonlinear least squares regression to fit the light response curves with a rectangular hyperbola (MATLAB, version 8.6.0, Mathworks Inc., Natick, MA, USA). This gave ε_0 values of 0.47 g C mol $PPFD^{-1}$ and 0.24 g C mol $PPFD^{-1}$ for the West Pond and Mayberry wetlands, respectively. Lower ecosystem-scale ε_0 at the Mayberry wetland reflects the fact that this is a heterogeneous canopy, and therefore at the canopy level ε_0 is influenced by the presence of both vegetation and open water.

For all VIs tested in the LUE model, T_{scalar} was estimated at each time step using the equation developed for the Terrestrial Ecosystem Model (Raich *et al.*, 1991), which is also used in the VPM model (Xiao *et al.*, 2004)

$$T_{scalar} = \frac{(T - T_{\min})(T - T_{\max})}{[(T - T_{\min})(T - T_{\max})] - (T - T_{opt})^2} \quad (7)$$

where T_{min}, T_{max}, and T_{opt} are minimum, maximum, and optimal temperature for photosynthesis, respectively. In this study, we used T_{min} of 0°C, T_{opt} of 22°C, and T_{max} of 50°C.

When Landsat-retrieved VIs were used in the LUE model, W_{scalar} was calculated using a simple approach utilizing a water-sensitive vegetation index (Xiao *et al.*, 2004)

$$W_{scalar} = \frac{1 + LSWI}{1 + LSWI_{max}} \quad (8)$$

where $LSWI_{max}$ is the maximum land surface water index (LSWI; Table 4.1) within the growing season, and was estimated separately for each year (Kang *et al.*, 2014).

3.5.5. Model parameter estimates and evaluation of model performance

Best-fit model parameters were estimated using linear least square regression implemented in MATLAB. At West Pond, model parameterization was conducted with data from 2012, 2013 and 2015, while data from 2014 were used for validation. Similarly, at Mayberry, all data excluding measurements from 2014 were used for model parameterization and data from 2014 were again used in validation. We selected 2014 as the validation period since there were minimal gaps in model drivers that year. Model performance was evaluated using the linear relationship between modeled and observed daily GPP (slope and intercept), the coefficient of determination (R^2), and the root mean square error (RMSE). We also explored the model's ability to predict annual and multi-year GPP budgets. When estimating modeled GPP sums, gaps in PAR and T_a were estimated using data from a nearby weather station. Continuous daily time series for both Landsat-derived and tower-based VIs were obtained by piecewise cubic interpolation (MATLAB).

4.4. Results

4.4.1. Seasonal dynamics of photosynthesis and vegetation indices

4.4.1.1. Tower-based indices

Both wetland sites exhibited clear seasonality in both daily GPP and GCC_{cam}, with high values during the primary growing season and low values during the inactive period (Figure 4.3). Both sites also showed considerable interannual variability

in GPP, particularly at the recently restored Mayberry wetland (Figure 4.3). GCC_{cam} closely paralleled year-to-year differences in GPP at both sites (Figure 4.3a,b). At Mayberry, with the exception of the first two growing seasons characterized by rapid vegetation growth and expansion, GCC_{cam} tracked daily GPP nearly synchronously, and was able to capture the decrease in GPP in the middle of the 2014 growing season caused by a caterpillar infestation at the site. At the West Pond wetland, daily GPP increased somewhat more slowly than GCC_{cam}, reaching maximum values up to ~4 weeks after GCC_{cam} reached peak values, and then tended to decline before the decrease in GCC_{cam}. Correlations between daily GPP and GCC_{cam} were high at both sites, ranging between 0.65 and 0.89 (Table 4.2). Lower correlations were observed at the Mayberry wetland in part due to the more heterogeneous nature of this site; as a result of the flux footprint moving over the mosaic of open water and vegetation, there was considerable day-to-day variability in GPP, however, this was not detected by GCC_{cam} (Figure 4.3b).

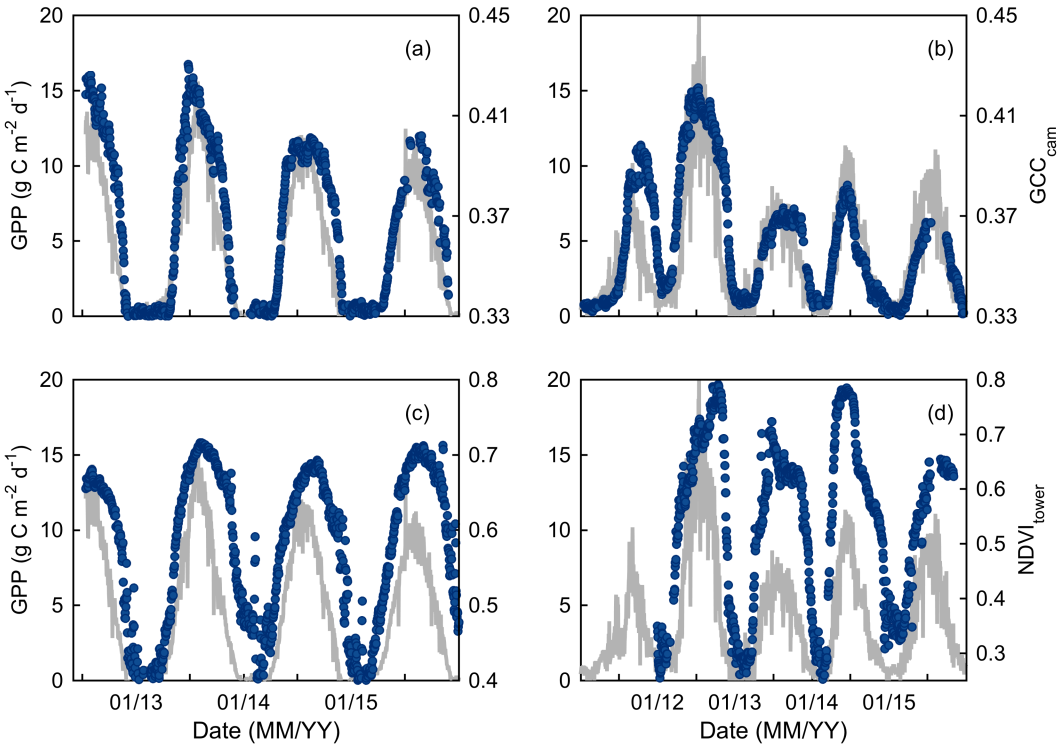

Figure 4.3. Time series of daily GPP (gray line; g C m^{-2} d^{-1}) and GCC_{cam} (camera-derived green chromatic coordinate, blue circles) for (a) West Pond and (b) Mayberry, and time series of daily GPP (gray line; g C m^{-2} d^{-1}) and $NDVI_{tower}$ (tower-based normalized difference vegetation index, blue circles) for (c) West Pond, and (d) Mayberry.

Across all years, the relationship between daily GPP and GCC_{cam} was essentially linear at both wetland sites (Table 4.2; Figure 4.4), although at Mayberry this relationship was influenced by the time since restoration. At this recently restored site,

in the first two years following restoration (2011 and 2012), when emergent marsh vegetation colonization and spread was rapid and there was very little accumulation of standing leaf litter, there was a non-linear relationship between daily GPP and GCC_{cam}, with higher GCC_{cam} values for a given daily GPP value than in subsequent years (Figure 4.4b). Following 2012, daily GPP scaled linearly with GCC_{cam} and the relationship between daily GPP and GCC_{cam} showed little variation between years, similar to the older West Pond wetland (Figure 4.4a,b).

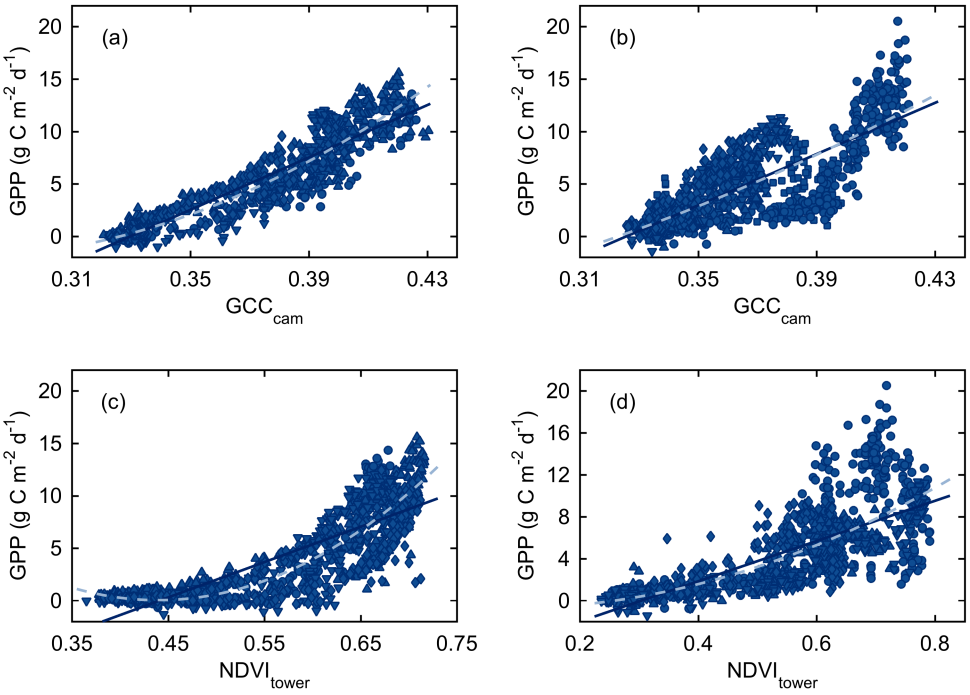

Figure 4.4. Scatter plots of daily GPP (g C m^{-2} d^{-1}) vs. GCC_{cam} for (a) West Pond, and (b) Mayberry, and vs. $NDVI_{tower}$ for (c) West Pond, and (d) Mayberry). Linear (dark blue) and quadratic lines (dashed light blue) are superimposed (see Table 4.2 for coefficients of determination). Different years are represented by difference symbols (2011 = squares, 2012 = circles; 2013 = upward-pointing triangles; 2014 = downward-pointing triangles; 2015 = diamonds).

At West Pond, the relationship between daily GPP and ExG_{cam} was similar to that observed for GCC_{cam} (Table 4.2), however, at Mayberry GCC_{cam} somewhat outperformed ExG_{cam} since GCC_{cam} was better able to capture interannual variability in GPP. Since GCC_{cam} was better correlated with daily GPP than ExG_{cam}, we focus on GCC_{cam} in the subsequent results.

Table 4.2. Coefficients of determination for linear (R^2) and quadratic regression (R^2_{quad}) of camera-derived greenness indices (GCC_{cam}, ExG_{cam}), tower-based NDVI ($NDVI_{tower}$), and Landsat-derived vegetation indices (EVI_L, $SAVI_L$, $NDVI_L$, $GNDVI_L$, ExG_L, GCC_L, $LSWI_L$) with daily GPP, and number of samples (n) corresponding to each vegetation index.

	West Pond			Mayberry		
	R^2	R^2_{quad}	n	R^2	R^2_{quad}	n
GCC_{cam}	0.88	0.89	1193	0.65	0.65	1650
GCC_{cam_L}[a]	0.93	0.92	41	0.85	0.71	59
ExG_{cam}	0.85	0.87	1193	0.55	0.55	1650
$NDVI_{tower}$	0.70	0.78	1307	0.58	0.59	1305
EVI_L	0.72	0.71	44	0.50	0.52	65
$SAVI_L$	0.71	0.70	44	0.47	0.49	65
$NDVI_L$	0.61	0.59	44	0.40	0.41	65
$GNDVI_L$	0.51	0.49	44	0.24	0.23	65
ExG_L	0.63	0.68	44	0.38	0.36	65
GCC_L	0.57	0.56	44	0.28	0.27	65
$LSWI_L$	0.64	0.62	44	0.40	0.39	65

[a]GCC_{cam_L} indicates GCC_{cam} measurements corresponding to the same dates as the Landsat imagery. Note that in 2015 there were three days when Landsat imagery was available but there were no available camera images, which explains the lower number of samples for GCC_{cam_L} (n = 41) compared with the Landsat VIs (n = 44).

Broadband NDVI measured at West Pond using radiometric measurements and narrowband NDVI estimated at Mayberry using an in-house built LED-sensor (both $NDVI_{tower}$) also showed clear seasonality, however, at both wetland sites $NDVI_{tower}$ showed poorer agreement with daily GPP compared with camera-derived indices (Table 4.2). Furthermore, $NDVI_{tower}$ at West Pond (and to a lesser extent at Mayberry) appeared to saturate at high GPP values (Figure 4.4c,d), making GCC_{cam} a better predictor of interannual variability in GPP (Table 4.2; Figure 4.3).

4.4.1.2. Landsat-based indices

All VIs retrieved from Landsat data showed strong seasonality, although some indices tracked GPP better than others (Table 4.2; Figure 4.5). Comparisons between VIs and daily GPP showed that at both wetland sites EVI_L and $SAVI_L$ had the strongest relationship with GPP (Table 4.2), as the seasonal dynamics of these indices followed the phase and amplitude of GPP better than the other VIs (Figure 4.5). Conversely, at

both wetlands, GCC_L and $GNDVI_L$ had the weakest relationship with GPP (Table 4.2). While VIs generally paralleled GPP relatively well across years, there were two notable discrepancies; all VIs at West Pond reached peaked values in 2015 although GPP was lowest during that growing season, and VIs at Mayberry remained high in 2013 despite a considerably drop in GPP that year. The regression of $LSWI_L$ against observed GPP also showed that land surface water content was significantly correlated with photosynthesis at both wetlands (Table 4.2). Again, GPP was better correlated with VIs at West Pond (R^2 = 0.49 to 0.72) than Mayberry (R^2 = 0.23 to 0.52) due to the more homogenous and less dynamic nature of the West Pond wetland.

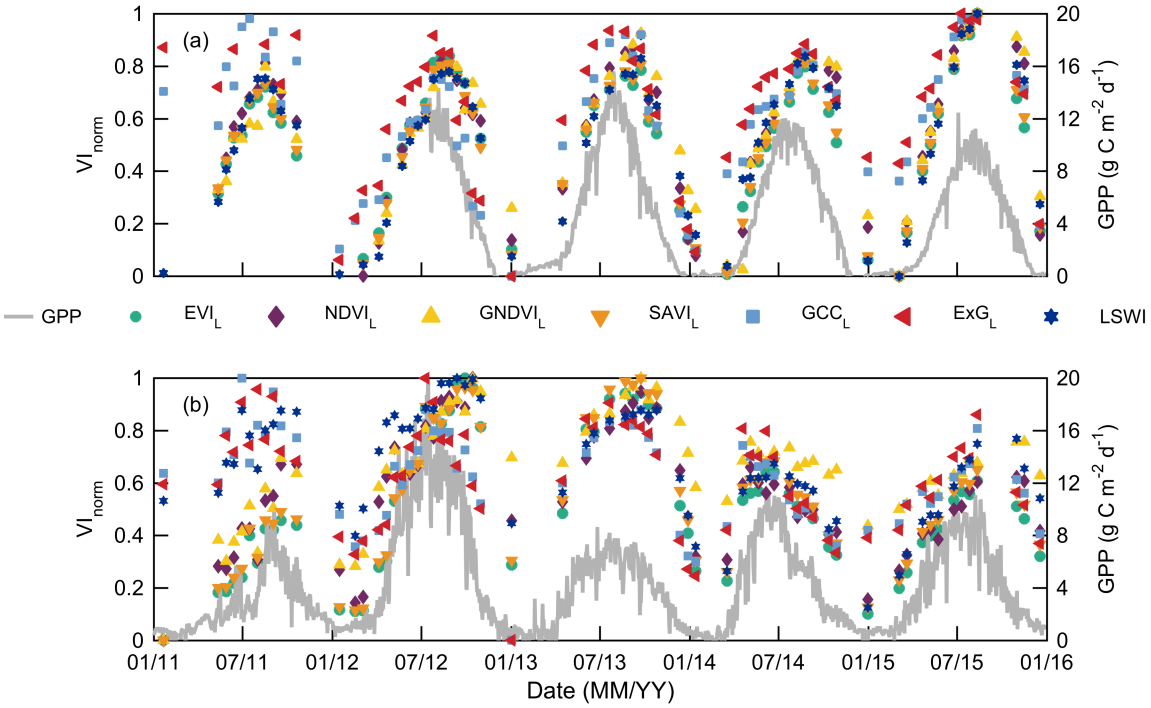

Figure 4.5. Time series of daily GPP (gray line; g C m^{-2} d^{-1}) and normalized vegetation indices (VI_{norm}) obtained from Landsat (see Table 4.1 for the description of each VI) for (a) West Pond and (b) Mayberry. Indices were normalized between 0 and 1 to allow all Landsat-derived VIs to be plotted on the same figure.

4.4.2. Model performance

4.4.2.1. Tower-based indices

Performance of the LUE model using GCC_{cam} as a proxy for fAPAR was strong, with high data-model agreement, particularly at the older, more homogeneous West Pond site (slope = 0.87, intercept = 0.71; R^2 = 0.90; RMSE = 1.32 g C m^{-2} d^{-1} calculated during the validation period) (Table 4.3; Figure 4.6). Nonetheless, despite higher

variability in GPP, model performance at the Mayberry wetland was also strong (slope = 0.75, intercept = 0.15; R^2 = 0.91; RMSE = 1.47 g C m^{-2} d^{-1} calculated during the validation period). At West Pond, the model overestimated GPP by only 3% during the validation period (2014) and underestimated GPP by 2% across the entire observation period (2013-2015) (Table 4.4). At Mayberry, discrepancies between measured and modeled annual GPP sums were larger, again due to the more dynamic nature of GPP within and across years, with the model overestimating GPP by 20% during the validation period (2014), but underestimating GPP by only 4% for the whole record (2011-2014) (Table 4.4). While modeled and observed daily GPP at Mayberry varied nearly in phase, at West Pond modeled GPP tended to peak a few weeks before observed GPP (Figure 4.6), largely as a result of daily GPP increasing somewhat more slowly than GCC_{cam} as described above (Figure 4.3). In addition, at both sites, the LUE model tended to underestimate GEP during less sunny conditions.

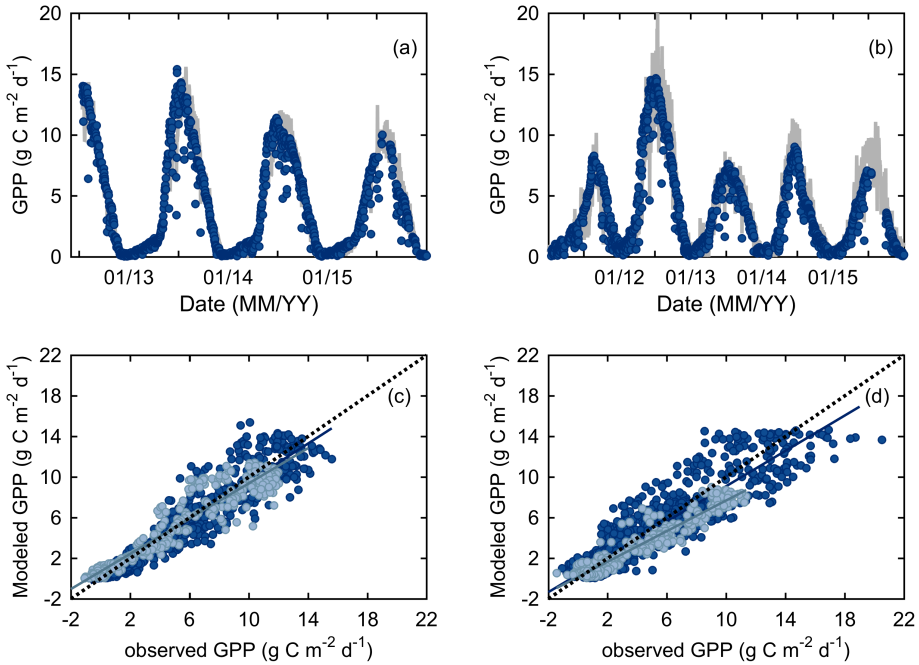

Figure 4.6. Modeled (blue circles), where GCC_{cam} was used as the vegetation index (VI) in the LUE model, and observed (gray line) daily GPP (g C m^{-2} d^{-1}) for (a) West Pond, and (b) Mayberry. For both wetlands, data from all years except 2014 were used in model parameterization and data from 2014 were used in model validation. (c) and (d) show data-model agreement for West Pond and Mayberry, respectively, where the dark blue circles indicate the parameterization period, and the light blue circles indicate the validation period. Solid dark blue and solid light blue lines indicate the line of best fit for the parameterization and validation periods, respectively, and the dotted line indicates the 1:1 line (see Table 4.3 for model performance statistics).

Table 4.3. Comparison of observed and simulated daily GPP at the West Pond (WP) and Mayberry (MB) wetlands during the parameterization (all years excluding 2014) and validation (2014) periods.

		R^2		Slope ($g\ C\ m^{-2}\ d^{-1}$)		Intercept ($g\ C\ m^{-2}\ d^{-1}$)		RMSE ($g\ C\ m^{-2}\ d^{-1}$)		n
		Param	Val	Param	Val	Param	Val	Param	Val	
WP	GCC_{cam}	0.91	0.90	0.94	0.87	0.16	0.71	1.29	1.32	1193
	GCC_{cam_L}	0.93	0.91	0.96	0.88	0.16	0.62	1.12	1.20	41
	$NDVI_{tower}$	0.90	0.93	0.86	0.84	0.79	1.17	1.36	1.31	1307
	EVI_L	0.83	0.97	0.81	0.76	1.21	0.99	1.74	1.16	44
	$SAVI_L$	0.83	0.98	0.80	0.79	1.23	0.93	1.75	1.04	44
	$NDVI_L$	0.83	0.97	0.79	0.78	1.34	1.12	1.75	1.09	44
	$GNDVI_L$	0.83	0.97	0.77	0.80	1.56	1.07	1.78	1.02	44
	ExG_L	0.79	0.85	0.74	0.70	1.64	2.23	1.97	1.78	44
	GCC_L	0.78	0.85	0.71	0.67	1.90	2.48	2.01	1.87	44
MB	GCC_{cam}	0.84	0.91	0.87	0.75	0.40	0.15	1.55	1.47	1650
	GCC_{cam_L}	0.83	0.90	0.86	0.63	0.60	0.90	1.55	1.75	59
	$NDVI_{tower}$	0.76	0.93	0.77	1.26	1.07	0.34	2.02	2.00	1305
	EVI_L	0.69	0.88	0.70	0.69	1.55	1.48	2.04	1.42	65
	$SAVI_L$	0.66	0.87	0.67	0.70	1.73	1.60	2.14	1.43	65
	$NDVI_L$	0.66	0.85	0.66	0.63	1.80	1.52	2.13	1.59	65
	$GNDVI_L$	0.62	0.80	0.59	0.63	2.19	2.33	2.26	1.81	65
	ExG_L	0.44	0.87	0.44	0.60	2.92	1.99	2.74	1.61	65
	GCC_L	0.42	0.80	0.40	0.56	3.21	2.56	2.78	1.90	65

Table 4.4. Average annual air temperature (T_a; °C) and time-integrated sums of photosynthetically active radiation (PAR; mol m^{-2}), eddy covariance estimated gross primary production (GPP_{obs}; g C m^{-2}), modeled GPP (GPP_{pred}; g C m^{-2}) for a range of vegetation indices, and comparison between observed and predicted GPP (relative error[a]; RE (%)) at both wetland sites.

			GCC_{cam}		$NDVI_{tower}$		EVI_L		$SAVI_L$		$NDVI_L$		$GNDVI_L$		ExG_L		GCC_L	
		GPP_{obs}	GPP_{pred}	RE	GPP_{pred}	RE	GPP_{pred}	RE	GPP_{pred}	RE	GPP_{pred}	RE	GPP_{pred}	RE	GPP_{pred}	RE	GPP_{pred}	RE
WP	2013	1780	1733	-3	1572	-12	1572	-12	1595	-10	1636	-8	1673	-6	1764	-1	1804	1
	2014	1513	1565	3	1442	-5	1442	-5	1462	-3	1507	0	1538	2	1708	13	1750	16
	2015	1411	1317	-7	1710	21	1710	21	1726	22	1757	25	1766	25	1783	26	1830	30
	2013-2015	4704	4615	-2	4724	0	4724	0	4783	2	4900	4	4977	6	5255	12	5384	14
MB	2011	974	1074	10	--	--	876	-10	904	-7	965	-1	919	-6	1443	48	1460	50
	2012	2318	2318	0	1902	-18	1702	-27	1649	-29	1772	-24	1688	-27	1482	-36	1543	-33
	2013	1276	1227	-4	1653	30	1931	51	1954	53	1850	45	1961	54	1572	23	1589	25
	2014	1405	1127	-20	1896	35	1306	-7	1352	-4	1246	-11	1495	6	1355	-4	1476	5
	2015	1514	--	--	--	--	1252	-17	1294	-15	1185	-22	1388	-8	1406	-7	1470	-3
	2011-2015	7487	5746[b]	-4[b]	5451[c]	9[c]	7067	-6	7153	-4	7018	-6	7451	0	7258	-3	7538	1

[a]$RE = [(GPP_{pred}-GPP_{obs})/ GPP_{obs}] \times 100\%$ (Kang *et al.*, 2014).

[b]Sum excludes 2015 due to the large gap in GCC_{cam} during peak growing season which makes gap-filling GCC_{cam} challenging and consequently annual integrated GPP_{pred} highly uncertain that year. The RE compares GPP_{pred} against GPP_{obs} across 2011-2014.

[c]Sum excludes 2011 and 2015 due to the limited number of $NDVI_{tower}$ in those years (Figure 4.3). The RE compares GPP_{pred} against GPP_{obs} across 2012-2014.

For both West Pond and Mayberry, model performance metrics indicated that data-model agreement tended to be slightly better when GCC_{cam} rather than $NDVI_{tower}$ was included in the LUE model (Table 4.3). Furthermore, when comparing observed and modeled GPP sums, the relative error was consistently lower when GCC_{cam} rather than $NDVI_{tower}$ was used as a proxy for fAPAR (Table 4.4). As noted previously, interannual dynamics of GCC_{cam} followed those of GPP better than $NDVI_{tower}$ since GCC_{cam}, unlike $NDVI_{tower}$, tended not to saturate.

4.4.2.2. Landsat-derived indices

All VIs resulted in overall reasonable agreement between predicted and observed GPP at the West Pond wetland (slope = 0.67 to 0.80, intercept = 0.99 to 2.48; R^2 = 0.85 to 0.98; RMSE = 1.02 to 1.87 g C m^{-2} d^{-1} calculated during the validation period). When considering individual VIs, EVI_L and $SAVI_L$ slightly outperformed the other indices while GCC_L and ExG_L resulted in the poorest agreement between predicted and observed GPP (Table 4.3). Despite the limited temporal frequency of Landsat, data were acquired at sufficient intervals to adequately capture seasonal dynamics of GPP (Figure 4.7). Interpolation of VIs between sampling dates resulted in overall good agreement between observed and modeled GPP sums when integrated across years (Table 4.4), with relative errors across the three full years of measurements (2013-2015) as low as 0% and 2% when EVI_L and $SAVI_L$ were included in the LUE model, respectively. Although relative errors across years were small, they were larger for individual years (Table 4.4). For instance, when considering EVI_L, the Landsat-derived VI resulting in best model performance, modeled GPP was underestimated by 12% in 2013 and overestimated by 21% in 2015 (Table 4.4; Figure 4.7).

Model performance across all VIs was lower at Mayberry, although again EVI_L resulted in best model performance (slope = 0.69, intercept = 1.48; R^2 = 0.88; RMSE = 1.42 g C m^{-2} d^{-1} calculated during the validation period), while GCC_L resulted in the lowest fit between predicted and observed GPP (Table 4.3). Similar to West Pond, the relative error across years was low (between -6% and 1%), although within years modeled GPP could be strongly over or underestimated (Table 4.4).

4.4.2.3. Tower-based vs. Landsat-derived VIs

Comparisons between VIs and GPP showed that GCC_{cam} followed the seasonal and interannual dynamics of GPP better than other VIs (Figure 4.3; Figure 4.5). As such, GCC_{cam} resulted in the best agreement between observed and predicted GPP when compared to the other VIs explored in this study (Table 4.3). Although this is in part related to the greater temporal frequency of GCC_{cam} relative to the VIs obtained from Landsat, even when GCC_{cam} was temporally downscaled to correspond to the

same dates as the Landsat imagery (GCC_{cam_L}), camera-derived GCC was still better correlated with daily GPP and resulted in stronger model performance compared with all Landsat-based VIs (Table 4.2; Table 4.3).

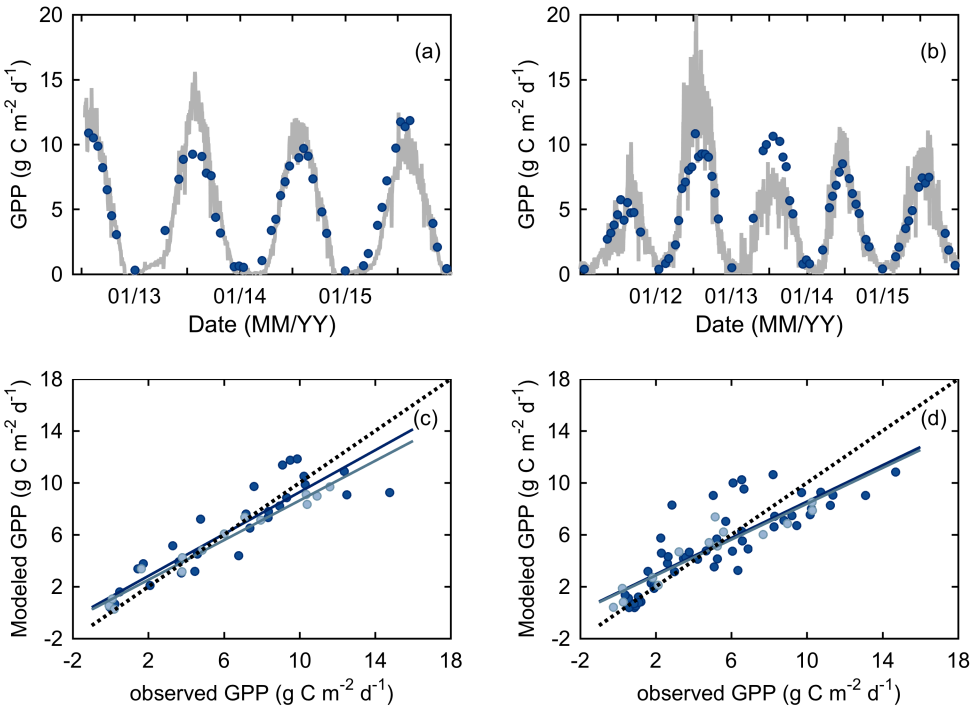

Figure 4.7. Modeled (blue circles), where EVI_L was used as the VI in the LUE model, and observed (gray line) daily GPP (g C m^{-2} d^{-1}) for (a) West Pond, and (b) Mayberry. For both wetlands, data from all years except 2014 were used in model parameterization and data from 2014 were used in model validation. (c) and (d) show data-model agreement for the West Pond and Mayberry wetlands, respectively, where the dark blue circles indicate the parameterization period, and the light blue circles indicate the validation period. Solid dark blue and solid light blue lines indicate the line of best fit for the parameterization and validation periods, respectively, and the dotted line indicates the 1:1 line (see Table 4.3 for model performance statistics).

4.5. Discussion

Wetlands are important ecosystems for C storage and thus provide valuable ecosystem services globally (Costanza et al. 1997, Syvitski et al. 2009). These systems have been degraded globally at a rapid rate (Zedler and Kercher 2005) and the cost of wetland restoration is high. With a growing interest in using C markets to fund

wetland restoration projects (Merrill et al. 2010, Mack et al. 2012), including California's Cap-and-Trade program (Deverel et al. 2016), there is a need for models that can precisely and cheaply predict C cycling in these ecosystems. In this study, we explored the potential of using a simple light use efficiency approach combining camera-derived greenness indices or Landsat-based vegetation indices and meteorological data to inexpensively and accurately estimate wetland photosynthesis.

4.5.1. Digital camera imagery for GPP modeling – strengths and limitations

As observed in other ecosystems, including forests, grasslands, and crops (Richardson et al. 2009, Migliavacca et al. 2011, Keenan et al. 2014, Toomey et al. 2015), GPP was highly correlated with greenness derived from camera imagery at both wetlands. At both sites, GCC_{cam} also strongly tracked interannual variability in GPP better than tower-based NDVI measurements, highlighting that interannual variation in annual GPP can be estimated using camera-derived color indices (Toomey et al. 2015). In freshwater marshes, the accumulation of standing litter is important for controlling interannual variability in CO_2 fluxes (Rocha and Goulden 2008, Rocha et al. 2008). GCC_{cam} at both sites was able to capture year-to-year differences in litter accumulation, with lower GCC_{cam} values reflecting years with higher standing litter, which shades the green leaves resulting in a reduction in GPP (Rocha et al. 2008).

We show that camera-based color indices combined with eddy covariance measurements are highly valuable for developing and testing LUE models to predict daily photosynthesis. Analysis of the LUE model highlighted that GPP can be accurately predicted by combining GCC_{cam} and meteorological data, similar to the results obtained by Migliavacca et al. (2011) for a subalpine grassland. We were able to explain up to 91% of the variation in GPP, and predict annual GPP budgets within 0% to 20% of observed budgets, and cumulative GPP across years to within 2% to 4% of observed values. However, as a result of the considerable differences between the wetlands, model parameters differed between sites (ε_0 = 47 g C mol $PPFD^{-1}$ and 0.24 g C mol $PPFD^{-1}$, a_0 = -1.4 and -2.6 and a_1 = 4.3 and 8.4 for West Pond and Mayberry, respectively). This reflects one of the drawbacks of using empirical approaches for estimating fAPAR (Hilker et al. 2008). Although re-parameterization of the model is required when applying it to other wetlands types (or when large differences are observed within wetland types), once the model has been developed for a representative site, it can be applied to other similar environments at minimal costs (i.e. the cost of a digital camera or webcam which runs from around $100 to $5000 USD; Brown et al. (2016)). While the West Pond wetland is representative of a densely vegetated freshwater marsh, most restored wetlands in the Sacramento-San Joaquin Delta resemble the Mayberry wetland, consisting of a mosaic of open water and

vegetation. From 2013 to 2015, over 3,000 acres of freshwater marshes were restored in the Delta, with more restoration projects anticipated in the future. Eddy covariance flux towers have recently been (or will be) installed at these newly restored sites and the use of cost-effective camera instruments will be particularly beneficial for validating and adapting the LUE model using measurements collected at these sites.

Since consumer-grade cameras are not calibrated scientific instruments, it is important to understand the strengths and limitations of the information they produce (Sonnentag et al. 2012, Brown et al. 2016). Camera hardware and image format have considerable impact on image quality (Brown et al. 2016), and GCC_{cam} and ExG_{cam} calculated for the same site and ROI using different camera types and models are not directly comparable (c.f. Figure 8 in Sonnentag et al. 2012). As such, consistency in camera hardware and image format, or the development of calibration protocols and standards is important when developing and applying LUE models across sites, particularly with a growing global digital camera – "phenocam" – network (Brown et al. 2016). These limitations and uncertainties need to be addressed in order to improve the reliability of camera-based color indices for monitoring and modeling canopy phenology and photosynthesis.

Several studies have suggested the use of a gray reference panel placed in the digital cameras' FOV to provide a first-order means of assessing the continuity and stability of GCC_{cam} over time and/or standardizing images taken under different lighting conditions or across sites (Richardson et al. 2009, Migliavacca et al. 2011, Sonnentag et al. 2012, Richardson et al. 2013). This is particularly important for multiyear studies as the sensitivity of different camera channels was observed change over time, and the drift appeared to be camera-specific (Ide and Oguma 2010). This was not assessed in this study, and future research focused on calibration and standard development is strongly needed to facilitate multi-site comparisons, and enhance the value of long-term studies from individual sites (Richardson et al. 2013).

Due to the changes in tower set-up and camera location at the Mayberry site, the FOV and ROI changed several times throughout the study (Figure 4.2). Despite these changes in the FOV, GCC_{cam} and daily GPP were strongly correlated and high data-model agreement was observed. However, the relationship between GCC_{cam} and GPP could have potentially been improved by minimizing changes in the FOV, since for phenocam data it is recommended to maintain a consistent FOV to ensure long-term data continuity and facilitate automated processing (Brown et al. 2016). Therefore, studies should be designed to minimize changes in camera positioning and location to maintain a continuous image record of a consistent FOV for as long as possible (Brown et al. 2016).

Our analysis also revealed a number of other limitations of using GCC_{cam} to model GPP. Similar to other studies, we observed that GCC_{cam} did not always vary synchronously with daily GPP (Keenan et al. 2014, Toomey et al. 2015), but rather daily GPP tended to lag behind increases in canopy greenness in spring and lead decreases in greenness in fall, particularly at the West Pond wetland. This was reflected in modeled daily GPP reaching peak values before daily GPP estimated from eddy covariance measurements. This is likely caused by seasonal variation in foliage pigments, and accentuated by the viewing angle of the camera (Keenan et al. 2014, Toomey et al. 2015). Although in this study we did not explicitly consider the spatial heterogeneity at Mayberry, the greater complexity of this site notably influenced the reliability of using camera-based indices for the development and parameterization of the LUE model. This can be explained by the fact that there is a strong nonlinear relationship between canopy greenness, canopy structure (i.e. seasonality of leaf area index and gap fraction), and leaf physiology (Keenan et al. 2014). While directly addressing spatial heterogeneity in LUE models is beyond the scope of this paper, this can potentially be done by considering vegetation patches and open water separately (rather than treating the canopy as a single entity as we did in this study, and is typically done by others), similar to the two-layer LUE model proposed by Huemmrich et al. (2010).

4.5.2. Landsat-derived indices for GPP modeling – strengths and limitations

Although GCC_{cam} resulted in better data-model agreement relative to the other VIs explored in this study, Landsat-derived VIs also resulted in overall good agreement between predicted and observed GPP at the homogeneous West Pond wetland. We chose Landsat data over MODIS imagery since despite the lower frequency of data acquisition, greater spatial resolution is needed when considering wetlands in the Sacramento-San Joaquin Delta and elsewhere since these ecosystems are often small and fragmented within the landscape (Byrd *et al.*, 2014). For example, in the Delta the area of remaining wetlands represents only 3% of its historical extent. As observed in other studies, EVI_L outperformed the other Landsat indices we investigated, since this index is designed to enhance the vegetation signal with improved sensitivity to high biomass thus de-coupling canopy background signals and reducing atmospheric influences (Hilker *et al.*, 2008, Huete *et al.*, 2002). This index is also a good estimate of the amount of PAR absorbed by photosynthetically active vegetation (Kalfas *et al.*, 2011, Kang *et al.*, 2014, Xiao *et al.*, 2004), and Rocha *et al.* (2008) observed that NEE and surface EVI were tightly correlated at a fresh water marsh in Southern California, with EVI responding strongly to variations in standing litter that appears to drive GPP in these systems. Although EVI_L typically followed seasonal and interannual dynamics in GPP at West Pond, EVI_L reached peak values in 2015 although GPP was lower relative to other years. This reflects the influence of a newly restored wetland built in 2013

surrounding the West Pond wetland. Emergent vegetation at this recently restored site expanded rapidly at the end of 2014 and during the 2015 growing season and the lack of litter (Byrd *et al.*, 2014), and the high reflectance of the young canopy (Ustin & Trabucco, 2000) likely influenced band reflectance values in some of the Landsat pixels falling within the flux footprint (Figure 4.1), contributing to the decoupling in the dynamics of Landsat-based VIs and GPP in 2015. Nonetheless, despite the limited temporal frequency of Landsat data, we show that LUE models using EVI_L can adequately predict daily and annual GPP in small, homogeneous wetland ecosystems, allowing for regional upscaling of wetland photosynthesis and representing an improvement over MODIS GPP. However, as with any empirical determination of absorbed PAR, a direct conversion of satellite spectral reflectance of surface fAPAR over large areas in difficult, since empirical relationships are site and sensor specific, can vary in time and space, and may be unsuitable for application to large areas (Hilker *et al.*, 2008). This empirical approach is even more limited in dynamic, heterogeneous wetland environments as observed by the poorer agreement between observed and modeled GPP at Mayberry. Issues of patch size, data saturation and water inundation need to be considered in these heterogeneous wetland sites (Byrd *et al.*, 2014). In particular, field spectra of emergent wetland vegetation show significant reduction in near-infrared reflectance and shift in the red-edge position with progressive water depth, which can highly influence VI-based estimates of wetland productivity (Byrd *et al.*, 2014, Kearney *et al.*, 2009). This represents a drawback of estimating GPP using Landsat data and explains in part why GCC_{cam}, which is less influenced by background effects due to the viewing angle of the camera, is a better predictor of GPP in these environments.

4.6. Conclusion

In this study, we show that digital repeat photography provides reliable information on canopy greenness that can be used to model canopy-scale photosynthesis in wetland ecosystems. By combining camera-derived greenness indices and meteorological data in a LUE model, we accurately predicted seasonal and interannual dynamics of C uptake in two restored temperate freshwater marshes. This suggests that digital cameras provide a low-cost method for monitoring C cycling in wetland environments. However, further work is needed to develop calibration protocols and standards to ensure congruency of long-term datasets across sites. Furthermore, future efforts should focus on explicitly considering spatial heterogeneity when modeling photosynthesis using LUE models since model performance decreased with increasing site complexity. Similarly, Landsat data also shows promise for

modeling GPP in wetland environments, particularly in more homogeneous systems, suggesting that this approach can be used for regional upscaling of wetland photosynthesis. However, again Landsat-based model performance was lower at the more heterogeneous site, reflecting potential limitations of Landsat data.

We conclude that digital repeat photography provides a simple and cost-effective means of estimating photosynthesis in wetland ecosystems. Wetland gross primary production can also be estimated in uniform systems using Landsat data, which is valuable for regional estimates of photosynthesis. The LUE approach presented in this study provides a valuable tool for C market-funded wetland conservation and restoration, thereby providing opportunities to counteract the widespread degradation of wetlands worldwide. Although in this study we focus only on modeling C uptake, the model we present can be integrated into full biogeochemical models designed for C market and Cap-and-Trade systems (e.g. Oikawa et al. 2016) to accurately estimate both CO_2 and CH_4 exchange, which is critical for evaluating the greenhouse gas mitigation potential of wetland restoration.

References

Ahrends HE, Etzold S, Kutsch WL *et al.* (2009) Tree phenology and carbon dioxide fluxes: use of digital photography for process-based interpretation at the ecosystem scale. *Climate Research,* **39**, 261-274.

Alberto MCR, Hirano T, Miyata A, Wassmann R, Kumar A, Padre A, Amante M (2012) Influence of climate variability on seasonal and interannual variations of ecosystem CO2 exchange in flooded and non-flooded rice fields in the Philippines. *Field Crops Research,* **134**, 80-94.

Alberto MCR, Wassmann R, Buresh RJ, Quilty JR, Correa Jr TQ, Sandro JM, Centeno CaR (2014) Measuring methane flux from irrigated rice fields by eddy covariance method using open-path gas analyzer. *Field Crops Research,* **160**, 12-21.

Anderson FE, Bergamaschi B, Sturtevant C *et al.* (2016) Variation of energy and carbon fluxes from a restored temperate freshwater wetland and implications for carbon market verification protocols. *Journal of Geophysical Research: Biogeosciences,* **121**, 777–795.

Armentano TV (1980) Drainage of organic soils as a factor in the world carbon cycle. *BioScience,* **30**, 825-830.

Aselmann I, Crutzen PJ (1989) Global distribution of natural freshwater wetlands and rice paddies, their net primary productivity, seasonality and possible methane emissions. *Journal of Atmospheric Chemistry,* **8**, 307-358.

Atwater BF, Belknap DF (1980) Tidal-wetland deposits of the Sacramento-San Joaquin Delta, California. In: *Quaternary depositional environments of the Pacific Coast.* (eds Field ME, Abuoma H, Coburn IP, Douglas RG, Ingle JC) pp 89-103. Pacific Section- Society for Sedimentary Geology.

Aubinet M, Grelle A, Ibrom A *et al.* (1999) Estimates of the annual net carbon and water exchange of forests: The EUROFLUX methodology. In: *Advances in Ecological Research.* (eds Fitter AH, Raffaelli DG) pp 113-175. Academic Press.

Aulakh MS, Wassmann R, Rennenberg H (2001) Methane emissions from rice fields—quantification, mechanisms, role of management, and mitigation options. In: *Advances in agronomy.* pp 193-260. Academic Press.

Bachelet D, Kern J, Tölg M (1995) Balancing the rice carbon budget in China using spatially-distributed data. *Ecological Modelling*, **79**, 167-177.

Bachelet D, Neue HU (1993) Methane emissions from wetland rice areas of Asia. *Chemosphere*, **26**, 219-237.

Badiou P, Mcdougal R, Pennock D, Clark B (2011) Greenhouse gas emissions and carbon sequestration potential in restored wetlands of the Canadian prairie pothole region. *Wetlands Ecology and Management*, **19**, 237-256.

Baldocchi DD (2003) Assessing the eddy covariance technique for evaluating carbon dioxide exchange rates of ecosystems: past, present and future. *Global Change Biology*, **9**, 479-492.

Baldocchi DD (2014) Measuring fluxes of trace gases and energy between ecosystems and the atmosphere – the state and future of the eddy covariance method. *Global Change Biology*, **20**, 3600-3609.

Baldocchi DD, Detto M, Sonnentag O, Verfaillie J, Teh YA, Silver W, Kelly NM (2012) The challenges of measuring methane fluxes and concentrations over a peatland pasture. *Agricultural and Forest Meteorology*, **153**, 177-187.

Baldocchi DD, Falge E, Gu L *et al.* (2001) FLUXNET: A New Tool to Study the Temporal and Spatial Variability of Ecosystem–Scale Carbon Dioxide, Water Vapor, and Energy Flux Densities. *Bulletin of the American Meteorological Society*, **82**, 2415-2434.

Baldocchi DD, Hicks BB, Meyers TP (1988) Measuring biosphere-atmosphere exchanges of biologically related gases with micrometeorological methods. *Ecology*, **69**, 1331-1340.

Baldocchi DD, Knox SH, Dronova I *et al.* (2016) The impact of expanding flooded land area on the annual evaporation of rice. *Agricultural and Forest Meteorology*, **accepted**.

Baldocchi DD, Sturtevant C (2015) Does day and night sampling reduce spurious correlation between canopy photosynthesis and ecosystem respiration? *Agricultural and Forest Meteorology*, **207**, 117-126.

Bellisario LM, Bubier JL, Moore TR, Chanton JP (1999) Controls on CH4 emissions from a northern peatland. *Global Biogeochemical Cycles*, **13**, 81-91.

Bernacchi CJ, Hollinger SE, Meyers T (2005) The conversion of the corn/soybean ecosystem to no-till agriculture may result in a carbon sink. *Global Change Biology*, **11**, 1867-1872.

Bernal B, Mitsch WJ (2012) Comparing carbon sequestration in temperate freshwater wetland communities. *Global Change Biology*, **18**, 1636-1647.

Bernal B, Mitsch WJ (2013) Carbon sequestration in two created riverine wetlands in the Midwestern United States. *Journal of Environmental Quality*, **42**, 1236-1244.

Bhattacharyya P, Neogi S, Roy KS, Dash PK, Nayak AK, Mohapatra T (2014) Tropical low land rice ecosystem is a net carbon sink. *Agriculture, Ecosystems & Environment*, **189**, 127-135.

Blais A-M, Lorrain S, Tremblay A (2005) Greenhouse gas fluxes (CO2, CH4 and N2O) in forests and wetlands of boreal, temperate and tropical regions. In: *Greenhouse Gas Emissions — Fluxes and Processes.* (eds Tremblay A, Varfalvy L, Roehm C, Garneau M) pp 87-127. Springer Berlin Heidelberg.

Bonneville M-C, Strachan IB, Humphreys ER, Roulet NT (2008) Net ecosystem CO2 exchange in a temperate cattail marsh in relation to biophysical properties. *Agricultural and Forest Meteorology*, **148**, 69-81.

Bossio DA, Horwath WR, Mutters RG, Van Kessel C (1999) Methane pool and flux dynamics in a rice field following straw incorporation. *Soil Biology and Biochemistry*, **31**, 1313-1322.

Bridgham S, Megonigal JP, Keller J, Bliss N, Trettin C (2006) The carbon balance of North American wetlands. *Wetlands*, **26**, 889-916.

Bridgham SD, Cadillo-Quiroz H, Keller JK, Zhuang Q (2013) Methane emissions from wetlands: biogeochemical, microbial, and modeling perspectives from local to global scales. *Global Change Biology*, **19**, 1325-1346.

Brinson MM, Lugo AE, Brown S (1981) Primary productivity, decomposition and consumer activity in freshwater wetlands. *Annual Review of Ecology and Systematics*, **12**, 123-161.

Bronson KF, Neue H-U, Abao, E. B., Singh U (1997) Automated chamber measurements of methane and nitrous oxide flux in a flooded rice soil: I. Residue, nitrogen, and water management. *Soil Science Society of America Journal*, **61**, 981-987.

Brown TB, Hultine KR, Steltzer H *et al.* (2016) Using phenocams to monitor our changing Earth: toward a global phenocam network. *Frontiers in Ecology and the Environment*, **14**, 84-93.

Byrd KB, O'connell JL, Di Tommaso S, Kelly M (2014) Evaluation of sensor types and environmental controls on mapping biomass of coastal marsh emergent vegetation. *Remote Sensing of Environment,* **149**, 166-180.

Cao M, Dent JB, Heal OW (1995) Modeling methane emissions from rice paddies. *Global Biogeochemical Cycles,* **9**, 183-195.

Casper P, Maberly SC, Hall GH, Finlay BJ (2000) Fluxes of methane and carbon dioxide from a small productive lake to the atmosphere. *Biogeochemistry,* **49**, 1-19.

Chanton JP, Whiting GJ, Blair NE, Lindau CW, Bollich PK (1997) Methane emission from rice: Stable isotopes, diurnal variations, and CO2 exchange. *Global Biogeochemical Cycles,* **11**, 15-27.

Chanton JP, Whiting GJ, Happell JD, Gerard G (1993) Contrasting rates and diurnal patterns of methane emission from emergent aquatic macrophytes. *Aquatic Botany,* **46**, 111-128.

Chapin FS, Iii, Woodwell GM, Randerson JT *et al.* (2006) Reconciling Carbon-cycle Concepts, Terminology, and Methods. *Ecosystems,* **9**, 1041-1050.

Chu H, Chen J, Gottgens JF, Ouyang Z, John R, Czajkowski K, Becker R (2014) Net ecosystem methane and carbon dioxide exchanges in a Lake Erie coastal marsh and a nearby cropland. *Journal of Geophysical Research: Biogeosciences,* **119**, 722-740.

Chu H, Gottgens JF, Chen J *et al.* (2015) Climatic variability, hydrologic anomaly, and methane emission can turn productive freshwater marshes into net carbon sources. *Global Change Biology,* **21**, 1165-1181.

Cicerone RJ, Delwiche CC, Tyler SC, Zimmerman PR (1992) Methane emissions from California rice paddies with varied treatments. *Global Biogeochemical Cycles,* **6**, 233-248.

Cicerone RJ, Shetter JD (1981) Sources of atmospheric methane: Measurements in rice paddies and a discussion. *Journal of Geophysical Research,* **86**, 7203-7209.

Cicerone RJ, Shetter JD, Delwiche CC (1983) Seasonal variation of methane flux from a California rice paddy. *Journal of Geophysical Research: Oceans,* **88**, 11022-11024.

Conrad R (2002) Control of microbial methane production in wetland rice fields. *Nutrient Cycling in Agroecosystems,* **64**, 59-69.

Conrad R (2007) Microbial ecology of methanogens and methanotrophs. *Advances in*

agronomy, **96**, 1-63.

Corton TM, Bajita JB, Grospe FS *et al.* (2000) Methane emission from irrigated and intensively managed rice fields in central luzon (Philippines). *Nutrient Cycling in Agroecosystems*, **58**, 37-53.

Costanza R, D'arge R, De Groot R *et al.* (1997) The value of the world's ecosystem services and natural capital. *Nature*, **387**, 253-260.

Couwenberg J, Dommain R, Joosten H (2010) Greenhouse gas fluxes from tropical peatlands in south-east Asia. *Global Change Biology*, **16**, 1715-1732.

Dannenberg S, Conrad R (1999) Effect of rice plants on methane production and rhizospheric metabolism in paddy soil. *Biogeochemistry*, **45**, 53-71.

Den Van Der Gon HA, Van Breemen N (1993) Diffusion-controlled transport of methane from soil to atmosphere as mediated by rice plants. *Biogeochemistry*, **21**, 177-190.

Dengel S, Zona D, Sachs T *et al.* (2013) Testing the applicability of neural networks as a gap-filling method using CH4 flux data from high latitude wetlands. *Biogeosciences*, **10**, 8185-8200.

Denier Van Der Gon HaC, Kropff MJ, Van Breemen N *et al.* (2002) Optimizing grain yields reduces CH4 emissions from rice paddy fields. *Proceedings of the National Academy of Sciences*, **99**, 12021-12024.

Denier Van Der Gon HaC, Van Bodegom PM, Houweling S, Verburg PH, Van Breemen N (2000) Combining upscaling and downscaling of methane emissions from rice fields: Methodologies and preliminary results. *Nutrient Cycling in Agroecosystems*, **58**, 285-301.

Detto M, Baldocchi D, Katul G (2010) Scaling Properties of Biologically Active Scalar Concentration Fluctuations in the Atmospheric Surface Layer over a Managed Peatland. *Boundary-Layer Meteorology*, **136**, 407-430.

Detto M, Katul GG (2007) Simplified expressions for adjusting higher-order turbulent statistics obtained from open path gas analyzers. *Boundary-Layer Meteorology*, **122**, 205-216.

Detto M, Montaldo N, Albertson JD, Mancini M, Katul G (2006) Soil moisture and vegetation controls on evapotranspiration in a heterogeneous Mediterranean

ecosystem on Sardinia, Italy. *Water Resources Research,* **42**, W08419.

Detto M, Verfaillie J, Anderson F, Xu L, Baldocchi D (2011) Comparing laser-based open- and closed-path gas analyzers to measure methane fluxes using the eddy covariance method. *Agricultural and Forest Meteorology,* **151**, 1312-1324.

Deverel S, Oikawa PY, Mack SK (2016) Wetland implementation and rice cultivation in the Sacramento-San Joaquin Delta, San Francisco estuary and the coast of California – Methodology for quantifying greenhouse gas emissions reductions. http://americancarbonregistry.org/carbon-accounting/standardsmethodologies/restoration-of-california-deltaic-and-coastal-wetlands.

Deverel SJ, Leighton DA (2010) Historic, recent, and future subsidence, Sacramento-San Joaquin Delta, California, USA. *San Francisco Estuary and Watershed Science,* **8**.

Deverel SJ, Rojstaczer S (1996) Subsidence of agricultural lands in the Sacramento-San Joaquin Delta, California: Role of aqueous and gaseous carbon fluxes. *Water Resources Research,* **32**, 2359-2367.

Ding A, Willis C, Sass R, Fisher F (1999a) Methane emissions from rice fields: Effect of plant height among several rice cultivars. *Global Biogeochemical Cycles,* **13**, 1045-1052.

Ding A, Willis CR, Sass RL, Fisher FM (1999b) Methane emissions from rice fields: Effect of plant height among several rice cultivars. *Global Biogeochemical Cycles,* **13**, 1045-1052.

Drewer J, Lohila A, Aurela M *et al.* (2010) Comparison of greenhouse gas fluxes and nitrogen budgets from an ombotrophic bog in Scotland and a minerotrophic sedge fen in Finland. *European Journal of Soil Science,* **61**, 640-650.

Drexler JZ, De Fontaine CS, Brown TA (2009a) Peat accretion histories during the past 6,000 years in marshes of the Sacramento–San Joaquin Delta, CA, USA. *Estuaries and Coasts,* **32**, 871-892.

Drexler JZ, Fontaine C, Deverel S (2009b) The legacy of wetland drainage on the remaining peat in the Sacramento — San Joaquin Delta, California, USA. *Wetlands,* **29**, 372-386.

Drexler JZ, Snyder RL, Spano D, Paw U KT (2004) A review of models and micrometeorological methods used to estimate wetland evapotranspiration.

Hydrological Processes, **18**, 2071-2101.

Drösler M, Freibauer A, Christensen T, Friborg T (2008) Observations and status of peatland greenhouse gas emissions in Europe. In: *The Continental-Scale Greenhouse Gas Balance of Europe.* (eds Dolman AJ, Valentini R, Freibauer A) pp 243-261. Springer New York.

Emmert-Mattox S, Crooks S, Findsen J (2010) Wetland grasses and gases: Are tidal wetlands ready for the carbon markets? *National Wetlands Newsletter32*, **6**, 6-10.

Emmett-Mattox S, Crooks S, Findsen J (2011) Gases and grasses: the restoration, conservation, or avoided loss of tidal wetlands carbon pools may help to mitigate climate change. In: *The Environmental Forum.* pp 30-35.

Eugster W, Moffat AM, Ceschia E *et al.* (2010) Management effects on European cropland respiration. *Agriculture, Ecosystems & Environment*, **139**, 346-362.

Eusufzai MK, Tokida T, Okada M, Sugiyama S-I, Liu GC, Nakajima M, Sameshima R (2010) Methane emission from rice fields as affected by land use change. *Agriculture, Ecosystems & Environment*, **139**, 742-748.

Foken T, Wichura B (1996) Tools for quality assessment of surface-based flux measurements. *Agricultural and Forest Meteorology*, **78**, 83-105.

Forster P, Ramaswamy V, Artaxo P *et al.* (2007) Changes in atmospheric constituents and in radiative forcing. *Climate Change 2007: The Physical Science Basis. Contribution of Working Group I to the Fourth Assessment Report of the Intergovernmental Panel on Climate Change*, 210-215.

Frolking SE, Bubier JL, Moore TR *et al.* (1998) Relationship between ecosystem productivity and photosynthetically active radiation for northern peatlands. *Global Biogeochemical Cycles*, **12**, 115-126.

Gitelson AA, Merzlyak MN (1997) Remote estimation of chlorophyll content in higher plant leaves. *International Journal of Remote Sensing*, **18**, 2691-2697.

Gitelson AA, Peng Y, Masek JG *et al.* (2012) Remote estimation of crop gross primary production with Landsat data. *Remote Sensing of Environment*, **121**, 404-414.

Griffin D, Anchukaitis KJ (2014) How unusual is the 2012–2014 California drought? *Geophysical Research Letters*, **41**, 9017-9023.

Grinsted A, Moore JC, Jevrejeva S (2004) Application of the cross wavelet transform and

wavelet coherence to geophysical time series. *Nonlinear processes in geophysics,* **11**, 561-566.

Han GH, Yoshikoshi H, Nagai H, Yamada T, Saito M, Miyata A, Harazono Y (2005) Concentration and carbon isotope profiles of CH4 in paddy rice canopy: Isotopic evidence for changes in CH4 emission pathways upon drainage. *Chemical Geology,* **218**, 25-40.

Hatala JA, Detto M, Baldocchi DD (2012a) Gross ecosystem photosynthesis causes a diurnal pattern in methane emission from rice. *Geophysical Research Letters,* **39**, L06409.

Hatala JA, Detto M, Sonnentag O, Deverel SJ, Verfaillie J, Baldocchi DD (2012b) Greenhouse gas (CO2, CH4, H2O) fluxes from drained and flooded agricultural peatlands in the Sacramento-San Joaquin Delta. *Agriculture, Ecosystems & Environment,* **150**, 1-18.

Heinsch FA, Maosheng Z, Running SW *et al.* (2006) Evaluation of remote sensing based terrestrial productivity from MODIS using regional tower eddy flux network observations. *IEEE Transactions on Geoscience and Remote Sensing*, **44**, 1908-1925.

Helfter C, Campbell C, Dinsmore KJ *et al.* (2015) Drivers of long-term variability in CO2 net ecosystem exchange in a temperate peatland. *Biogeosciences,* **12**, 1799-1811.

Hendriks DMD, Van Huissteden J, Dolman AJ (2010) Multi-technique assessment of spatial and temporal variability of methane fluxes in a peat meadow. *Agricultural and Forest Meteorology,* **150**, 757-774.

Hendriks DMD, Van Huissteden J, Dolman AJ, Van Der Molen MK (2007) The full greenhouse gas balance of an abandoned peat meadow. *Biogeosciences,* **4**, 411-424.

Herbst M, Friborg T, Schelde K *et al.* (2013) Climate and site management as driving factors for the atmospheric greenhouse gas exchange of a restored wetland. *Biogeosciences,* **10**, 39-52.

Hilker T, Coops NC, Wulder MA, Black TA, Guy RD (2008) The use of remote sensing in light use efficiency based models of gross primary production: A review of current status and future requirements. *Science of The Total Environment,* **404**, 411-423.

Hiraishi T, Krug T, Tanabe K, Srivastava N, Baasansuren J, Fukuda M, Troxler T (2014) 2013 Supplement to the 2006 IPCC Guidelines for National Greenhouse Gas

Inventories: Wetlands. *IPCC, Switzerland*.

Hirano T, Segah H, Kusin K, Limin S, Takahashi H, Osaki M (2012) Effects of disturbances on the carbon balance of tropical peat swamp forests. *Global Change Biology*, **18**, 3410-3422.

Hollinger SE, Bernacchi CJ, Meyers TP (2005) Carbon budget of mature no-till ecosystem in North Central Region of the United States. *Agricultural and Forest Meteorology*, **130**, 59-69.

Holzapfel-Pschorn A, Seiler W (1986) Methane emission during a cultivation period from an Italian rice paddy. *Journal of Geophysical Research: Atmospheres*, **91**, 11803-11814.

Hsieh C-I, Katul G, Chi T-W (2000) An approximate analytical model for footprint estimation of scalar fluxes in thermally stratified atmospheric flows. *Advances in Water Resources*, **23**, 765-772.

Huang YaO, Sass R, Fisher F (1997a) Methane emission from Texas rice paddy soils. 1. Quantitative multi-year dependence of CH4 emission on soil, cultivar and grain yield. *Global Change Biology*, **3**, 479-489.

Huang YaO, Sass R, Fisher F (1997b) Methane emission from Texas rice paddy soils. 2. Seasonal contribution of rice biomass production to CH4 emission. *Global Change Biology*, **3**, 491-500.

Huang YaO, Sass RL, Fisher JFM (1998) A semi-empirical model of methane emission from flooded rice paddy soils. *Global Change Biology*, **4**, 247-268.

Huemmrich KF, Gamon JA, Tweedie CE *et al.* (2010) Remote sensing of tundra gross ecosystem productivity and light use efficiency under varying temperature and moisture conditions. *Remote Sensing of Environment*, **114**, 481-489.

Huete A (1988) A soil-adjusted vegetation index (SAVI). *Remote Sensing of Environment*, **25**, 295-309.

Huete A, Didan K, Miura T, Rodriguez EP, Gao X, Ferreira LG (2002) Overview of the radiometric and biophysical performance of the MODIS vegetation indices. *Remote Sensing of Environment*, **83**, 195-213.

Humphreys ER (2004) Net ecosystem production of three coastal Douglas-fir stands at different stages of development after harvesting. Unpublished Doctor of

Philosophy University of British Columbia.

Humphreys ER, Lafleur PM, Flanagan LB, Hedstrom N, Syed KH, Glenn AJ, Granger R (2006) Summer carbon dioxide and water vapor fluxes across a range of northern peatlands. *Journal of Geophysical Research: Biogeosciences,* **111**, G04011.

Huxman T, Snyder K, Tissue D *et al.* (2004) Precipitation pulses and carbon fluxes in semiarid and arid ecosystems. *Oecologia,* **141**, 254-268.

Ide R, Oguma H (2010) Use of digital cameras for phenological observations. *Ecological Informatics,* **5**, 339-347.

Ipcc (1997) *Revised 1996 IPCC guidelines for national greenhouse gas inventories,* Cambridge, Cambridge University Press.

Jackowicz-Korczyński M, Christensen TR, Bäckstrand K, Crill P, Friborg T, Mastepanov M, Ström L (2010) Annual cycle of methane emission from a subarctic peatland. *Journal of Geophysical Research: Biogeosciences,* **115**, G02009.

Janssens IA, Lankreijer H, Matteucci G *et al.* (2001) Productivity overshadows temperature in determining soil and ecosystem respiration across European forests. *Global Change Biology,* **7**, 269-278.

Kaimal JC, Gaynor JE (1991) Another look at sonic thermometry. *Boundary-Layer Meteorology,* **56**, 401-410.

Kalfas JL, Xiao X, Vanegas DX, Verma SB, Suyker AE (2011) Modeling gross primary production of irrigated and rain-fed maize using MODIS imagery and CO2 flux tower data. *Agricultural and Forest Meteorology,* **151**, 1514-1528.

Kang X, Wang Y, Chen H *et al.* (2014) Modeling carbon fluxes using multi-temporal MODIS imagery and CO2 eddy flux tower data in Zoige alpine wetland, South-West China. *Wetlands,* **34**, 603-618.

Katul GG, Schieldge J, Hsieh C-I, Vidakovic B (1998) Skin temperature perturbations induced by surface layer turbulence above a grass surface. *Water Resources Research,* **34**, 1265-1274.

Kayranli B, Scholz M, Mustafa A, Hedmark Å (2009) Carbon storage and fluxes within freshwater wetlands: a critical review. *Wetlands,* **30**, 111-124.

Kearney MS, Stutzer D, Turpie K, Stevenson JC (2009) The effects of tidal inundation on the reflectance characteristics of coastal marsh vegetation. *Journal of Coastal*

Research, **25**, 1177-1186.

Keenan TF, Darby B, Felts E *et al.* (2014) Tracking forest phenology and seasonal physiology using digital repeat photography: a critical assessment. *Ecological Applications,* **24**, 1478-1489.

Khalil MaK, Butenhoff CL (2008) Spatial variability of methane emissions from rice fields and implications for experimental design. *Journal of Geophysical Research: Biogeosciences,* **113**.

Khalil MaK, Rasmussen RA, Shearer MJ, Dalluge RW, Ren L, Duan C-L (1998) Factors affecting methane emissions from rice fields. *Journal of Geophysical Research: Atmospheres,* **103**, 25219-25231.

Kim J, Verma SB, Billesbach DP (1999) Seasonal variation in methane emission from a temperate Phragmites-dominated marsh: effect of growth stage and plant-mediated transport. *Global Change Biology,* **5**, 433-440.

Knox SH, Sturtevant C, Matthes JH, Koteen L, Verfaillie J, Baldocchi D (2015) Agricultural peatland restoration: effects of land-use change on greenhouse gas (CO2 and CH4) fluxes in the Sacramento-San Joaquin Delta. *Global Change Biology,* **21**, 750–765.

Koebsch F, Jurasinski G, Koch M, Hofmann J, Glatzel S (2015) Controls for multi-scale temporal variation in ecosystem methane exchange during the growing season of a permanently inundated fen. *Agricultural and Forest Meteorology,* **204**, 94-105.

Kramer RA, Shabman L (1993) The effects of agricultural and tax policy reform on the economic return to wetland drainage in the Mississippi Delta region. *Land Economics,* **69**, 249-262.

Kriegler FJ, Malila WA, Nalepka RF, Richardson W (1969) Preprocessing transformations and their effects on multispectral recognition. *Proceedings of the 6th international symposium on remote sensing of environment*, 97-131.

Kroon PS, Schrier-Uijl AP, Hensen A, Veenendaal EM, Jonker HJJ (2010) Annual balances of CH4 and N2O from a managed fen meadow using eddy covariance flux measurements. *European Journal of Soil Science,* **61**, 773-784.

Le Mer J, Roger P (2001) Production, oxidation, emission and consumption of methane by soils: A review. *European Journal of Soil Biology,* **37**, 25-50.

Leuning R, Van Gorsel E, Massman WJ, Isaac PR (2012) Reflections on the surface energy imbalance problem. *Agricultural and Forest Meteorology*, **156**, 65-74.

Lindau CW, Bollich PK, Delaune RD, Patrick WH, Jr., Law VJ (1991) Effect of urea fertilizer and environmental factors on CH4 emissions from a Louisiana, USA rice field. *Plant and Soil*, **136**, 195-203.

Linquist BA, Anders MM, Adviento-Borbe MaA, Chaney RL, Nalley LL, Da Rosa EFF, Van Kessel C (2015) Reducing greenhouse gas emissions, water use, and grain arsenic levels in rice systems. *Global Change Biology*, **21**, 407-417.

Lloyd J, Taylor JA (1994) On the Temperature Dependence of Soil Respiration. *Functional Ecology*, **8**, 315-323.

Ma S, Baldocchi DD, Hatala JA, Detto M, Curiel Yuste J (2012) Are rain-induced ecosystem respiration pulses enhanced by legacies of antecedent photodegradation in semi-arid environments? *Agricultural and Forest Meteorology*, **154–155**, 203-213.

Mack SK, Lane RR, Day JW (2012) The restoration of degraded deltaic wetlands of the Mississippi Delta. Tierra Resources, American Carbon Registry.

Maljanen M, Sigurdsson BD, Guðmundsson J, Óskarsson H, Huttunen JT, Martikainen PJ (2010) Greenhouse gas balances of managed peatlands in the Nordic countries – present knowledge and gaps. *Biogeosciences*, **7**, 2711-2738.

Malone SL, Staudhammer CL, Loescher HW *et al.* (2014) Seasonal patterns in energy partitioning of two freshwater marsh ecosystems in the Florida Everglades. *Journal of Geophysical Research: Biogeosciences*, **119**, 1487-1505.

Massman WJ, Lee X (2002) Eddy covariance flux corrections and uncertainties in long-term studies of carbon and energy exchanges. *Agricultural and Forest Meteorology*, **113**, 121-144.

Matlab (2014), Natick, Mass, The Mathworks Inc.

Matthes JH, Sturtevant C, Verfaillie J, Knox S, Baldocchi D (2014) Parsing the variability in CH4 flux at a spatially heterogeneous wetland: Integrating multiple eddy covariance towers with high-resolution flux footprint analysis. *Journal of Geophysical Research: Biogeosciences*, **119**, 2014JG002642.

Mcdermitt D, Burba G, Xu L *et al.* (2011) A new low-power, open-path instrument for

measuring methane flux by eddy covariance. *Applied Physics B,* **102**, 391-405.

Mcleod E, Chmura GL, Bouillon S *et al.* (2011) A blueprint for blue carbon: toward an improved understanding of the role of vegetated coastal habitats in sequestering CO2. *Frontiers in Ecology and the Environment,* **9**, 552-560.

Mcmillan AMS, Goulden ML, Tyler SC (2007) Stoichiometry of CH4 and CO2 flux in a California rice paddy. *Journal of Geophysical Research: Biogeosciences,* **112**, G01008.

Meijide A, Manca G, Goded I, Magliulo V, Di Tommasi P, Seufert G, Cescatti A (2011) Seasonal trends and environmental controls of methane emissions in a rice paddy field in Northern Italy. *Biogeosciences,* **8**, 3809-3821.

Merrill A, Siegel S, Morris B *et al.* (2010) Greenhouse gas reduction and environmental benefits in the Sacramento-San Joaquin Delta: advancing carbon capture wetland farms and exploring potential for low carbon agriculture. Prepared for The Nature Conservancy, Sacramento, California. Accessed online: http://www.stillwatersci.com/search.php.

Meyer GE, Mehta T, Kocher M, Mortensen DA, Samal A (1998) Textural imaging and discriminant analysis for distinguishing weeds for spot spraying. *Transactions of the ASAE,* **41**, 1189-1197.

Migliavacca M, Galvagno M, Cremonese E *et al.* (2011) Using digital repeat photography and eddy covariance data to model grassland phenology and photosynthetic CO2 uptake. *Agricultural and Forest Meteorology,* **151**, 1325-1337.

Miller R, Hastings L, Fujii R (2000) Hydrologic treatments affect gaseous carbon loss from organic soils, Twitchell Island, California, October 1995-December 1997. *Report Number: USGS/WRI-00-4042. 32*, 2000.

Miller RL (2011) Carbon gas fluxes in re-established wetlands on organic soils differ relative to plant community and hydrology. *Wetlands,* **31**, 1055-1066.

Miller RL, Fram M, Fujii R, Wheeler G (2008) Subsidence reversal in a re-established wetland in the Sacramento-San Joaquin Delta, California, USA. *San Francisco Estuary and Watershed Science,* **6**.

Miller RL, Fujii R (2010) Plant community, primary productivity, and environmental conditions following wetland re-establishment in the Sacramento-San Joaquin Delta, California. *Wetlands Ecology and Management,* **18**, 1-16.

Minoda T, Kimura M (1994) Contribution of photosynthesized carbon to the methane emitted from paddy fields. *Geophysical Research Letters,* **21**, 2007-2010.

Minoda T, Kimura M, Wada E (1996) Photosynthates as dominant source of CH4 and CO2 in soil water and CH4 emitted to the atmosphere from paddy fields. *Journal of Geophysical Research: Atmospheres,* **101**, 21091-21097.

Mitra S, Wassmann R, Vlek PL (2005) An appraisal of global wetland area and its organic carbon stock. *Current Science,* **88**, 25-35.

Mitsch W, Bernal B, Nahlik A *et al.* (2013) Wetlands, carbon, and climate change. *Landscape Ecology,* **28**, 583-597.

Miyata A, Iwata T, Nagai H *et al.* (2005) Seasonal variation of carbon dioxide and methane fluxes at single cropping paddy fields in central and western Japan. *Phyton,* **45**, 89-97.

Moffat AM, Papale D, Reichstein M *et al.* (2007) Comprehensive comparison of gap-filling techniques for eddy covariance net carbon fluxes. *Agricultural and Forest Meteorology,* **147**, 209-232.

Monteith J (1969) Light interception and radiative exchange in crop stands. In: *Physiological Aspects of Crop Yield: Proceedings of a symposium sponsored by the University of Nebraska, the American Society of Agronomy, and the Crop Science Society of America.* (eds Eastin JD, Haskins FA, Sullivan CY, Van Bavel CHM, Dinauer RC) pp 89-115, University of Nebraska, Lincoln.

Monteith J (1972) Solar radiation and productivity in tropical ecosystems. *Journal of applied ecology,* **9**, 747-766.

Monteith JL, Moss CJ (1977) Climate and the efficiency of crop production in Britain *Philosophical Transactions of the Royal Society of London B: Biological Sciences,* **281**, 277-294.

Moore CJ (1986) Frequency response corrections for eddy correlation systems. *Boundary-Layer Meteorology,* **37**, 17-35.

Morin TH, Bohrer G, Frasson RPDM, Naor-Azreli L, Mesi S, Stefanik KC, Schäfer KVR (2014) Environmental drivers of methane fluxes from an urban temperate wetland park. *Journal of Geophysical Research: Biogeosciences,* **119**, 2188-2208.

Morris J (2014) Biogeochemical consequences of converting corn into rice fields: An

analysis of greenhouse gas (CH4 and N2O) emissions in the Sacramento-San Joaquin Delta, California. Unpublished M.Sc. University of California, Davis.

Mount J, Twiss R (2005) Subsidence, sea level rise, and seismicity in the Sacramento-San Joaquin Delta. *San Francisco Estuary and Watershed Science*, **3**.

Murray BC, Pendleton L, Jenkins WA, Sifleet S (2011) Green payments for blue carbon: Economic incentives for protecting threatened coastal habitats. *Nicholas Institute for Environmental Policy Solutions, Report NI*, **11**.

Myhre G, Shindell D, BréOn F-M *et al.* (2013) Anthropogenic and natural radiative forcing. In: *Climate Change 2013: The Physical Science Basis. Contribution of Working Group I to the Fifth Assessment Report of the Intergovernmental Panel on Climate Change.* (eds Stocker TF, Qin D, Plattner G-K, Tignor M, Allen SK, Boschung J, Nauels A, Xia Y, Bex V, Midgley PM) pp 659–740. Cambridge, United Kingdom and New York, NY, USA, Cambridge University Press.

Nahlik A, Mitsch W (2010) Methane emissions from created riverine wetlands. *Wetlands,* **30**, 783-793.

Naser HM, Nagata O, Tamura S, Hatano R (2007) Methane emissions from five paddy fields with different amounts of rice straw application in central Hokkaido, Japan. *Soil Science and Plant Nutrition,* **53**, 95-101.

Neubauer SC, Megonigal JP (2015) Moving beyond global warming potentials to quantify the climatic role of ecosystems. *Ecosystems,* **18**, 1000-1013.

Neue HU, Sass R (1994) Trace gas emissions from rice fields. In: *Global Atmospheric-Biospheric Chemistry.* (ed Prinn R) pp 119-147. Springer US.

Neue HU, Wassmann R, Kludze HK, Bujun W, Lantin RS (1997) Factors and processes controlling methane emissions from rice fields. *Nutrient Cycling in Agroecosystems,* **49**, 111-117.

Nieveen JP, Campbell DI, Schipper LA, Blair IJ (2005) Carbon exchange of grazed pasture on a drained peat soil. *Global Change Biology,* **11**, 607-618.

Nilsson M, Sagerfors J, Buffam I *et al.* (2008) Contemporary carbon accumulation in a boreal oligotrophic minerogenic mire – a significant sink after accounting for all C-fluxes. *Global Change Biology,* **14**, 2317-2332.

Nishimura S, Sawamoto T, Akiyama H, Sudo S, Yagi K (2004) Methane and nitrous

oxide emissions from a paddy field with Japanese conventional water management and fertilizer application. *Global Biogeochemical Cycles,* **18**, GB2017.

Nouchi I, Mariko S (1993) Mechanism of methane transport by rice plants. In: *Biogeochemistry of Global Change.* (ed Oremland R) pp 336-352. Springer US.

Novick KA, Oishi AC, Ward EJ, Siqueira MBS, Juang J-Y, Stoy PC (2015) On the difference in the net ecosystem exchange of CO2 between deciduous and evergreen forests in the southeastern United States. *Global Change Biology,* **21**, 827-842.

Oikawa P, Jenerette G, Knox S *et al.* (2016) Introducing a biogeochemical model for estimating CO2 and CH4 exchange in restored wetlands. *Journal of Geophysical Research: Biogeosciences,* **Submitted**.

Olson DM, Griffis TJ, Noormets A, Kolka R, Chen J (2013) Interannual, seasonal, and retrospective analysis of the methane and carbon dioxide budgets of a temperate peatland. *Journal of Geophysical Research: Biogeosciences,* **118**, 226-238.

Page KL, Dalal RC (2011) Contribution of natural and drained wetland systems to carbon stocks, CO2, N2O, and CH4 fluxes: an Australian perspective. *Soil Research,* **49**, 377-388.

Papale D, Reichstein M, Aubinet M *et al.* (2006) Towards a standardized processing of Net Ecosystem Exchange measured with eddy covariance technique: algorithms and uncertainty estimation. *Biogeosciences,* **3**, 571-583.

Pendleton L, Donato DC, Murray BC *et al.* (2012) Estimating global "blue carbon" emissions from conversion and degradation of vegetated coastal ecosystems. *PloS one,* **7**, e43542.

Pennypacker S, Baldocchi D (2015) Seeing the fields and forests: Application of surface-layer theory and flux-tower data to calculating vegetation canopy height. *Boundary-Layer Meteorology,* **158**, 165-182.

Petrescu AMR, Lohila A, Tuovinen J-P *et al.* (2015) The uncertain climate footprint of wetlands under human pressure. *Proceedings of the National Academy of Sciences,* **112**, 4594-4599.

Poffenbarger H, Needelman B, Megonigal JP (2011) Salinity influence on methane emissions from tidal marshes. *Wetlands,* **31**, 831-842.

Raich JW, Rastetter EB, Melillo JM *et al.* (1991) Potential net primary productivity in South America: Application of a global model. *Ecological Applications,* **1**, 399-429.

Reeburgh W (2003) Global methane biogeochemistry. *Treatise on geochemistry,* **4**, 65-89.

Reichstein M, Falge E, Baldocchi D *et al.* (2005) On the separation of net ecosystem exchange into assimilation and ecosystem respiration: review and improved algorithm. *Global Change Biology,* **11**, 1424-1439.

Reid MC, Tripathee R, Schäfer KVR, Jaffé PR (2013) Tidal marsh methane dynamics: Difference in seasonal lags in emissions driven by storage in vegetated versus unvegetated sediments. *Journal of Geophysical Research: Biogeosciences,* **118**, 1802-1813.

Richardson A, Jenkins J, Braswell B, Hollinger D, Ollinger S, Smith M-L (2007) Use of digital webcam images to track spring green-up in a deciduous broadleaf forest. *Oecologia,* **152**, 323-334.

Richardson AD, Braswell BH, Hollinger DY, Jenkins JP, Ollinger SV (2009) Near-surface remote sensing of spatial and temporal variation in canopy phenology. *Ecological Applications,* **19**, 1417-1428.

Richardson AD, Klosterman S, Toomey M (2013) Near-surface sensor-derived phenology. In: *Phenology: An Integrative Environmental Science.* (ed Schwartz DM) pp 413-430. Dordrecht, Springer Netherlands.

Rinne J, Riutta T, Pihlatie M *et al.* (2007) Annual cycle of methane emission from a boreal fen measured by the eddy covariance technique. *Tellus B,* **59**, 449-457.

Rocha AV, Goulden ML (2008) Large interannual CO2 and energy exchange variability in a freshwater marsh under consistent environmental conditions. *Journal of Geophysical Research: Biogeosciences,* **113**, G04019.

Rocha AV, Goulden ML (2009) Why is marsh productivity so high? New insights from eddy covariance and biomass measurements in a Typha marsh. *Agricultural and Forest Meteorology,* **149**, 159-168.

Rocha AV, Potts DL, Goulden ML (2008) Standing litter as a driver of interannual CO2 exchange variability in a freshwater marsh. *Journal of Geophysical Research: Biogeosciences,* **113**, G04020.

Rojstaczer S, Deverel SJ (1993) Time dependence in atmospheric carbon inputs from

drainage of organic soils. *Geophysical Research Letters,* **20**, 1383-1386.

Rojstaczer S, Deverel SJ (1995) Land subsidence in drained histosols and highly organic mineral soils of California. *Soil Science Society of America Journal,* **59**, 1162-1167.

Rossini M, Meroni M, Migliavacca M *et al.* (2010) High resolution field spectroscopy measurements for estimating gross ecosystem production in a rice field. *Agricultural and Forest Meteorology,* **150**, 1283-1296.

Roulet NT, Lafleur PM, Richard PJH, Moore TR, Humphreys ER, Bubier J (2007) Contemporary carbon balance and late Holocene carbon accumulation in a northern peatland. *Global Change Biology,* **13**, 397-411.

Rouse J, Haas R, Scheel J, Deering D (1974) Monitoring vegetation systems in the Great Plains with ERTS. *Proceedings, 3rd Earth Resource Technology Satellite (ERTS) Symposium,* **1**, 48-62.

Ruimy A, Kergoat L, Bondeau A, Intercomparison TPOFTPNM (1999) Comparing global models of terrestrial net primary productivity (NPP): analysis of differences in light absorption and light-use efficiency. *Global Change Biology,* **5**, 56-64.

Running SW, Nemani RR, Heinsch FA, Zhao M, Reeves M, Hashimoto H (2004) A continuous satellite-derived measure of global terrestrial primary production. *BioScience,* **54**, 547-560.

Running SW, Thornton PE, Nemani R, Glassy JM (2000) Global terrestrial gross and net primary productivity from the Earth Observing System. In: *Methods in Ecosystem Science.* (eds Sala OE, Jackson RB, Mooney HA, Howarth RW) pp 44-57. New York, NY, Springer New York.

Ryu Y, Baldocchi DD, Kobayashi H *et al.* (2011) Integration of MODIS land and atmosphere products with a coupled-process model to estimate gross primary productivity and evapotranspiration from 1 km to global scales. *Global Biogeochemical Cycles,* **25**, GB4017.

Ryu Y, Baldocchi DD, Verfaillie J *et al.* (2010) Testing the performance of a novel spectral reflectance sensor, built with light emitting diodes (LEDs), to monitor ecosystem metabolism, structure and function. *Agricultural and Forest Meteorology,* **150**, 1597-1606.

Saarnio S, Morero M, Shurpali N, Tuittila E-S, M M, J A (2007) Annual CO2 and CH4

fluxes of pristine boreal mires as a background for the lifecycle analyses of peat energy. *Boreal Environmental Research,* **12**, 101-113.

Saito M, Miyata A, Nagai H, Yamada T (2005) Seasonal variation of carbon dioxide exchange in rice paddy field in Japan. *Agricultural and Forest Meteorology,* **135**, 93-109.

Sass RL, Fisher FM, Harcombe PA, Turner FT (1990) Methane production and emission in a Texas rice field. *Global Biogeochemical Cycles,* **4**, 47-68.

Sass RL, Fisher FM, Harcombe PA, Turner FT (1991a) Mitigation of methane emissions from rice fields: Possible adverse effects of incorporated rice straw. *Global Biogeochemical Cycles,* **5**, 275-287.

Sass RL, Fisher FM, Jr., Huang Y (2000) A process-based model for methane emissions from irrigated rice fields: experimental basis and assumptions. In: *Methane Emissions from Major Rice Ecosystems in Asia.* (eds Wassmann R, Lantin R, Neue H-U) pp 249-258. Springer Netherlands.

Sass RL, Fisher FM, Lewis ST, Jund MF, Turner FT (1994) Methane emissions from rice fields: Effect of soil properties. *Global Biogeochemical Cycles,* **8**, 135-140.

Sass RL, Fisher FM, Turner FT, Jund MF (1991b) Methane emission from rice fields as influenced by solar radiation, temperature, and straw incorporation. *Global Biogeochemical Cycles,* **5**, 335-350.

Satpathy SN, Rath AK, Ramakrishnan B, Rao VR, Adhya TK, Sethunathan N (1997) Diurnal variation in methane efflux at different growth stages of tropical rice. *Plant and Soil,* **195**, 267-271.

Schotanus P, Nieuwstadt FTM, Bruin HaR (1983) Temperature measurement with a sonic anemometer and its application to heat and moisture fluxes. *Boundary-Layer Meteorology,* **26**, 81-93.

Schrier-Uijl A, Kroon P, Leffelaar P, Huissteden JC, Berendse F, Veenendaal E (2010) Methane emissions in two drained peat agro-ecosystems with high and low agricultural intensity. *Plant and Soil,* **329**, 509-520.

Schrier-Uijl AP, Kroon PS, Hendriks DMD *et al.* (2013) Agricultural peat lands; towards a greenhouse gas sink – a synthesis of a Dutch landscape study. *Biogeosciences Discuss.,* **10**, 9697-9738.

Schütz H, Holzapfel-Pschorn A, Conrad R, Rennenberg H, Seiler W (1989a) A 3-year continuous record on the influence of daytime, season, and fertilizer treatment on methane emission rates from an Italian rice paddy. *Journal of Geophysical Research: Atmospheres,* **94**, 16405-16416.

Schütz H, Seiler W, Conrad R (1989b) Processes involved in formation and emission of methane in rice paddies. *Biogeochemistry,* **7**, 33-53.

Schütz H, Seiler W, Conrad R (1990) Influence of soil temperature on methane emission from rice paddy fields. *Biogeochemistry,* **11**, 77-95.

Seiler W, Holzapfel-Pschorn A, Conrad R, Scharffe D (1983) Methane emission from rice paddies. *Journal of Atmospheric Chemistry,* **1**, 241-268.

Shlemon R, Begg EL (1975) Late Quaternary evolution of the Sacramento-San Joaquin Delta, California. *Quaternary Studies, Bulletin,* **13**, 259-266.

Shurpali NJ, Verma SB (1998) Micrometeorological measurements of methane flux in a Minnesota peatland during two growing seasons. *Biogeochemistry,* **40**, 1-15.

Sims DA, Rahman AF, Cordova VD *et al.* (2008) A new model of gross primary productivity for North American ecosystems based solely on the enhanced vegetation index and land surface temperature from MODIS. *Remote Sensing of Environment,* **112**, 1633-1646.

Sjöström M, Ardö J, Arneth A *et al.* (2011) Exploring the potential of MODIS EVI for modeling gross primary production across African ecosystems. *Remote Sensing of Environment,* **115**, 1081-1089.

Sonnentag O, Detto M, Runkle BRK, Teh YA, Silver WL, Kelly M, Baldocchi DD (2011) Carbon dioxide exchange of a pepperweed (Lepidium latifolium L.) infestation: How do flowering and mowing affect canopy photosynthesis and autotrophic respiration? *Journal of Geophysical Research: Biogeosciences,* **116**, G01021.

Sonnentag O, Hufkens K, Teshera-Sterne C *et al.* (2012) Digital repeat photography for phenological research in forest ecosystems. *Agricultural and Forest Meteorology,* **152**, 159-177.

Stallard RF (1998) Terrestrial sedimentation and the carbon cycle: Coupling weathering and erosion to carbon burial. *Global Biogeochemical Cycles,* **12**, 231-257.

Stephens JC, Allen Jr L, Chen E (1984) Organic soil subsidence. *Man-induced land*

subsidence. Reviews in Engineering Geology VI. Geological Society of America, 107-122.

Stoy PC, Katul GG, Siqueira MBS *et al.* (2005) Variability in net ecosystem exchange from hourly to inter-annual time scales at adjacent pine and hardwood forests: a wavelet analysis. *Tree Physiology*, **25**, 887-902.

Stoy PC, Mauder M, Foken T *et al.* (2013) A data-driven analysis of energy balance closure across FLUXNET research sites: The role of landscape scale heterogeneity. *Agricultural and Forest Meteorology*, **171–172**, 137-152.

Strachan I, Nugent K, Crombie S, Bonneville MC (2015) Carbon dioxide and methane exchange at a cool-temperate freshwater marsh. *Environmental Research Letters*, **10**, 065006.

Ström L, Ekberg A, Mastepanov M, Røjle Christensen T (2003) The effect of vascular plants on carbon turnover and methane emissions from a tundra wetland. *Global Change Biology*, **9**, 1185-1192.

Sturtevant C, Oechel WC (2013) Spatial variation in landscape-level CO2 and CH4 fluxes from arctic coastal tundra: influence from vegetation, wetness, and the thaw lake cycle. *Global Change Biology*, **19**, 2853-2866.

Sturtevant C, Oechel WC, Zona D, Kim Y, Emerson CE (2012) Soil moisture control over autumn season methane flux, Arctic Coastal Plain of Alaska. *Biogeosciences*, **9**, 1423-1440.

Sturtevant C, Ruddell BL, Knox SH, Verfaillie J, Matthes JH, Oikawa PY, Baldocchi D (2016) Identifying scale-emergent, nonlinear, asynchronous processes of wetland methane exchange. *Journal of Geophysical Research: Biogeosciences*, **121**, 188–204.

Sun L, Song C, Miao Y, Qiao T, Gong C (2013) Temporal and spatial variability of methane emissions in a northern temperate marsh. *Atmospheric Environment*, **81**, 356-363.

Suyker AE, Verma SB, Burba GG, Arkebauer TJ, Walters DT, Hubbard KG (2004) Growing season carbon dioxide exchange in irrigated and rainfed maize. *Agricultural and Forest Meteorology*, **124**, 1-13.

Syvitski JPM, Kettner AJ, Overeem I *et al.* (2009) Sinking deltas due to human activities. *Nature Geoscience*, **2**, 681-686.

Taylor JA, Brasseur GP, Zimmerman PR, Cicerone RJ (1991) A study of the sources and

sinks of methane and methyl chloroform using a global three-dimensional Lagrangian tropospheric tracer transport model. *Journal of Geophysical Research: Atmospheres,* **96**, 3013-3044.

Teh Y, Silver W, Sonnentag O, Detto M, Kelly M, Baldocchi D (2011) Large greenhouse gas emissions from a temperate peatland pasture. *Ecosystems,* **14**, 311-325.

Toomey M, Friedl MA, Frolking S *et al.* (2015) Greenness indices from digital cameras predict the timing and seasonal dynamics of canopy-scale photosynthesis. *Ecological Applications,* **25**, 99-115.

Torrence C, Compo GP (1998) A practical guide to wavelet analysis. *Bulletin of the American Meteorological Society,* **79**, 61-78.

Treat CC, Bubier JL, Varner RK, Crill PM (2007) Timescale dependence of environmental and plant-mediated controls on CH4 flux in a temperate fen. *Journal of Geophysical Research: Biogeosciences,* **112**, G01014.

Turetsky MR, Kotowska A, Bubier J *et al.* (2014) A synthesis of methane emissions from 71 northern, temperate, and subtropical wetlands. *Global Change Biology,* **20**, 2183–2197.

Ustin SL, Trabucco A (2000) Using hyperspectral data to assess forest structure. *Journal of Forestry,* **98**, 47-49.

Van Der Nat F-FWA, Middelburg* JJ, Van Meteren D, Wielemakers A (1998) Diel methane emission patterns from Scirpus lacustris and Phragmites australis. *Biogeochemistry,* **41**, 1-22.

Veenendaal EM, Kolle O, Leffelaar PA *et al.* (2007) CO2 exchange and carbon balance in two grassland sites on eutrophic drained peat soils. *Biogeosciences,* **4**, 1027-1040.

Waddington JM, Day SM (2007) Methane emissions from a peatland following restoration. *Journal of Geophysical Research: Biogeosciences,* **112**, G03018.

Waddington JM, Strack M, Greenwood MJ (2010) Toward restoring the net carbon sink function of degraded peatlands: Short-term response in CO2 exchange to ecosystem-scale restoration. *Journal of Geophysical Research: Biogeosciences,* **115**, G01008.

Wang B, Neue HU, Samonte HP (1997) Role of rice in mediating methane emission. *Plant and Soil,* **189**, 107-115.

Wassmann R, Aulakh MS (2000) The role of rice plants in regulating mechanisms of methane missions. *Biology and Fertility of Soils,* **31**, 20-29.

Wassmann R, Lantin RS, Neue HU, Buendia LV, Corton TM, Lu Y (2000a) Characterization of methane emissions from rice fields in Asia. III. Mitigation options and future research needs. *Nutrient Cycling in Agroecosystems,* **58**, 23-36.

Wassmann R, Neue HU, Lantin RS, Buendia LV, Rennenberg H (2000b) Characterization of methane emissions from rice fields in Asia. I. Comparison among field sites in five countries. *Nutrient Cycling in Agroecosystems,* **58**, 1-12.

Webb EK, Pearman GI, Leuning R (1980) Correction of flux measurements for density effects due to heat and water vapour transfer. *Quarterly Journal of the Royal Meteorological Society,* **106**, 85-100.

Westergaard-Nielsen A, Lund M, Hansen BU, Tamstorf MP (2013) Camera derived vegetation greenness index as proxy for gross primary production in a low Arctic wetland area. *ISPRS Journal of Photogrammetry and Remote Sensing,* **86**, 89-99.

Whalen S (2005) Biogeochemistry of methane exchange between natural wetlands and the atmosphere. *Environmental Engineering Science,* **22**, 73-94.

Whiting GJ, Chanton JP (1993) Primary production control of methane emission from wetlands. *Nature,* **364**, 794-795.

Whiting GJ, Chanton JP (2001) Greenhouse carbon balance of wetlands: methane emission versus carbon sequestration. *Tellus B,* **53**, 521-528.

Wille C, Kutzbach L, Sachs T, Wagner D, Pfeiffer E-M (2008) Methane emission from Siberian arctic polygonal tundra: eddy covariance measurements and modeling. *Global Change Biology,* **14**, 1395-1408.

Wilson K, Goldstein A, Falge E *et al.* (2002) Energy balance closure at FLUXNET sites. *Agricultural and Forest Meteorology*, **113**, 223-243.

Woebbecke D, Meyer G, Vonbargen K, Mortensen D (1995) Color indexes for weed identification under various soil, residue, and lighting conditions. *Transactions of the ASAE*, **38**, 259-269.

Wu M, Muhammad S, Chen F, Niu Z, Wang C (2015) Combining remote sensing and eddy covariance data to monitor the gross primary production of an estuarine wetland ecosystem in East China. *Environmental Science: Processes & Impacts,* **17**,

753-762.

Xiao X, Hollinger D, Aber J, Goltz M, Davidson EA, Zhang Q, Moore Iii B (2004) Satellite-based modeling of gross primary production in an evergreen needleleaf forest. *Remote Sensing of Environment,* **89**, 519-534.

Xin F, Xiao XM, Zhao BIN *et al.* (2016) Modeling gross primary production of paddy rice cropland through analyses of data from CO2 eddy flux tower sites and MODIS images. *Remote Sensing of Environment,* **submitted**.

Yagi K, Minami K (1990) Effect of organic matter application on methane emission from some Japanese paddy fields. *Soil Science and Plant Nutrition,* **36**, 599-610.

Yagi K, Minami K (1993) Spatial and Temporal Variations of Methane Flux from a Rice Paddy Field. In: *Biogeochemistry of Global Change.* (ed Oremland R) pp 353-368. Springer US.

Yagi K, Tsuruta H, Kanda KI, Minami K (1996) Effect of water management on methane emission from a Japanese rice paddy field: Automated methane monitoring. *Global Biogeochemical Cycles,* **10**, 255-267.

Yan X, Yagi K, Akiyama H, Akimoto H (2005) Statistical analysis of the major variables controlling methane emission from rice fields. *Global Change Biology*, **11**, 1131-1141.

Ye R, Doane TA, Morris J, Horwath WR (2015) The effect of rice straw on the priming of soil organic matter and methane production in peat soils. *Soil Biology and Biochemistry*, **81**, 98-107.

Ye R, Espe MB, Linquist B, Parikh SJ, Doane TA, Horwath WR (2016) A soil carbon proxy to predict CH4 and N2O emissions from rewetted agricultural peatlands. *Agriculture, Ecosystems & Environment,* **220**, 64-75.

Yvon-Durocher G, Allen AP, Bastviken D *et al.* (2014) Methane fluxes show consistent temperature dependence across microbial to ecosystem scales. *Nature,* **507**, 488-491.

Zedler JB, Kercher S (2005) Wetland resources: status, trends, ecosystem services, and restorability. *Annual Review of Environment and Resources,* **30**, 39-74.